DIGITAL ACCESS TO SCHOLARSHIP AT HARVARD
DASH.HARVARD.EDU

HARVARD LIBRARY
Office for Scholarly Communication

Reconstructing Oxygen Isotope Seasonality in Large Herbivores Through Mineralization Modeling, Experimentation and Optimization

Permanent link
http://nrs.harvard.edu/urn-3:HUL.InstRepos:37944994

Terms of Use
This article was downloaded from Harvard University's DASH repository, and is made available under the terms and conditions applicable to Other Posted Material, as set forth at http://nrs.harvard.edu/urn-3:HUL.InstRepos:dash.current.terms-of-use#LAA

Share Your Story

The Harvard community has made this article openly available.
Please share how this access benefits you. Submit a story .

Accessibility

Reconstructing oxygen isotope seasonality in large herbivores through mineralization modeling, experimentation and optimization

A dissertation presented by

DANIEL RUSSELL GREEN

to

The Department of Human Evolutionary Biology

in partial fulfillment of the requirements
for the degree of
Doctor of Philosophy
in the subject of
Human Evolutionary Biology

Harvard University
Cambridge, Massachusetts

December 2016

© 2016 Daniel Russell Green

All rights reserved

Dissertation Advisor: Dr. Tanya Smith Daniel Russell Green

Reconstructing oxygen isotope seasonality in large herbivores through mineralization modeling, experimentation and optimization

ABSTRACT

The seasonality of climate shapes behavior, adaptation and evolution, and figures in environmental theories of human origins. Because blood and tooth oxygen isotope ($\delta^{18}O$) values reflect landscape hydrology, and because teeth mineralize incrementally, tooth $\delta^{18}O$ values preserve information about past seasonality. However, efforts to reconstruct seasonal patterns from teeth are constrained by uncertainty in the relationship between environmental and blood $\delta^{18}O$, and in the nature of tooth mineralization. This dissertation addresses these uncertainties and builds tools that can reconstruct past seasonality from isotopes in teeth, using sheep as representatives of large herbivores common in fossil assemblages. First, I characterize molar mineralization in a population of Dorset sheep using synchrotron x-ray density mapping. I employ Markov Chain Monte Carlo (MCMC) sampling to transform variation in mineralization timing and magnitude from the entire population into a dynamic model. Teeth mineralize primarily in two stages, each distinct in morphology and timing, and mineralization slows towards the end of formation. Next, I test models that link environmental and blood oxygen by raising a population of Dorset sheep, and by providing them with Massachusetts ($\delta^{18}O$ enriched) and Montana water ($\delta^{18}O$ depleted). Blood rapidly tracks environmental water, recovering discrete precipitation events, and is sensitive to animal evaporative water loss. Under controlled conditions, individual and population blood $\delta^{18}O$ variation exceeds rain $\delta^{18}O$ variation at some tropical sites relevant to human evolution. Lastly, I produce a method for reconstructing seasonal

drinking water $\delta^{18}O$ from tooth $\delta^{18}O$ patterns. To do this I test the mineralization and blood models developed here by finely sampling $\delta^{18}O$ from the molars of my experimental sheep. These tests broadly confirm mineralization patterns, but show mineralization appears to include resetting of hydroxyapatite (HAp) constituents. Seasonal drinking water $\delta^{18}O$ histories are reconstructed from tooth $\delta^{18}O$ values through iterative, computational techniques that draw upon mineralization and blood physiology models. I find that conventional serial sampling without modeling fails to reflect the timing and magnitude of drinking water $\delta^{18}O$ seasonality. By contrast, approaches combining mineralization, blood models and optimization accurately reconstruct seasonality. Simulations show that higher resolution sampling is more important for seasonality reconstruction in the tropics. This work makes the reconstruction of seasonal climates relevant to human evolution more feasible, and will help elucidate the environmental context of our own origins.

Contents

Abstract iii
Contents v
Authorship and Attribution vii
Acknowledgements viii

Chapter 1 – Introduction: Seasonality and Human Evolution
1.1 Climate and competition in evolution 1
1.2 The savanna hypothesis 2
1.3 Seasonality and human origins 6
1.4 Reconstructing seasonality 11
1.5 Approach 17
1.6 References 21

Chapter 2 – High-resolution synchrotron imaging and Markov Chain Monte Carlo reveal tooth mineralization patterns
2.1 Abstract 31
2.2 Introduction 32
2.2.1 Tooth mineralization in health, material science, and evolutionary biology 32
2.2.2 Tooth formation and the problem of mineralization 33
2.3 Methods 37
2.3.1 Synchrotron imaging 37
2.3.2 Standardizing enamel coordinates and estimating extension 39
2.3.3 Mineralization model construction using MCMC method 43
2.4 Results 45
2.4.1 Synchrotron μCT imaging 45
2.4.2 Gaussian mineralization model 47
2.4.3 MCMC mineralization model 49
2.5 Discussion 50
2.5.1 Relationship to previous models 50
2.5.2 Implications beyond mineralization 51
2.6 Conclusions 53
2.7 References 54

Chapter 3 – Determinants of blood $\delta^{18}O$ turnover and variation in a population of experimental sheep
3.1 Abstract 59
3.2 Introduction 60
3.2.1 Oxygen isotopes in the environment and body 60
3.2.2 Modeling body water $\delta^{18}O$ steady-state: inputs and outputs 62
3.2.3 Luz *et al.* (1984) model 63
3.2.4 Gretebeck *et al.* (1997) and Podlesak *et al.* (2008) models 64

3.2.5 Kohn (1996) 65
3.3 Methods 67
3.3.1 Sheep experiment 67
3.3.2 Stable isotope analyses 69
3.3.3 Weight, VO2, feed and temperature parameterization 70
3.3.4 Water flux modeling 72
3.4 Results 74
3.4.1 Blood values, turnover and variance 75
3.4.2 Model performances 76
3.5 Discussion 82
3.6 Conclusions 86
3.7 References 87

Chapter 4 – High-resolution stable isotope analyses reveal tooth mineralization patterns for climate reconstruction
4.1 Abstract 91
4.2 Introduction 92
4.2.1 Seasonality, evolution and adaptation 92
4.2.2 Documenting seasonality in teeth 93
4.2.3 Tooth mineralization and inverse method reconstruction 95
4.3 Methods 96
4.3.1 Experimental water switch and dicing 96
4.3.2 Oxygen isotope measurements 98
4.3.3 Blood-water $\delta^{18}O$ modeling 101
4.3.4 $\delta^{18}O$ integration with tooth mineralization 102
4.4 Results and Discussion 107
4.4.1 Experimental validation of mineralization model 107
4.4.2 Hydroxyapatite PO_4 resetting 107
4.4.3 Development of inverse procedure to estimate $\delta^{18}O$ inputs 109
4.4.4 Inverse reconstruction results 115
4.4.5 Resetting optimization 119
4.5 Conclusions 123
4.6 References 125

Chapter 5 – Conclusions: the future of seasonality reconstruction
5.1 A method for seasonality reconstruction 131
5.2 Importance of modeling mineralization 131
5.3 Human mineralization patterns 134
5.4 Inverse modeling in other taxa 135
5.5 Probability frameworks for seasonality reconstruction 136
5.6 Multiproxy approach to paleoseasonality 139
5.7 Conclusions 139
5.8 References 142

Authorship, Attribution and Presentations

Chapter 1 - Introduction. Daniel Green (DG) wrote the manuscript.

Chapter 2 - High-resolution synchrotron imaging and Markov Chain Monte Carlo reveal tooth mineralization patterns. Daniel Green (DG) designed the research with supervision from Tanya Smith (TS) and Paul Tafforeau (PT). DG dissected teeth, DG and PT conducted synchrotron imaging, DG digitally prepared sections, Gregory Green (GG) wrote python scripts flattening sections and conducting MCMC searches. DG wrote the manuscript with contributions from TS, PT, GG, Albert Colman (AC) and Felicitas Bidlack (AB).

This work has been presented at the following conferences: American Association of Physical Anthropologists (AAPA) annual meeting in Knoxville, TN (2013); Gordon Research Seminar on Biominalization, New London, NH (2014).

Chapter 3 – Determinants of blood $\delta^{18}O$ turnover and variation in a population of experimental sheep. DG designed the research with supervision from TS. DG raised animals with the aid of Pedro Ramirez, and DG conducted all water and blood sampling. DG conducted isotopic measurements with AC and Gerard Olack (GO). DG analyzed data and wrote the manuscript with contributions from TS and AC.

A portion of this work was presented at the following conferences: Gordon Research Seminar on Biominalization, New London, NH (2014); AAPA annual meeting in St. Louis, MO (2015); Cleveland Museum of Natural History Symposium on Paleoclimate (2015).

Chapter 4 – High-resolution stable isotope analyses reveal tooth mineralization patterns for climate reconstruction. DG designed the research with supervision from TS. DG conducted tooth physical sampling, performed Ag_3PO_4 precipitations and made $\delta^{18}O$ measurements with supervision from AC and GO and help from Johanna Holo (JH). DG wrote python scripts for blood isotopic modeling, integration with mineralization, optimization routines, and analysis with contributions from GG and supervision by AC and GG. DG wrote the manuscript with editing by TS, AC, FB and GG.

A portion of this work has been presented at the Cleveland Museum of Natural History Symposium on Paleoclimate (2015), and at the AAPA annual meeting in Atlanta, GA (2016).

Chapter 5 – Conclusions: the future of seasonality reconstruction. DG wrote the manuscript.

Acknowledgements

Many people made this work possible. I am thankful to Mary Smith and Mike Thonney at the Cornell Sheep Program for all of their wisdom and interest in my project. At the Wyss institute James Weaver was kind to share his toys and his ideas, and Fettah Kosar at the Center for Nanoscale Systems provided CT time and knowledge of Turkish politics. From Harvard's Earth and Planetary Science Department, I am grateful to Charlie Langmuir and Zhongxing Chen for generous lab space in their clean room. I am grateful to Dan Schrag for support when I very much needed it, and to Denise Sadler, Greg Eischied, Sarah Manley and Kate Dennis for putting up with my highly unusual "geological" samples.

Several people throughout the United States and the world advanced my research and helped me think in new ways. Paul Tafforeau's enthusiasm and commitment were a major factor in making the synchrotron portion of this research feasible. In Kenya, I am grateful to Kyalo Manthi and Emma Mbua for their support at the National Museums of Kenya. I am especially grateful to Meave and Richard Leakey, and to their team including Ikal Angelei, Emekwi, Esekon, Martin, John Lonyericho, and Cyprian Nyete, for all their generosity and genius. I am grateful to Dr. Edward Kariuki and Dr. Samuel Andanje for their help at KWS. Because of their support in the field and in the lab I must thank Gerry Olack, Johanna Holo, Thure Cerling, Frank Brown, Craig Feibel, Dino Martins, Chris Lepre, Rhonda Quinn, Sonia Harmand, Jason Lewis, Kendra Chritz, Scott Blumenthal, Aric Mine, Anna Waldeck, Andy Masterson and Sora Kim. Tyson Alvanos, Lisa Milliard, David Eneguess and Robert Savoy at Disco were kind to let me use their machines. I am grateful to Felicitas Bidlack for her support, and for pushing us to think about mineralization in new, better ways.

In the care of my sheep, I am above all thankful to Pedro Ramirez, whose secrets about animal care and human life have helped many graduate students and sheep. Moira Sheehan and Steve Niemi provided veterinary care for the animals above and beyond the call of duty. At the Concord Field Station I am grateful to Andy Biewener for his generosity and expertise, to Lisa Litchfield, Somer O'Brien, and Jen Carr for their help, and to Carolyn Eng and Zack Lewis for falling in love with 948. I am grateful to 947, 949, 950, 951, 957, 961, 962, 963 and 964. Stephanie Meredith and Katie Zink made hard tasks easier with compassion and professionalism.

In the department of Human Evolutionary Biology, I am grateful to many faculty for generously sharing their insights into physiology and evolution, including Noreen Tuross, Richard Wrangham, Rachel Carmody, Terry Capellini, Katie Hinde, Maryellen Ruvolo, and Christian Tryon in Archeology. I never understood potential of bureaucracy before I met Meg Lynch and Lenia Constaninou, and cannot thank them enough for all they have done for me and other students. I'm also grateful to Meg Jarvi and Monica Oyama for supporting them. There are many HEB students who have made HEB an interesting and wonderful home. I have especially appreciated the friendship and guidance of my cohort Sam Urlacher, Bridget Alex, Brian Addison and honorary member Bastien Varoutsikas; the old folks including Karola Kirsanow, Tina Warinner, Neil Roach and Amanda Lobell, Zarin Machanda, Alicia Breakey, Liz Brown, Tory Wobber, and Erik Otarollo-Castillo; and many of the young folks including Kate Carter, Eric Castillo, Andy Cunningham, Andrew Yegian, Tory Tobolski and Manvir Singh. Michele Morgan, Larry Flynn, John Barry, Carol Hooven, Meir Barack, Anna Warrener, Linda Reynard, Brenda Frazier and Kristi Lewton have all helped make HEB the fascinating intellectual environment and friendly place that it is.

I am so lucky to have a committee of brilliant, fascinating and dedicated scientists who genuinely care about their students. Dan, thank you for pushing me to do the hard but good things I dreaded most, and for being more than just an evolutionary biologist. David, thank you for your endless knowledge and careful thought regarding adaptation, speciation, evolution, biogeography, and diplomacy: I genuinely believe Darwin would have loved meeting you. Albert, all I've learned about chemistry I've learned from you. Your deep engagement and effort in this project have made it so much more rewarding, and productive. Tanya, no graduate student has

ever been so supported at every step by their advisor. Thank you for your constant advocacy on my behalf, for your unparalleled understanding of tooth formation in all its complexity, and for your insistence in the highest standard of rigor at every level. Thank you for all your support and advice in writing, for your patience, and for the fact that when I say I'm Tanya Smith's student, people pay attention. Thank you most of all for your friendship.

I've had many friends who have made Cambridge and Harvard a wonderful place. At Eliot House, I'm especially indebted to Gail O'Keefe and Doug Melton, to the tutors who made Eliot home, and to the students whose curiosity and optimism continue to make the earth turn. Sensei Eiji Toryu and the Boston JKA have been astonishingly kind to welcome me into their community. I'd like to thank Colleen and Christine for helping make the world a place I love. Ben and Richa, you've taught me about new ways of being, of intelligence, and kindness. Sarah Rugheimer, Trevor Stark, Mircea Raianu, Alix Lactoste and AJ Kumar, thank you for reminding me that academia can be bigger than academia.

My parents Heather and David have encouraged my interest in science my whole life, and without them, their support and their community, I could never have done this research. Anthony, thank you for your humor, your many interests, and for forging your own brilliant path: your love and support has helped me get through this work. Gregory, my PhD changed forever when you sat me down at Simon's on Mass Ave and began teaching me Python. Since that time you've given me tutorials on partial differential equations (some of them at 3am) and introduced me to the beauty of Bayes' theorem. If I could make you a member of my committee,

I would. I also want to thank my cousin Oles Szejman (1927-2014) for being the most cantankerous, knowledgeable, and beloved scholar-in-residence of Cambridge.

Lastly, Karen you have been the best part of my PhD these last seven-and-a-half years. Thank you for your curiosity, companionship, and love of life.

By June our brook's run out of song and speed.
Sought for much after that, it will be found
Either to have gone groping underground
(And taken with it all the Hyla breed
That shouted in the mist a month ago,
Like ghost of sleigh-bells in a ghost of snow)—
Or flourished and come up in jewel-weed,
Weak foliage that is blown upon and bent
Even against the way its waters went.
Its bed is left a faded paper sheet
Of dead leaves stuck together by the heat—
A brook to none but who remember long.
This as it will be seen is other far
Than with brooks taken otherwhere in song.
We love the things we love for what they are.

Robert Frost, *Hyla Brook*

Despised; the wood her sad retreat receives:
Who covers her ashamed face with leaves;
And skulks in desert caves. Love still possessed
Her soul; through grief of her repulse, increased.
Her wretched body pines with sleepless care:
Her skin contracts: her blood converts to air.
Nothing was left her now but voice and bones:
The voice remains; the other turn to stones.

Ovid, *Metamorphoses*
(tr. George Sandys)

1

Introduction: Seasonality and Human Evolution

1.1 Climate and competition in evolution

The environment of hominin origins has long been a central focus of human evolutionary biology, because it places the emergence of highly complex, apparently extraordinary behaviors into the context of ordinary, if still complex, ecological processes. Understanding the ecological context of adaptation and evolution is a central task of evolutionary biology. Even in Darwin's first formulation of evolution by natural selection, he reviewed the competing processes – abiotic environmental challenges, and competition - that would tend to shape selection and adaptive response:

> *"Climate plays an important part in determining the average numbers of a species, and periodical seasons of extreme cold or drought, I believe to be the most effective of all checks. In so far as climate chiefly acts in reducing food, it brings on the most severe struggle between the individuals, whether of the same or of distinct species… Nor do I believe that any great physical change, as of climate… is actually necessary to produce new and unoccupied places for natural selection. For as all the inhabitants of each country are struggling together with nicely balanced forces, extremely slight modifications in the structure or habits of one inhabitant would often give it an advantage over others." (Darwin, 1859)*

The evolutionary origin of primate and human cognitive ability is often considered in terms of climate or competition, but of course neither can be wholly separated in nature (Milton 1988; Dunbar *et al.*, 2007). As always, Darwin's intuitive sense was to eschew simple explanations, and

to recognize the multiplicity of interacting forces that had, in the long history of the earth, produced the vast complexity of life we observe today.

1.2 The savanna hypothesis

Announcing the discovery of the first fossil australopithecine in 1925, Raymond Dart speculated that while most primates are well suited to tropical forests, the African savanna had been the laboratory of human evolution (Dart 1925, cited in Domínguez-Rodrigo 2014). Subsequent investigations demonstrated that many Australopithecine fossils formed in more open habitats, and the savanna hypothesis remains a powerful force in thinking about human evolution today (Coppens, 1978; Foley 1987; Domínguez-Rodrigo 2014). The savanna hypothesis is not unique to hominins: it is justifiably invoked to explain the increasing domination of large, cursorial (running) and hypsodont (high-crowned) ungulate herbivores throughout Eurasia and Africa (Fortelius *et al.*, 2014). This process appears to have occurred globally as the planet cooled and grasslands spread from their earliest origins in Africa and South America. In regions of uplift like Patagonia, or spreading grasslands in North America, horse and camelid herbivores grew in size, and grew large teeth, to follow the opening habitats now recognized from pollen, phytolith and macrofossil remains (Stromberg 2011). This phenomenon began later in Eurasia, as global cooling and aridification continued, probably driven by Antarctic glaciation. Starting with the central Asian steppes in the early Miocene, and spreading into previously forested regions of Europe, savannas appeared in patches or in plains, favoring herbivores with adaptations to exploit them. By the late Miocene, culminating in the end-Messinian crisis, expanding open habitats had generated an extraordinary evolutionary radiation of bovids, and to a lesser extent

other herbivores, many associated with classical African savanna communities (Fig. 1.1) (Stromberg, 2011; Fortelius *et al.*, 2014).

The East African environments where hominins are first found are famously variable and complex, acting as a geographical conduit for organisms with diverse niches and adaptations across northern and Sub-Saharan habitats. The region included a mix of open and heavily forested, even wet environments in the early Miocene, but by the middle Miocene, ocean-core pollen records show that grasses were abundant (Leakey *et al.*, 2011; Feakins *et al.*, 2013). Towards the end of the Miocene, the global spread of arid, low-CO_2 adapted C4 plants and associated open floral and faunal communities expanded throughout East Africa as well (Fig. 1.1) (Stromberg 2011; Uno *et al.*, 2011). Tooth carbon isotope ($\delta^{13}C$) values show that herbivores responded in a range of ways. Hipparionins – early equids – quickly became C4 grazers, followed soon afterwards by many suids and elephantids. Bovids, rhinos and hippos also transitioned to more C4 plants, though slowly and variably, and giraffids became C3 specialists (Uno *et al.*, 2011).

The earliest putative hominin found in Chad, *Sahelanthropus*, likely lived in a mosaic environment characterized by seasonal, broad floodplains, not unlike those found at the eastern site of Lothagam in the late Miocene c. 7 million years ago (Ma) (Brunet *et al.*, 2005; Feibel 2011). The other Miocene hominins *Orrorin* in the Tugen Hills, Kenya and *Ardipithecus* in Aramis, Ethiopia are also thought to have lived in mixed environments, with denser forests near rivers and lakes grading into bush and grassland, where tooth $\delta^{13}C$ value suggest *Ardipithecus* foraged

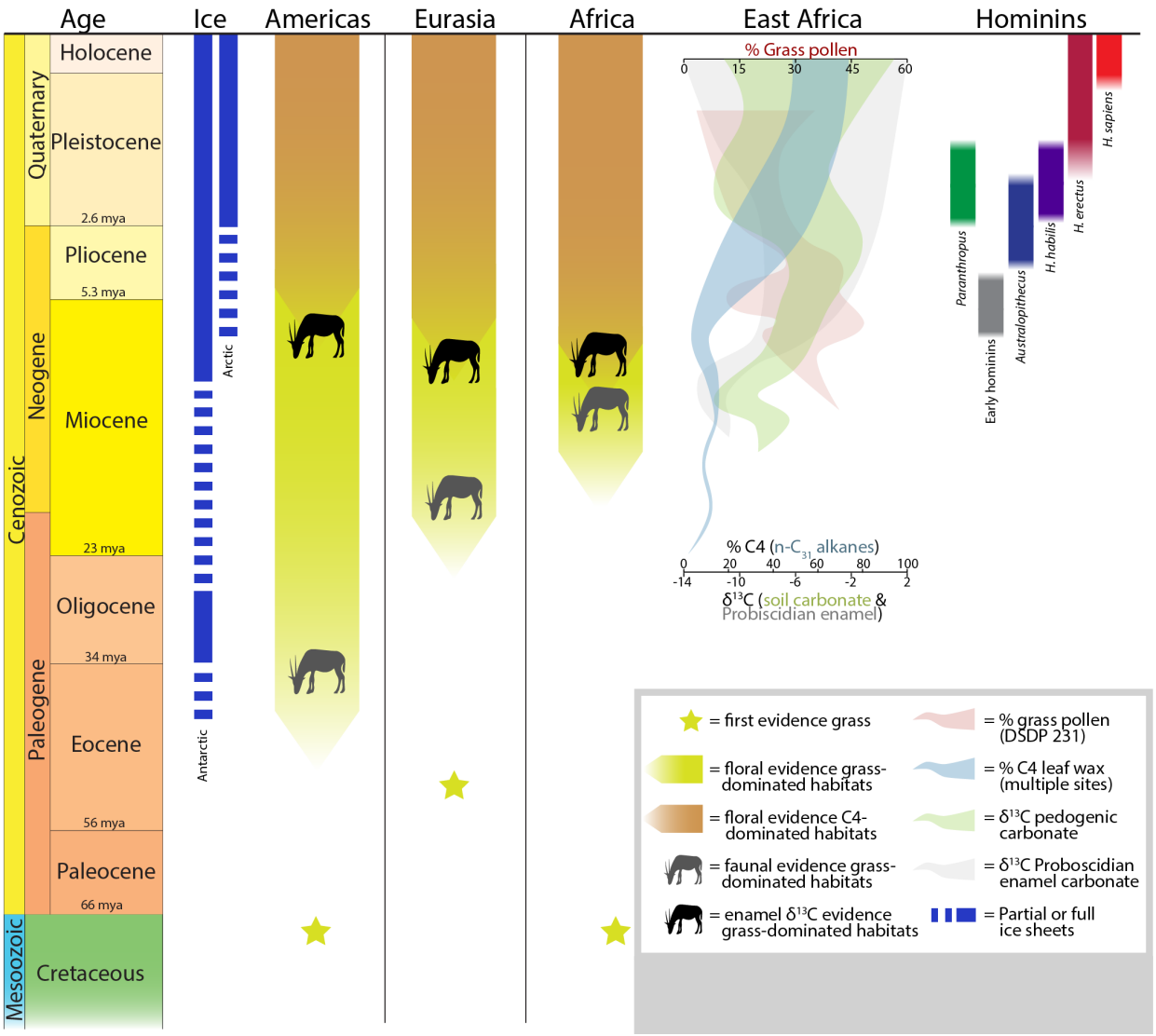

Figure 1.1: Cenozoic grassland habitat expansion and the context of human evolution. Over the last 65 million years (mya, scale shown at left), the appearance of ice at either pole (partial/ephemeral or full glaciation shown as dashed or full blue line, respectively) and presence of grass habitats are plotted for the Americas, Eurasia and Africa. First pollen evidence of grass is shown as a yellow star, while first floral (macrofossil, phytolith and pollen) evidence for grass habitats (yellow bar) or C4-dominated habitats (brown bars, reconstructed through $\delta^{13}C$ values) appear later. Evidence of large herbivore communities dedicated to grassland habitats or C4-grass habitats (detected from tooth $\delta^{13}C$ values) are shown as gray and black grazers, respectively. To the right, east African vegetation indices include % grass pollen (red, measured from Somali gulf ocean core DSDP 231), estimated % C4 leaf waxes (blue, DSDP sites 228, 232, 235 and 241), and $\delta^{13}C$ values of soil nodule and elephantid enamel carbonate (green and gray, respectively, shown in V-PDB scale). Far right, larger clades of hominins, not necessarily monophyletic, include early putative hominins, Australopithecines, Paranthropines, early *Homo*, *H. erectus* and *H. sapiens*. Data and figure adapted from Zachos *et al.*, (2001), Stromberg (2011), Feakins *et al.*, (2013), Wood and Grabowski (2015), and Uno *et al.*, (2016).

(Woldegabriel *et al.*, 2009; Roche *et al.*, 2013; Cerling *et al.*, 2014; Suwa and Ambrose 2014; Cerling *et al.*, 2015). Hominins may have exploited savanna resources through bipedal locomotion, which is four times more efficient than quadrupedal locomotion terrestrially, and may have increased hominin foraging range into spreading grassland ecosystems (Sockol *et al.*, 2007; Pontzer *et al.*, 2009; Vrba 2015). Tooth $\delta^{13}C$ values indicate that *Ardipithecus* foraged at least partially in C4-dominated habitats (White *et al.*, 2009; Cerling *et al.*, 2015), though both *Ardipithecus* and the later *Australopithecus anamensis* in Turkana, Kenya consumed primarily C3-based resources, almost certainly plants, and not unlike savanna chimpanzees (Ungar and Sponheimer, 2011; Cerling *et al.*, 2013).

Hominins attributed to the genus *Homo* first appear during the radiation of hominin species at fossil assemblages in east and south Africa across the Plio-Pleistocene transition, 1.5-3.5 Ma (Kimbel and Lockwood 2006). Recent discoveries Lomekwi, Kenya and Dikika, Ethiopia suggest that large scale stone tool industries were produced by Australopithecines, and predate the earliest known expansions in brain size in *Homo* (McPherron *et al.*, 2011; Harmand *et al.*, 2015). Numerous environmental recorders including dust transport to marine and lake sediments, soil carbonate $\delta^{13}C$, faunal abundance, and fossil $\delta^{13}C$ and oxygen isotope ($\delta^{18}O$) values all indicate that after an early Pliocene warm and wet period, the later Pliocene and Pleistocene witnessed repeated drying, and the associated expansion of arid environments. This process was a part of global changes likely brought about by the onset of Northern Hemisphere glaciations, and in east Africa the pace and extent of change was highly variable geographically (Partridge et al., 1995; Kingston 2007; Elton 2008; Blois and Hadly 2009; Uno *et al.,* 2011; Joordens *et al.*, 2011; Levin *et*

al., 2011). Both hominin and herbivore taxa diversity reached a maximum at East African fossil sites during this interval (Bobe and Leakey 2009; Bobe 2011).

The explosion of hominin diversity at the Plio-Pleistocene boundary, and the concurrence of hominin evolution with the spread of savanna habitats and climatic instability, give the savanna hypothesis an enduring attraction. But how and why did hominins exploit expanding arid landscapes? Did diverse species occupy different habitats, or exploit niches preferentially according to their physical adaptations, social organizations, or technological industries?

1.3 Seasonality and human origins

Seasonality of rainfall is a major determinant of plant community structure, and prolonged, seasonal dry periods remain central to technical definitions of savanna landscapes (Domínguez-Rodrigo 2014, Levin 2015). Seasonality contributes to the fire regimes that have become important fixtures of some grassland communities (Archibald *et al.*, 2012; Hoetzel *et al.*, 2013). In the complex mosaic of environments in east Africa, specific seasonal rainfall regimes associated with the Inter-Tropical Convergence Zone (ITCZ) pattern the distribution of plant communities (Levin 2015). These help form adjacent but distinct associated faunal communities that may be local, or belong to larger geographic ranges extending throughout Africa (Lorenzen *et al.*, 2012). The recent discovery of four species of giraffe via genomics, all coexisting side-by-side in east African wooded savannas, also reveals that their geographical ranges accord with ITCZ-determined seasonality regimes, possibly influencing species birth seasonality (Brown *et al.*, 2007; Thomassen *et al.*, 2012; Fenessy *et al.*, 2016). In the restricted area of South Africa's Kruger National Park, species abundance is regulated in part by differential survivorship of

juveniles during prolonged droughts, for instance depressing Zebra offspring survivorship more in arid zones, but affecting wildebeest offspring in all areas equally (Owen-Smith *et al.*, 2005).

Many diverse taxa maintain niche separation through differential seasonal access to resources. On the Galapagos island of Santa Cruz, woodpecker finches compete with thicker-billed competitors by using twig and cactus spines as tools to hunt insects during dry seasons (Tebbich *et al.*, 2004; Rundell and Price 2009). In some primate lineages, seasonal resource availability is thought to promote complex behavior and intelligence, giving preferential access to energy-rich foods through planning, social coordination during foraging, or tool use (Melin *et al.*, 2014; Janmaat *et al.*, 2016). Access to high quality resources may increase overall energy available for cognition, or increase brain caloric expenditure through reduced gastrointestinal or muscular costs (Aiello and Wheeler, 1995; Isler and Van Schaik, 2014; Liao *et al.*, 2016).

It is almost certain that various hominin taxa exploited different niches available to them in east Africa and throughout the continent, based upon their morphological adaptations (Kimbel and Lockwood 2006; Sponheimer et al., 2006; Ungar et al., 2006; Ungar et al., 2008; Straight et al., 2009; Cerling et al., 2011; Wood and Leakey 2011) and tooth $\delta^{13}C$ values (Cerling *et al.*, 2013; Sponheimer *et al.*, 2013). Unlike the earliest hominins, the Pliocene and Pleistocene *Kenyanthropus*, *Australopithecus afarensis*, *Au. africanus* and *Paranthropus robustus* consumed a mix of C3 and C4 resources, while the east African *Au. bahrelghazali* and the Paranthropines *P. aethiopicus* and *P. boisei* specialized on C4 resources (Fig. 1.2). Like gracile east African and all south African

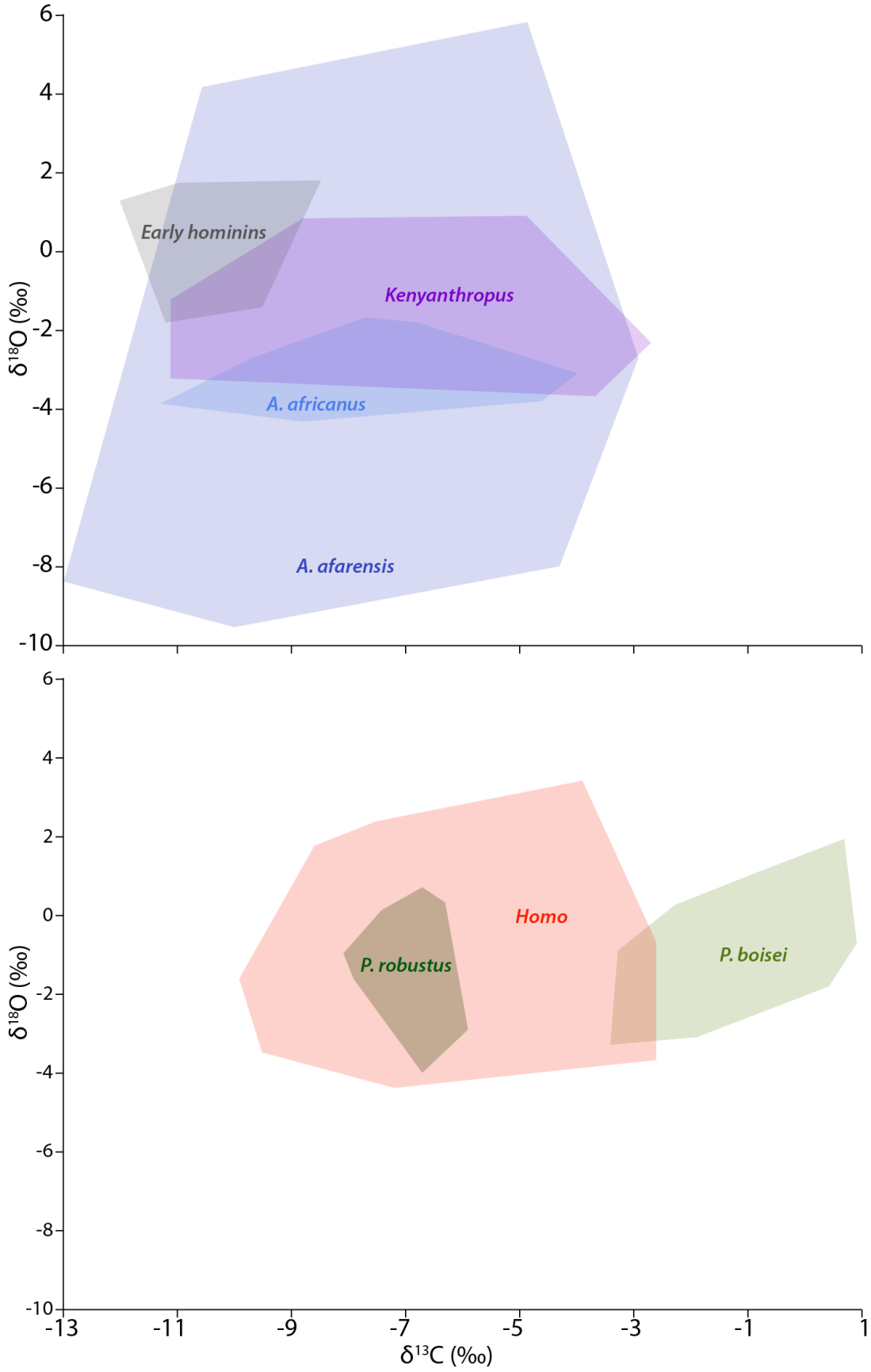
Early hominins
Kenyanthropus
A. africanus
A. afarensis
Homo
P. robustus
P. boisei
δ18O (‰)
δ13C (‰)
6
4
2
0
-2
-4
-6
-8
-10
-13
-11
-9
-7
-5
-3
-1
1

Figure 1.2: Hominin carbon and oxygen isotope values. Above, enamel carbonate $\delta^{13}C$ and $\delta^{18}O$ values from the early hominins *Ardipithecus* and *Australopithecus anamensis* (gray), *A. afarensis* (dark blue), *A. africanus* (light blue), and *Kenyanthropus* (purple). Below, values from *P. robustus* (dark green), *P. boisei* (light green) and *Homo* (red). Low $\delta^{13}C$ values indicate early hominins consumed C3 resources almost exclusively, and high $\delta^{13}C$ values suggest *P. boisei*, like other east African paranthropines, relied heavily upon C4 resources. Intermediate values suggest that other hominins acquired a wide range of C3 and C4 resources. Varied $\delta^{18}O$ values may reflect preferential use of certain landscape water sources, but is also linked to differences in landscape hydrology. *A afarensis*, which shows a large range of $\delta^{18}O$ values, nevertheless has $\delta^{18}O$ values similar to those of equids and suids found in the same sedimentary layers (Wynn *et al.*, 2013). Data from Sponheimer *et al.*, (2013).

Australopithecines, specimens attributed to *Homo* also consumed a mix of C3 and C4 resources (Cerling *et al.*, 2013; Sponheimer *et al.*, 2013).

Did the seasonal availability of C3 and C4-related resources drive the more diverse foraging patterns of Pliocene *Australopithecus*, of south African *Paranthropus*, and of *Homo* throughout Africa? Might stone tool industries have provided hominins access to resources previously unavailable to them, and if so, where and when did they seek them? Sponheimer *et al.* (2006) shows that both $\delta^{13}C$ and $\delta^{18}O$ values in *P. robustus* teeth varied substantially over time, and in coordinated fashion. As Sponheimer *et al.* (2006) ask:

> *"About 2.4 to 1.4 million years ago, our earliest stone tool–making ancestors, Homo habilis and H. erectus, shared African savannas with their close relatives, Paranthropus. How variable were their environments? How much did their diets overlap in different seasons? And how did these two bipedal hominins manage to coexist for 1 million years?"*

Seasonality may have contributed to niche partitioning among early hominins and within *Homo*, promoted social and cognitive flexibility, increased stone tool use, or led to *H. erectus* range expansion in response to environmental instability (Ambrose *et al.*, 2001; Lieberman *et al.*, 2009; Anton *et al.*, 2014; Vrba 2015). Rainfall seasonality is thought to have influenced later human dispersals from Africa, the largescale domestication of plants, and the geographic range of pastoralist practices. Because of its importance to understanding the environment and behavior of early hominins, seasonality remains an important focus of human paleoenvironmental reconstruction. Nevertheless, reconstructing paleoseasonality remains a daunting task because of its ephemeral nature.

1.4 Reconstructing seasonality

Climatic changes that alter environments and provoke adaptive or behavioral responses may be long term and directional (secular) or cyclical on a variety of timescales. In addition to facing long term cooling and aridification, Plio-Pleistocene tropical African climate was subject to variation caused by precession in the earth's orbit around the sun on 24,000, 41,000 and c. 100,000-year cycles. Even el-Niña related effects generated by heat anomalies in the southern Pacific, occurring on 5-7 year timescales, influence climatic patterns in east Africa. Seasonality is a more temporally detailed form of largescale cyclic climatic variation, and for this reason has a great impact on individual behavior and survivorship. It is also therefore the most difficult form of variation to reconstruct from stratigraphic records. Past rainfall seasonality can be reconstructed through a variety of recorders with different temporal and spatial sensitivity. Many reconstructions rely upon stable isotopes, particularly oxygen and carbon, that partition unevenly across landscapes, ecosystems, and organisms over time, and are preserved in fossils or sediments. Isotope ratios are often described using δ notation

$$\delta = 10^3(R - R_{std})/R_{std} \qquad \text{(eq. 1.1)}$$

where R and R_{std} are the abundance of the rare over the common isotope in a sample of interest and standard, respectively, and sample δ is reported in units per thousand, ‰ (per mil)(Friedman and O'Neil 1977; Bowen 2010).

In general terms, higher $\delta^{13}C$ values indicate the prevalence of plants that use arid and low-CO2 adapted C4 rather than C3 photosynthesis. This is because C4 photosynthesis does not

discriminate as powerfully against the heavy carbon isotope during carbon fixation as C3 photosynthesis. Higher $\delta^{18}O$ values indicate that water on the landscape or in the body is evaporating at a higher rate (Gat 1996, Bowen 2010). Because of their intimate relationship with landscape hydrology, $\delta^{18}O$ values are the focus of this work.

At the largest scale, past tropical seasonality over large timescales can be roughly predicted by known precessional patterns in the earth's orbit, with increased insolation increasing monsoon intensities (Kingston *et al.*, 2007). Regionally, prolonged or intense dry seasons increase Aeolian dust transport to lake or ocean cores, though these proxies are indirect, influenced by wind, and may not reflect local patterns (deMenocal 2004). Within terrestrial sedimentary sequences, paleosol carbonate nodules are important indicators of landscape aridity, an indirect measure of rainfall seasonality, and capture C3 and C4 plant community composition through $\delta^{13}C$ values (Levin *et al.*, 2009). Paleosols are problematic indicators of seasonality however because they form over 10^3-10^4 year timeframes, cannot form under mesic or rapid depositional environments, and like dust records reflect water budget deficit, not specific rainfall patterns (Breecker *et al.*, 2009; Uno *et al.*, 2016).

Plant fossil remains are another indirect indicator of past seasonality and have seen renewed interest in recent years. Both pollens and phytoliths – amorphous calcium carbonate precipitates that form in plant tissues – are deposited in low-energy lacustrine, floodplain and marine sediments, and can be identified to broad taxonomic or functional groups (Bonnefille 2010; Feakins *et al.*, 2013; Mander *et al.*, 2013). Preservation is unreliable, and because different plant groups may produce or disperse these materials on vastly different scales, data must be analyzed

with caution. Phytoliths may allow isotopic analysis for C3/C4 presence, and both pollens and phytoliths record floral community composition where certain taxa (e.g. grasses or trees) indicate disruptive and seasonal, or stable and forested environments (Woldegabriel *et al.*, 2009; Bonnefille 2010). In recent years plant leaf wax and lipid isotopic composition have become another important source of plant community analysis (Feakins 2013; Magill *et al.*, 2013; Uno *et al.*, 2016a; Uno *et al.*, 2016b).

Faunal community composition can be another critical, indirect indicator of landscape seasonality. Aquatic or primate taxa may demonstrate year-round water availability or dense forest, while particular small mammal or large herbivore remains may indicate arid or seasonal grassland landscapes (Manthi 2007; Bobe and Leakey 2009; Bobe 2011). Particular faunal morphological characteristics may represent adaptations to specific environments, and the discipline of "ecometrics" – correlating environmental parameters with these adaptations – may be used to infer past rainfall patterns (Eronen *et al.*, 2010a; Eronen *et al.*, 2010b; Fortelius *et al.*, 2012; Liu *et al.*, 2012; Fortelius *et al.*, 2016). Recently, analyses of herbivore dental characteristics have been used to approach reconstruction of dry and wet season intensities, and suggest that dental adaptations may be especially driven by drought-induced fallback food diets (Žliobaitė *et al.*, 2016).

Because higher $\delta^{18}O$ and $\delta^{13}C$ values on a landscape indicate greater evaporative water loss and plant use of arid-adapted C4 photosynthesis, respectively, these have been measured in teeth as recorders of herbivore interactions with wetter or drier environments (Longinelli 1984; Bowen 2010; Wynn *et al.*, 2013). In particular, $\delta^{18}O$ values in blood and teeth can reflect landscape

hydrology: blood $\delta^{18}O$ is in equilibrium with landscape $\delta^{18}O$, and landscape $\delta^{18}O$ values are shaped by hydrological regimes (Longinelli 1984; Bowen 2010; Quinn 2015).

Teeth form and erupt during an animal's lifetime, and isotope measurements across the tooth row can therefore record environmental change, animal migration, or variation in foraging and physiology (Bryant *et al.*, 1996). Even greater detail can be recorded within a single tooth that formed incrementally over time, and many studies have therefore sampled isotopes sequentially from cusp to cervix, to capture information related to different periods of tooth formation (Fricke and O'Neil 1996; Fricke *et al.*, 1998; Balasse *et al.*, 2003; Sponheimer *et al.*, 2006; Smith and Tafforeau 2008; Zazzo *et al.*, 2012). Sequential isotope values from teeth bring us tantalizingly close to original seasonal variation in the environment, but importantly, measurements reflect environmental chemistry only through an animal's foraging behavior, body chemistry, and the complex and often unknown process of tooth mineralization.

Passey and Cerling (2002) addressed this problem by building a quantitative model of mineralization, and integrating it with tooth isotope measurements to solve for the original blood isotope values over time (Passey *et al.*, 2005). Passey and Cerling (2002) developed their model from the traditional conceptualization of tooth enamel mineralization where mineral increases monotonically in two stages: secretion and maturation (Simmer *et al.*, 2012). Secreted enamel accounts for only 20-30% of mature mineral weight (Passey and Cerling, 2002; Simmer *et al.*, 2012), and contains ordered increments marking formation time (Boyde, 1989; Smith, 2006; Smith and Tafforeau, 2008). Suga (1982) proposed that maturation phase geometry and timing includes a series of waves of increasing mineralization moving to and from the EDJ (Suga, 1982).

Passey and Cerling (2002) proposed that an initial secretory front is followed immediately by a single maturation wave in the same geometric orientation.

Passey *et al.* (2005) integrated conceptions of mineralization with tooth isotopic sampling in an effort to solve for blood isotopic composition. In this sense, Passey *et al.*, (2005)'s method represented a major advance over the previous and still common practice of leaving the seasonal significance of varying isotope values measured from a tooth to subjective interpretation. Nevertheless the method has been employed infrequently, being experimentally validated for $\delta^{13}C$ inputs in rabbits and sheep (Passey *et al.*, 2005; Zazzo *et al.*, 2010), $\delta^{18}O$ inputs in woodrats (Blumenthal *et al.*, 2014), and used to estimate potential $\delta^{13}C$ inputs in fossil hippopotamuses (Passey *et al.*, 2005). One reason for underutilization is that this method was designed for ever-growing teeth like rodent incisors or hippo tusks, whereas molar mineralization processes tend to be more complex (Passey *et al.*, 2005; Zazzo *et al.*, 2010). For instance, molars are known to form at nonlinear rates that differ across the tooth row, and between taxa (Passey *et al.*, 2005; Zazzo *et al.*, 2010; Zazzo *et al.*, 2012; Kierdorf *et al.*, 2013; Bendrey *et al.*, 2015). Furthermore the pattern of enamel maturation – the phase of mineralization when the bulk of enamel constituents are formed – has remained difficult to characterize spatially and temporally (Suga 1982; Hoppe *et al.*, 2004; Tafforeau *et al.*, 2007: Taylor and Kohn, 2016). Reconstructions of the magnitude and timing of seasonal oscillations in blood and environmental $\delta^{18}O$ (see below) crucially depend upon an accurate, quantitative understanding of mineralization.

This understanding is further complicated by the discovery that organisms precipitate biominerals through a variety of pathways that influence the geochemical composition of teeth.

Arthropods commonly precipitate calcium carbonate shells and sometimes more exotic materials with the aid of amorphous precursors, mineral impurities, and proteins to speed the mineralization process (Simmer *et al.*, 2012; Wang *et al.*, 2013; De Yoreo *et al.*, 2015). Amorphous mineral precursors and intermediates allow early particle formation at lower ion concentrations and with reduced activation costs before the eventual formation of crystalline mineral (Wang *et al.*, 2013; De Yoreo *et al.*, 2015). Recently these processes have been observed in mammals, alongside repeated, pH-mediated dissolution and reprecipitation of the maturing enamel (Beniash *et al.*, 2009; Damkier *et al.*, 2014). These mineralization processes may improve material performance (Bentov *et al.*, 2016). Importantly, they are also likely to influence isotopic compositions as mineral structure evolves over time, and continues interacting with changing body chemistry (Giuffre *et al.*, 2014; De Yoreo *et al.*, 2015).

Another obstacle to reconstructing rainfall seasonality using Passey *et al.* (2005)'s approach is the complexity of linking herbivore tooth $\delta^{18}O$ values to landscape hydrology. Passey *et al.* (2005) and other experimental large animal projects have focused on tooth carbonate $\delta^{13}C$ values that more clearly reflect browsing and grazing on C3 or C4 plants, but whose relationship to seasonal rainfall patterns may be tenuous (Ayliffe *et al.*, 2004; Cerling *et al.*, 2007; Zazzo *et al.*, 2010). A series of more or less complex models are available that predict blood (and ultimately tooth) $\delta^{18}O$ values from environmental sources, but it is unclear which are appropriate for paleoecological reconstruction (Luz *et al.*, 1984; Kohn 1996; Podlesak *et al.*, 2008). In addition to the complexity of animal physiology, understanding the impact of animal behavior on blood $\delta^{18}O$ values may be an even more vexing problem (Kohn *et al.*, 1998). To complicate matters further, the ‰ offset between blood and tooth phosphate $\delta^{18}O$ values is poorly constrained in mammals (Longinelli

and Nuti, 1973; Lecuyer *et al.*, 2013; Chang and Blake, 2015). Few studies have recorded the changes and variation in $\delta^{18}O$ values from environmental sources through the blood and into teeth, and none have done so for large herbivores in a controlled setting (Luz *et al.*, 1984; Podlesak *et al.*, 2008; Balasse *et al.*, 2012). Such an experiment is vital to efforts to make meaningful statements about environmental seasonality from body oxygen values.

1.5 Approach

This thesis approaches the reconstruction of past seasonality using a combination of modeling, experimental, and computational approaches focused on $\delta^{18}O$ values in large herbivores. This approach develops or adopts mathematical models that approximate each of the many steps that link seasonal climatic and environmental $\delta^{18}O$ chemistry to transformations in animal blood $\delta^{18}O$, and final tooth $\delta^{18}O$ values and spatial patterns. These models are often described as "forward" models because they recreate the chemical changes that occur moving from the environment forward to blood and finally teeth, which are abundant at fossil and archaeological sites. Experimentation with sheep, large domesticated herbivores whose tooth morphology and digestive physiology resemble the bovids that dominate fossil assemblages of the Cenozoic, produces data that evaluates and refines these models, bringing them closer to the processes in nature they attempt to describe. Lastly, computational methods make use of forward models and $\delta^{18}O$ data collected from teeth to move backwards from teeth to original, seasonally varying blood and environmental water $\delta^{18}O$ histories. These methods are often described as "inverse" methods because they take final products, like tooth $\delta^{18}O$ values, and move backwards in time to estimate the original water $\delta^{18}O$ histories that produced them.

The second chapter in this thesis resolves longstanding uncertainty in the process of mineralization using synchrotron x-ray based density measurements from the developing first and second molars of 45 Dorset sheep that died at known ages. I assume that within any given sheep population, a pattern of mineralization exists that is approximated, with variation, among all individuals. Density measurements from these individuals, for all tooth locations, are combined to produce an estimate of the average mineralization pattern, and the variation in the pattern typical for the population. This chapter documents significant inter-individual variability in tooth morphology and maturation geometry. It also demonstrates that an overall spatial and temporal pattern of maturation emerges from the entire dataset, and reconciles a number of previous and contradictory theories of mineralization.

The third chapter reports the results of an experiment in a population of Dorset sheep, where changing blood $\delta^{18}O$ values are measured as drinking water, feed and air are controlled and experimentally altered. The results are used to evaluate and improve existing models that predict blood $\delta^{18}O$ from environmental sources, and also reveal substantial variation within and between individuals over time. Relatively rapid body water turnover in this population is situated within the context of observations in other taxa.

The fourth chapter integrates the models created and refined in the second and third chapters to reconstruct drinking water $\delta^{18}O$ histories from tooth $\delta^{18}O$ values. To accomplish this, data are collected from a tooth at very high resolution, and assembled into a tooth $\delta^{18}O$ map. Hypothetical environmental water $\delta^{18}O$ histories are then iteratively proposed, and combined with mineralization and blood oxygen modeling to construct "forward" modeled tooth $\delta^{18}O$

maps. These maps are compared to real tooth data until modeled and data maps converge. Known water intake history in our experimental animal demonstrates that this method can quantitatively reconstruct drinking water $\delta^{18}O$ intake history from tooth isotope measurements. Computational methods for improving convergence speed and reconstruction accuracy are discussed. I also explore how increased sample resolution would or would not be expected to improve reconstruction of seasonal $\delta^{18}O$ detail and magnitude in the context of different global rainfall regimes.

Despite having relatively little variation in seasonal meteoric (rainfall) water $\delta^{18}O$ values, east African sites of past hominin occupation contain a great range of available water and vegetation sources that are reflected in herbivore tooth values from the past and present (Fig. 1.3) (Levin *et al.*, 2009; Bowen 2010; Quinn 2015). The diversity of these resources available to savanna fauna increases the likelihood that seasonal variations, relevant to human habitats and behavior, may be preserved and reconstructed. In the conclusion of this work, I discuss how methods presented here can be applied to data collected from fossil herbivore teeth to reconstruct patterns of seasonal behavior and hydrology at prehistoric sites of human occupation.

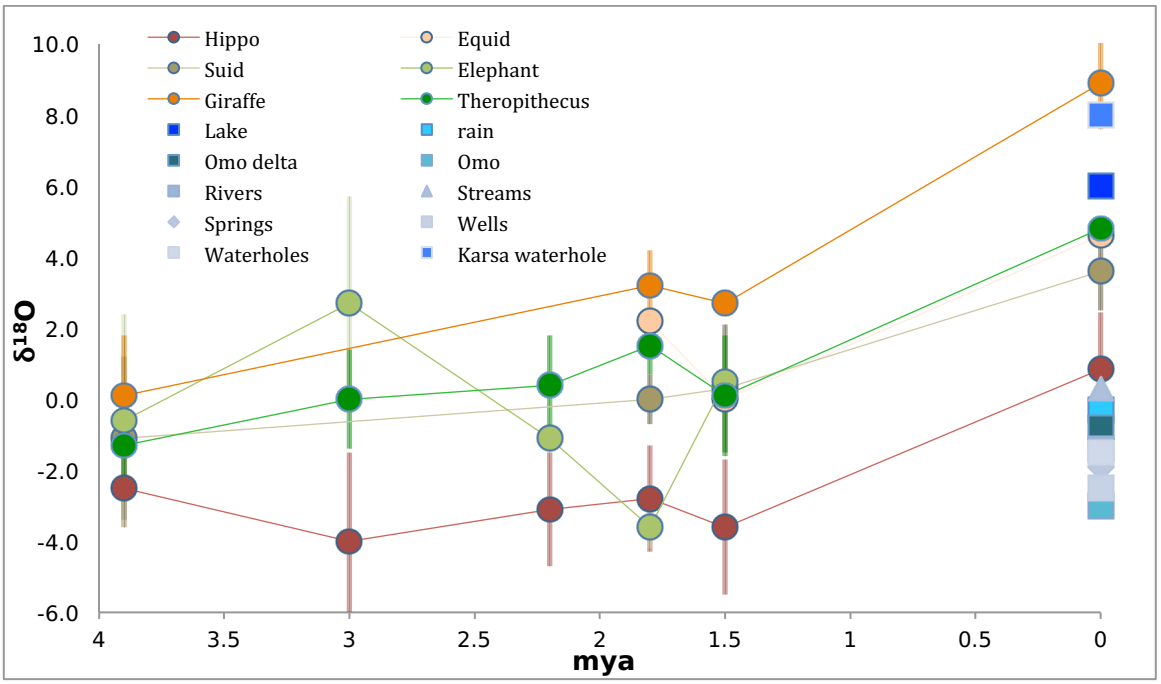

Figure 1.3: Oxygen isotope values of contemporary water sources (blue, Vienna Standard Mean Ocean Water (VSMOW) scale) and large herbivore tooth carbonate values (other colors, Vienna Pee Dee Belemnite (VPDB) scale) in the Turkana Basin over the Plio-Pleistocene. Data from Quinn (2015).

1.6 References

Aiello LC, Wheeler P (1995) The expensive-tissue hypothesis: the brain and the digestive system in human and primate evolution. Current anthropology. 36(2):199-221.

Ambrose, S. H., 2006. "A tool for all seasons." Science vol.314 pp.930

Antón SC, Potts R, Aiello LC (2014) Evolution of early Homo: An integrated biological perspective. *Science* 345:1236828.

Archibald S, Staver AC, Levin SA (2012) Evolution of human-driven fire regimes in Africa. Proceedings of the National Academy of Sciences. 109(3):847-52.

Balasse M, Smith AB, Ambrose SH, Leigh SR (2003) Determining sheep birth seasonality by analysis of tooth enamel oxygen isotope ratios: the Late Stone Age site of Kasteelberg (South Africa). Journal of Archaeological Science. 30(2):205-15.

Balasse, M., Obein, G., Ughetto-Monfrin, J., and I. Mainland, 2011. "Investigating seasonality and season of birth in past herds: a reference set of sheep enamel stable isotope oxygen ratios." Archaeometry, vol.54, no.2, pp.349-368.

Beniash E, Metzler RA, Lam RS, Gilbert PU (2009) Transient amorphous calcium phosphate in forming enamel. Journal of structural biology. 166(2):133-43.

Bird, R. B. and D. W. Bird. "Human hunting seasonality." In, "Seasonality in Primates: Studies of Living and Extinct Human and Non-Human Primates." Eds. Brockman, D. K. and C. P. Van Schaik. Cambridge University Press, Cambridge 2005.

Blois, J. L. and Hadly, E. A., 2009. "Mammalian response to Cenozoic climate change." Annual Reviews in Earth and Planetary Sciences, vol.37 pp.181-208.

Blumenthal S, Cerling T, Chritz K, Bromage T, Kozdon R, Valley J (2014) Stable isotope time-series in mammalian teeth: In situ δ18O from the innermost enamel layer. *Geochim Cosmochim Acta* 124:223236.

Brown DM, Brenneman RA, Koepfli KP, Pollinger JP, Milá B, Georgiadis NJ, Louis EE, Grether GF, Jacobs DK, Wayne RK (2007) Extensive population genetic structure in the giraffe. BMC biology. 5(1):1.

Brunet M, Guy F, Pilbeam D, Lieberman DE, Likius A, Mackaye HT, de Leon MS, Zollikofer CP, Vignaud P (2005) New material of the earliest hominid from the Upper Miocene of Chad. Nature. 434(7034):752-5.

Bobe, R., 2011, "Fossil mammals and paleoenvironments in the Omo-Turkana Basin," Evolutionary Anthropology, vol.20 pp.254-263.

Bobe, Rene and Leakey, Meave G., "Ecology of Plio-Pleistocene Mammals in the Omo-Turkana Basin and the Emergence of Homo." In Grine, F. E., Fleagle, J. G. and Leakey, R. E., Eds., "The First Humans – Origin and Early Evolution of the Genus Homo," pp.173-184, Springer, 2009.

Bonnefille R. Cenozoic vegetation, climate changes and hominid evolution in tropical Africa (2010) Global and Planetary Change. 72(4):390-411.

Bowen, G., 2010. "Isoscapes: spatial pattern in isotopic biogeochemistry." Annual Review of Earth and Planetary Sciences, vol.38 pp.161-87.

Breecker DO, Sharp ZD, McFadden LD (2009) Seasonal bias in the formation and stable isotopic composition of pedogenic carbonate in modern soils from central New Mexico, USA. Geological Society of America Bulletin. 121(3-4):630-40.

Bryant JD, Froelich PN, Showers WJ, Genna BJ (1996) A tale of two quarries: biologic and taphonomic signatures in the oxygen isotope composition of tooth enamel phosphate from modern and Miocene equids. Palaios. 1:397-408.

Cerling, T.E., Ayliffe, L. K., Dearing, M. D., Ehleringer, J. R., Passey, B. H., Podlesak, D. W., Torregrossa, A.- M., West, A G., 2007. "Determining biological tissue turnover using stable isotopes: the reaction progress variable." Oecologia, vol.151 pp.175–189.

Cerling, T. E., Wynn, J. G., Andanje, S. A., Bird, M. I., Korir, D. K., Levin, N. E., Mace, W., Macharia, A. N., Quade, J. and C. H. Remien, 2011. "Woody cover and hominin environments in the past 6 million years." Nature, vol.476 pp.51-57.

Cerling, T.E., Mbua, E., Kirera, F. M., Manthi, F. K., Grine, F. E., Leakey, M. G., Sponheimer, M., Uno, K. T., 2011. "Diet of Paranthropus boisei in the early Pleistocene of East Africa." Proceedings of the National Academy of Sciences, vol.108 no.23 pp.9337-9341.

Cerling TE, Manthi FK, Mbua EN, Leakey LN, Leakey MG, Leakey RE, Brown FH, Grine FE, Hart JA, Kaleme P, Roche H (2013) Stable isotope-based diet reconstructions of Turkana Basin hominins. Proceedings of the National Academy of Sciences. 110(26):10501-6.

Cerling TE, Brown FH, Wynn JG (2014) On the environment of Aramis. Current Anthropology. 55(4):469-70.

Cerling TE, Brown FH, Wynn JG (2015) On the environment of Aramis: concerning comment and replies of August 2014. Current Anthropology. 56(3):445-6.

Chang SJ, Blake RE (2015) Precise calibration of equilibrium oxygen isotope fractionations between dissolved phosphate and water from 3 to 37 C. Geochimica et Cosmochimica Acta. 150:314-29.

Damkier HH, Josephsen K, Takano Y, Zahn D, Fejerskov O, Frische S (2014) Fluctuations in surface pH of maturing rat incisor enamel are a result of cycles of H+-secretion by ameloblasts and variations in enamel buffer characteristics. Bone. 60:227-34.

Darwin Charles R. On the origin of species by means of natural selection, or the preservation of favoured races in the struggle for life. Murray, London. 1859.

deMenocal PB (2004) African climate change and faunal evolution during the Pliocene–Pleistocene. Earth and Planetary Science Letters. 220(1-2):3-24.

De Yoreo JJ, Gilbert PU, Sommerdijk NA, Penn RL, Whitelam S, Joester D, Zhang H, Rimer JD, Navrotsky A, Banfield JF, Wallace AF (2015) Crystallization by particle attachment in synthetic, biogenic, and geologic environments. Science. 349(6247):aaa6760.

Domínguez-Rodrigo M (2014) Is the "savanna hypothesis" a dead concept for explaining the emergence of the earliest hominins?. Current Anthropology. 55(1):59-81.

Dunbar RI, Shultz S (2007) Evolution in the social brain. Science. 317(5843):1344-7.

Ellison, P. T., Valeggia, C. R., and D. S. Sherry, "Human Birth Seasonality." In, "Seasonality in Primates: Studies of Living and Extinct Human and Non-Human Primates." Eds. Brockman, D. K. and C. P. Van Schaik. Cambridge University Press, Cambridge 2005.

Elton S (2008) The environmental context of human evolutionary history in Eurasia and Africa. Journal of Anatomy. 212(4):377-93.

Eronen JT, Polly PD, Fred M, Damuth J, Frank DC, Mosbrugger V, Scheidegger C, Stenseth NC, Fortelius M (2010) Ecometrics: the traits that bind the past and present together. Integrative zoology. 5(2):88-101.

Eronen JT, Puolamäki K, Liu L, Lintulaakso K, Damuth J, Janis C, Fortelius M (2010) Precipitation and large herbivorous mammals I: estimates from present-day communities. Evolutionary Ecology Research. 12(2):217-33.

Feakins SJ, Levin NE, Liddy HM, Sieracki A, Eglinton TI, Bonnefille R (2013) Northeast African vegetation change over 12 my. Geology. 41(3):295-8.

Feibel CS (2011) A geological history of the Turkana Basin. Evolutionary Anthropology: Issues, News, and Reviews. 20(6):206-16.

Fennessy J, Bidon T, Reuss F, Kumar V, Elkan P, Nilsson MA, Vamberger M, Fritz U, Janke A (2016) Multi-locus Analyses Reveal Four Giraffe Species Instead of One. Current Biology. 26(18):2543-9.

Foley, R. A., "The influence of seasonality on hominid evolution," In Ulijazek, S. J. and S. S. Strickland, "Seasonality and human ecology: 35th symposium volume of the Society for the Study of Human Biology." Cambridge University Press, New York: 1993.

Fortelius M, Eronen JT, Kaya F, Tang H, Raia P, Puolamäki K (2014) Evolution of Neogene mammals in Eurasia: environmental forcing and biotic interactions. Annual Review of Earth and Planetary Sciences. 42:579-604.

Fortelius M, Žliobaitė I, Kaya F, Bibi F, Bobe R, Leakey L, Leakey M, Patterson D, Rannikko J, Werdelin L (2016) An ecometric analysis of the fossil mammal record of the Turkana Basin. Phil. Trans. R. Soc. B. 371(1698):20150232.

Fricke HC, Clyde WC, O'Neil JR (1998) Intra-tooth variations in δ18O (PO4) of mammalian tooth enamel as a record of seasonal variations in continental climate variables. Geochimica et Cosmochimica Acta. 62(11):1839-50.

Friedman I, O'Neil JR. Data of geochemistry: Compilation of stable isotope fractionation factors of geochemical interest. US Government Printing Office; 1977.

Garcia RA, Cabeza M, Rahbek C, Araújo MB (2014) Multiple dimensions of climate change and their implications for biodiversity. *Science* 344:1247579.

Giuffre AJ, Gagnon AC, De Yoreo JJ, Dove PM (2015) Isotopic tracer evidence for the amorphous calcium carbonate to calcite transformation by dissolution–reprecipitation. Geochimica et Cosmochimica Acta. 165:407-17.

Good SP, Caylor KK (2011) Climatological determinants of woody cover in Africa. *Proc Natl Acad Sci USA* 108:4902-4907.

Harmand S, Lewis JE, Feibel CS, Lepre CJ, Prat S, Lenoble A, Boës X, Quinn RL, Brenet M, Arroyo A, Taylor N (2015) 3.3-million-year-old stone tools from Lomekwi 3, West Turkana, Kenya. Nature. 521(7552):310-5.

Hoetzel S, Dupont L, Schefuß E, Rommerskirchen F, Wefer G (2013) The role of fire in Miocene to Pliocene C4 grassland and ecosystem evolution. *Nat Geosci* 6:1027-1030.

Hoppe KA, Stover SM, Pascoe JR, Amundson R (2004) Tooth biomineralization in horses: implications for isotopic microsampling. *Palaeogeogr, Palaeoclim, Palaeoecology* 206:355–365.

Isler K, Van Schaik CP (2014) How Humans Evolved Large Brains: Comparative Evidence. *Ev Anthr* 23:65-75.

Janmaat KR, Boesch C, Byrne R, Chapman CA, Bi G, Zoro B, Head JS, Robbins MM, Wrangham RW, Polansky L (2016) Spatio-temporal complexity of chimpanzee food: How cognitive adaptations can counteract the ephemeral nature of ripe fruit. American journal of primatology.

Joordens, J. C. A., Vonhof, H. B., Feibel, C. S., Lourens, L. J., Dupont-Nivet, G., van der Lubbe, J. H. J. L., Sier, M. J., Davies, G. R., Kroon, D., 2011. "An astronomically tuned climate framework for hominins in the Turkana Basin." Earth and Planetary Sciences vol.307 pp.1-8.

Kierdorf, H., Witzel, C., Upex, B., Dobney, K. and U. Kierdorf, 2012. "Enamel hypoplasia in molars of sheep and goats, and its relationship to the pattern of tooth growth." Journal of Anatomy, vol.220 pp.484-495.

Kierdorf H, Kierdorf U, Frölich K, Witzel C (2013) Lines of evidence–incremental markings in molar enamel of Soay sheep as revealed by a fluorochrome labeling and backscattered electron imaging study. PloS one. 8(9):e74597.

Kimbel, W. H., C. A. Lockwood, et al. 2006. "Was Australopithecus anamensis ancestral to A. afarensis? A case of anagenesis in the hominin fossil record." Journal of Human Evolution 51(2): 134-152.

Kingston, J. D., 2007. "Shifting adaptive landscapes: progress and challenges in reconstructing early hominid environments." American Journal of Physical Anthropology vol.134 iss.S45 pp.20

Kohn MJ (1996) Predicting animal δ18O: accounting for diet and physiological adaptation. *Geochimica et Cosmochimica Acta.* 60(23):4811-29.

Kohn MJ, Schoeninger MJ, Valley JW (1998) Variability in oxygen isotope compositions of herbivore teeth: reflections of seasonality or developmental physiology? *Chem Geo* 152:97.

Kohn M (2004) Comment: Tooth Enamel Mineralization in Ungulates: Implications for Recovering a Primary Isotopic Time-Series, by B. H. Passey and T. E. Cerling (2002). *Geochim Cosmochim Acta* 68:403405.

Leakey M, Grossman A, Gutiérrez M, Fleagle JG (2011) Faunal change in the Turkana Basin during the late Oligocene and Miocene. Evolutionary Anthropology: Issues, News, and Reviews. 20(6):238-53.

Lécuyer C, Amiot R, Touzeau A, Trotter J. Calibration of the phosphate δ18O thermometer with carbonate–water oxygen isotope fractionation equations (2013) Chemical Geology. 347:217-26.

Levin NE, Zipser EJ, Cerling TE (2009) Isotopic composition of waters from Ethiopia and Kenya: insights into moisture sources for eastern Africa. Journal of Geophysical Research: Atmospheres. 114(D23).

Levin, N. E., Brown, F. H., Behrensmeyer, A. K., Bobe, R. and T. E. Cerling, 2011. "Paleosol carbonates from the Omo Group: Isotopic records of local and regional environmental change in East Africa." Paleogeography, Paleoclimatology, Paleoecology, vol.307 pp.75-89

Levin NE (2015) Environment and climate of early human evolution. Annual Review of Earth and Planetary Sciences. 43:405-29.

Liao WB, Lou SL, Zeng Y, Kotrschal A (2016) Large Brains, Small Guts: The Expensive Tissue Hypothesis Supported within Anurans. The American Naturalist. 188(6):000-.

Lieberman, D.E., Pilbeam, D. R. and R. W. Wrangham, "The transition from Australopithecus to Homo." In Shea, J. J. and D. E. Lieberman, Eds., "Transitions in Prehistory: Essays in honor of Ofer Bar-Yosef." American School of Prehistory Research, Oxbow Books, United States: 2009.

Liu L, Puolamäki K, Eronen JT, Ataabadi MM, Hernesniemi E, Fortelius M (2012) Dental functional traits of mammals resolve productivity in terrestrial ecosystems past and present. Proceedings of the Royal Society of London B: Biological Sciences. rspb20120211.

Longinelli A, Nuti S. Revised phosphate-water isotopic temperature scale (1973) Earth and Planetary Science Letters. 19(3):373-6.

Lorenzen ED, Heller R, Siegismund HR (2012) Comparative phylogeography of African savannah ungulates. Molecular Ecology. 21(15):3656-70.

Luz B, Kolodny Y, and Horowitz M (1984) Fractionation of oxygen isotopes between mammalian bone-phosphate and environmental drinking water. *Geochimica et Cosmochimica Acta*. 48:1689-93.

Magill CR, Ashley GM, Domínguez-Rodrigo M, Freeman KH (2016) Dietary options and behavior suggested by plant biomarker evidence in an early human habitat. Proceedings of the National Academy of Sciences. p.201507055.

Mander L, Li M, Mio W, Fowlkes CC, Punyasena SW (2013) Classification of grass pollen through the quantitative analysis of surface ornamentation and texture. Proceedings of the Royal Society of London B: Biological Sciences. 280(1770):20131905.

Marshall AJ, Wrangham RW (2007) Evolutionary consequences of fallback foods. *Int J Prim* 28:1219-1235.

Mayer AL, Khalyani AH (2011) Grass trumps trees with fire. Science, 334:188-189.

McPherron, S. P., Alemseged, Z., Marean, C., Wynn, J. W., Reed, D., Bobe, R., and H. Bearat, 2011. "Tool-marked bones from before the Oldowan change the paradigm." Proceedings of the National Academy of Sciences, vol.108, no.21, p.E116.

Melin AD, Young HC, Mosdossy KN, Fedigan LM (2014) Seasonality, extractive foraging and the evolution of primate sensorimotor intelligence. *J Hum Ev* 71:77-86.

Milton K (1988) Foraging behaviour and the evolution of primate intelligence. R. Byrne & A. Whiten (Eds.), Machiavellian intelligence: Social expertise and the evolution of intellect in monkeys, apes, and humans. Oxford University Press.

Morin CW, Comrie AC (2010) Modeled response of West Nile virus vector *C. quinquefasciatus* to climate using dynamic mosquito simulation. *Int J Biometeor.* 54:517-529.

Owen-Smith NO, Mason DR (2005) Comparative changes in adult vs. juvenile survival affecting population trends of African ungulates. Journal of Animal Ecology. 74(4):762-73.

Passey BH, Cerling TE (2002) Tooth enamel mineralization in ungulates: implications for recovering a primary isotopic time-series. *Geochim Cosmochim Acta* 66:3225-3234.

Passey B, Cerling T, Schuster G, Robinson T, Roeder B, Krueger S (2005) Inverse methods for estimating primary input signals from time-averaged isotope profiles. *Geochim Cosmochim Acta* 69:4101-4116.

Podlesak DW, Torregrossa AM, Ehleringer JR, Dearing MD, Passey BH, Cerling TE (2008) Turnover of oxygen and hydrogen isotopes in the body water, CO 2, hair, and enamel of a small mammal. *Geochim Cosmochim Acta*, *72*:19-35.

Pontzer H, Raichlen DA, Sockol MD (2009) The metabolic cost of walking in humans, chimpanzees, and early hominins. Journal of Human Evolution. 56(1):43-54.

Potts R (2013) Hominin evolution in settings of strong environmental variability. *Quat Science Rev* 73:1-13.

Quinn RL (2015) Influence of Plio-Pleistocene basin hydrology on the Turkana hominin enamel carbonate δ18O values. Journal of human evolution. 86:13-31.

Roche D, Ségalen L, Senut B, Pickford M (2013) Stable isotope analyses of tooth enamel carbonate of large herbivores from the Tugen Hills deposits: Palaeoenvironmental context of the earliest Kenyan hominids. Earth and Planetary Science Letters. 381:39-51.

Rundell RJ, Price TD (2009) Adaptive radiation, nonadaptive radiation, ecological speciation and nonecological speciation. Trends in Ecology & Evolution. 24(7):394-9.

Simmer J, Richardson A, Hu Y-Y, Smith C, Hu J (2012) A post-classical theory of enamel biomineralization… and why we need one. *Int J Oral Sci* 4:129–134.

Smith, T. M. and Tafforeau, P. 2008 "New Visions of Dental Tissue Research: Tooth Development, Chemistry and Structure." Evolutionary Anthropology, v.17 pp.213-226.

Sockol, M. D., Raichlen, D. A., and H. Pontzer, 2007, "Chimpanzee locomotor energetic and the origin of human bipedalism." Proceedings of the National Academy of Sciences, vol.104 no.30 pp.12265-12269.

Sponheimer M, Passey B H, de Ruiter D J, Guatelli-Steinberg D, *et al.* (2006) Isotopic Evidence for Dietary Variability in the Early Hominin P. robustus. *Science* 314:980-982.

Sponheimer M, Alemseged Z, Cerling TE, Grine FE, Kimbel WH, Leakey MG, Lee-Thorp JA, Manthi FK, Reed KE, Wood BA, Wynn JG (2013) Isotopic evidence of early hominin diets. Proceedings of the National Academy of Sciences. 110(26):10513-8.

Strömberg CA (2011) Evolution of grasses and grassland ecosystems. Annual Review of Earth and Planetary Sciences. 39:517-44.

Suga S 1982. Progressive mineralization pattern of developing enamel during the maturation stage. *J Dent Res* 1532-1542.

Suga, S., 1989. "Enamel Hypmineralization Views From the Pattern of Progressive Mineralization of Human ad Monkey Developing Enamel." Advances in Dental Research v.3 pp.188-198.

Suwa G, Ambrose SH (2014) Reply to Cerling et al. Current Anthropology. 55(4):473-4.

Tafforeau, P., Bentaleb, I., Jaeger, J-J., Martin, C., 2007 "Nature of laminations and mineralization in rhinoceros enamel using histology and X-ray synchrotron microtomography: Potential implications for paleoenvironmental isotopic studies." Paleogeography, Paleoclimatology, Paleoecology v.246 pp.206- 227.

Taylor and Kohn 2016, GCA.

Tebbich S, Taborsky M, Fessl B, Dvorak M, Winkler H (2004) Feeding behavior of four arboreal Darwin's finches: adaptations to spatial and seasonal variability. The Condor. 106(1):95-105.

Tebbich S, Irmgard T, Erica C, Sophia S (2012) Use of a barbed tool by an adult and a juvenile woodpecker finch (Cactospiza pallida). Behavioural processes. 89(2):166-71.

Thomassen HA, Freedman AH, Brown DM, Buermann W, Jacobs DK (2013) Regional differences in seasonal timing of rainfall discriminate between genetically distinct East African giraffe taxa. PloS one. 8(10):e77191.

Ungar, P. S., et al. (2006) "Dental microwear and diets of African early Homo." Journal of Human Evolution v.50 pp.78-95

Ungar PS, Grine FE, Teaford MF, 2008. "Dental Microwear and Diet of the Plio-Pleistocene Hominin Paranthropus boisei." PLoS ONE 3(4): e2044.

Ungar PS, Sponheimer M (2011) The diets of early hominins. Science. 334(6053):190-3.

Uno, K. T., Cerling, T. E., Harris, J. M., Kunimatsu, Y., Leakey, M. G., Nakatsukasa, M. and H. Nakaya, 2011. "Late Miocene to Pliocene carbon isotope record of differential diet change among East African herbivores." Proceedings of the National Academy of Sciences, vol.108 pp.6509-6514.

Vincens A, Garcin Y, Buchet G (2007) Influence of rainfall seasonality on African vegetation in the Late Quaternary: pollen evidence, Lake Masoko, Tanzania. *J Biogeogr* 34:1274-1288.

Vrba ES. Role of environmental stimuli in hominid origins. Handbook of paleoanthropology. 2015:1837-86.

Wang Q, Nemoto M, Li D, Weaver JC, Weden B, Stegemeier J, Bozhilov KN, Wood LR, Milliron GW, Kim CS, DiMasi E (2013) Phase transformations and structural developments in the radular teeth of Cryptochiton stelleri. Advanced Functional Materials. 23(23):2908-17.

Watson JE, Iwamura T, Butt N (2013) Mapping vulnerability and conservation adaptation strategies under climate change. *Nat Clim Change* 3:989-994.

White TD, Ambrose SH, Suwa G, Su DF, DeGusta D, Bernor RL, Boisserie JR, Brunet M, Delson E, Frost S, Garcia N (2009) Macrovertebrate paleontology and the Pliocene habitat of Ardipithecus ramidus. *Science* 326(5949):67-93.

WoldeGabriel G, Ambrose SH, Barboni D, Bonnefille R, Bremond L, Currie B, DeGusta D, Hart WK, Murray AM, Renne PR, Jolly-Saad MC (2009) The geological, isotopic, botanical, invertebrate, and lower vertebrate surroundings of Ardipithecus ramidus. Science. 326(5949):65-e5.

Wynn, J. G. 2004. "Influence of Plio-Pleistocene Aridification on Human Evolution: Evidence from Paleosols of the Turkana Basin, Kenya." American Journal of PaleoAnthropology, vol.123 pp.106-118.

Wynn JG, Sponheimer M, Kimbel WH, Alemseged Z, Reed K, Bedaso ZK, Wilson JN (2013). Diet of Australopithecus afarensis from the Pliocene Hadar formation, Ethiopia. Proceedings of the National Academy of Sciences. 110(26):10495-500.

Zazzo A, Balasse M, Passey B, Moloney A, Monahan F, Schmidt O (2010) The isotope record of short- and long-term dietary changes in sheep tooth enamel: Implications for quantitative reconstruction of paleodiets. *Geochim Cosmochim Acta* 74:3571-3586.

Zazzo A, Bendrey R, Vella D, Moloney A, Monahan F, Schmidt O (2012) Refined sampling strategy for intra-tooth stable isotope analysis of enamel. *Geochim Cosmochim Acta* 84:113.

Žliobaitė I, Rinne J, Tóth AB, Mechenich M, Liu L, Behrensmeyer AK, Fortelius M (2016) Herbivore teeth predict climatic limits in Kenyan ecosystems. Proceedings of the National Academy of Sciences. 201609409.

2

High-resolution synchrotron imaging and Markov Chain Monte Carlo reveal tooth mineralization patterns

2.1 Abstract

The incremental character of tooth formation is critical to enamel integrity, oral health, and can help reconstruct life history, diet, and even seasonal climate. Despite decades of study in diverse fields, the spatial and temporal pattern of enamel maturation is not well characterized. Here we use synchrotron x-ray microtomography and Markov Chain Monte Carlo sampling to estimate mineralization trajectories from an ontogenetic series of sheep first molars. To model mineralization, we adopt a Bayesian approach that posits a general pattern of maturation estimated via measurement, individual and population level mineral density variation over time. Dynamic tooth mineralization reconstructions demonstrate that enamel secretion and maturation waves advance at nonlinear rates with distinct geometries. While enamel secretion is ordered, maturation geometry is variable within a population. This model and methodology provide an avenue for characterizing complex tooth mineralization patterns in other taxa, and in other biomineralizing structures. Our synchrotron imaging data and model are available for possible application to multiple disciplines, including health, material science, and paleontological research.

2.2 Introduction

2.2.1 Tooth mineralization in health, material science, and evolutionary biology. Teeth form incrementally, creating microscropic features that have been a subject of study since they were first observed microscopically by van Leeuwenhoek (Hillson, 2005; Ungar, 2010). Mineralization remains a focus of research today due to its relevance to the development of material science, comparative and evolutionary biology, and contemporary health (Smith 2008; Wang *et al.*, 2013; Andra *et al.*, 2015). Mineralization defects with potentially serious consequences for oral health are estimated to affect from 2-40% of individuals in populations globally (Jälevik, 2010), and are typically identified by radiography (Huang *et al.*, 2010). In healthy teeth, layered organic and inorganic components give remarkable teeth hardness and stiffness characteristics typically superior to manufactured counterparts (Chai *et al.*, 2009; Wang *et al.*, 2013). Because mineralization impacts health through tooth structural properties (Chai *et al.*, 2009), material scientists seek to understand how mineral nucleation and subsequent growth are mediated by cell structure, protein deposition and solution composition (Weaver *et al.*, 2010). Experiments in invertebrates and mice suggest that protein-mineral interactions and amorphous to crystalline phase transitions help form dental tissues within relatively rapid timeframes (amorphous minerals consist of nanoparticles or droplets adhered into unordered solids, whereas crystalline minerals are formed by steady molecular accretion onto a single, ordered molecule) (Beniash *et al.*, 2009; Wang *et al.*, 2013; de Yoreo *et al.*, 2015). Understanding mineralization can therefore contribute to improved oral health and efforts to engineer materials that mimic natural dental mechanical properties.

Because they grow incrementally teeth also record dynamic processes in the body and environment of the animal. This is because hydroxyapatite (HAp) tooth mineral forms in equilibrium with changing blood chemistry, trapping transitory environmental, dietary and behavioral signals. Sampling teeth for trace element incorporation (e.g., lead) therefore facilitates assessment of childhood health, exposure and risk (Andra *et al.*, 2015), and aids reconstruction of individual dietary or health histories in a variety of contexts (Austin *et al.*, 2013; Humphrey 2014). Sampling of stable isotopes in teeth can yield information about seasonal changes in habitat or climate including monsoon intensity (Nelson 2007), and has been used to reconstruct seasonal contexts as diverse as recent husbandry practices (Balasse *et al.*, 2012; Zazzo *et al.*, 2012), or migration patterns in dinosaurs (Fricke *et al.*, 2011). Reconstructing the timing and magnitude of health, behavioral or environmental histories through teeth requires, however, a precise understanding of the geometry and timing of mineralization (Passey *et al.*, 2005).

2.2.2 Tooth formation and the problem of mineralization. Tooth enamel mineralization is traditionally conceptualized in two stages: secretion and maturation (Simmer *et al.*, 2012). During secretion, enamel-forming cells (ameloblasts) secrete a proteinaceous matrix that controls the formation of amorphous calcium phosphate and its transformation into ordered HAp crystallites (Beniash *et al.*, 2009; Simmer *et al.*, 2012; Diekwisch, 1998; Smith, 1998). This process begins at the interface between ameloblasts and dentin-forming cells (odontoblasts), where the future cusp will form. The secretory front advances towards

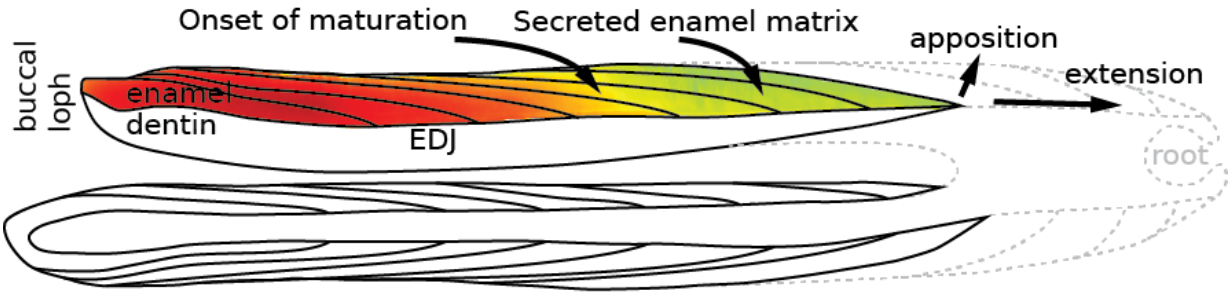

Figure 2.1 Growing sheep molar sectioned longitudinally across lingual and buccal (colored) loph. Solid lines represent formed enamel and dentin, while dotted lines depict future crown outlines. Mineralization initiates at both lingual and buccal dentin horns (left) and proceeds towards the cervix via extension and apposition until crown formation completes. Lines within enamel show incremental addition over time, and colors indicate maturation extent from low (green) to high (red).

the future enamel cervix and root by successively activating neighboring ameloblasts, a process known as extension (Fig. 2.1). Simultaneously, ameloblasts in this front add organic matrix and mineral lattice from the enamel-dentin junction (EDJ) towards the enamel surface during apposition. Secreted enamel accounts for only 20-30% of mature mineral weight (Passey and Cerling, 2002; Simmer *et al.*, 2012), and contains ordered increments marking formation time (Boyde, 1989; Smith, 2006; Smith and Tafforeau, 2008). The majority of mineral is added during maturation, a more complex and diffuse process that largely begins once ameloblasts complete secretion and the full enamel thickness is reached (Smith, 1998; Driessens and Verbeeck, 1990).

Two principle models have been proposed to explain maturation phase geometry and timing during mineralization. One model describes a series of waves of increasing mineralization moving to and from the EDJ, and is based on radiographs of primates and ungulates (Suga, 1982; Hoppe *et al.*, 2004). A more recent model proposes that an initial secretory front is followed immediately by a single maturation wave in the same geometric orientation (Passey and Cerling,

2002). This later model has been employed to estimate original body fluid isotope composition in an experimentally manipulated rabbit and in domesticated sheep (Passey *et al.*, 2005; Zazzo *et al.*, 2010). However, mineral density estimates from phosphorus concentration measurements, scanning electron microscopy and X-ray imaging of mammalian molars reveal temporal pauses between mineralization phases, and observed differences between enamel secretion and maturation geometry are not accounted for in these models (Longinelli and Padalino, 1980; Blumenthal *et al.*, 2014; Passey and Cerling, 2002; Suga, 1982; Hoppe *et al.*, 2004; Tafforeau *et al.*, 2007).

Here we aim to address longstanding uncertainty in the timing and geometry of mineralization by constructing an empirical model describing ungulate molar mineralization over time. Our model is built using quantitative monochromatic synchrotron X-ray microtomography (μCT) (Tafforeau *et al.*, 2007) and Markov Chain Monte Carlo (MCMC) methods using the molars of sheep that died between the ages of 0-1.5 years old. This sampling method allows us to construct a dynamic picture of mineralization, including secretion and maturation phases, from discrete density measurements made from different individuals. Importantly, this method captures diversity in the timing and magnitude of mineralization over time, among all individuals, and yields a model that reflects mineralization variation in nature.

Box 2.1 Definitions of Terms Used

Maturation: process of mineral density increase of the secreted mineral lattice from an initial 20-30% density. This is driven primarily by ion and protein diffusion and characterized by HAp crystal growth until mineralization is completed. Recent advances in the field of biomineralization have revised our understanding of maturation and how it may contribute to isotopic compositions within mineralized enamel (De Yoreo *et al.*, 2015). Maturation is marked by fluctuations in pH related to matrix protein removal and HAp production (Smith *et al.*, 2005; Simmer *et al.*, 2009; Hu *et al.*, 2011; Smith *et al.*, 2011; Kawasaki *et al.*, 2014). These processes may, via dissolution and reprecipitation, contribute to slower crystal growth and HAp characterized by fewer lattice defects (Damkier *et al.*, 2014; Josephson *et al.*, 2010).

Maturation onset and completion: maturation onset is here defined as the steep rise in mineral density after secretion, when enamel mineral density has achieved approximately 40% of mature levels for a given location (see Methods for more information). This definition allows maturation to be reliable identified in all synchrotron-scanned teeth. Completion is likewise defined as the achievement of approximately 85% of mature enamel mineral density for a given location; most locations continue to increase in mineral density beyond this threshold.

Mineralization: the entire process of ACP/HAp mineral deposition and maturation from the onset of secretion until the complete formation of the enamel crown.

Secretion: the initial ordered deposition of mineral and organic enamel matrix where ACP, other mineral precursors or HAp develop into a mineral lattice at 20 - 30% mature mineral density. Matrix proteins, proteases and water constitute the remaining weight %. This process is regulated by ameloblast activity, and the alignment and control of the mineral phase is achieved by concerted deposition and cleavage of the enamel matrix proteins amelogenin, ameloblastin, and enamelin, thus leading to HAp mineral formation (Catarina *et al.*, 2002; Kwak *et al.*, 2009; Pugach *et al.*, 2013; Wright *et al.*, 2009).

2.3 Methods

2.3.1 Synchrotron imaging. We dissected M1s from the mandibles of 45 Dorset sheep sourced from the Cornell Sheep Program that died of natural causes between the ages of 0-450 days. All 45 dissected teeth appeared free of significant pathology, and were stored in ethanol prior to scanning on beamline ID17 of the European Synchrotron Radiation Facility in Grenoble, France. We dissected and similarly prepared 18 M2s from the same animals. Teeth were scanned in two batches with an isotropic voxel size of 46μm, monochromatic beam set at 100keV, 60μm thick scintillator detector, and CCD FreLoN 2K14 ESRF camera. The scintillator screen detector was powder gadolinium oxysulfide (gadox) based and coupled through a lens based optical device. The ESRF camera used a Fast Readout Low Noise system (Labiche *et al.*, 2007). A propagation distance of 11 meters improved phase contrast fringes. PyHST2 reconstruction software was developed by Mirone *et al.*, (2012), and single distance phase retrieval by Paganin *et al.*, (2002) and Sanchez *et al.*, (2012). Displacement distance was half the field of view.

While polychromatic beams in conventional μCT (with a complex mixture of x-ray keV energies) can provide qualitative density estimates (Zou *et al.*, 2009; Zou *et al.*, 2011), we use synchrotron imaging because monochromatic X-ray beams (with single keV values) can quantitatively characterize hydroxyapatite densities in mineralizing ungulate teeth (Tafforeau *et al.*, 2007). For synchrotron imaging and measurement purposes, tooth composition can be assessed from variations of hydroxyapatite densities. Single distance phase retrieval in monochromatic mode can provide quantitative mineral density measurements analogous to absorption contrast data, but with improved signal to noise. Density values from attenuation

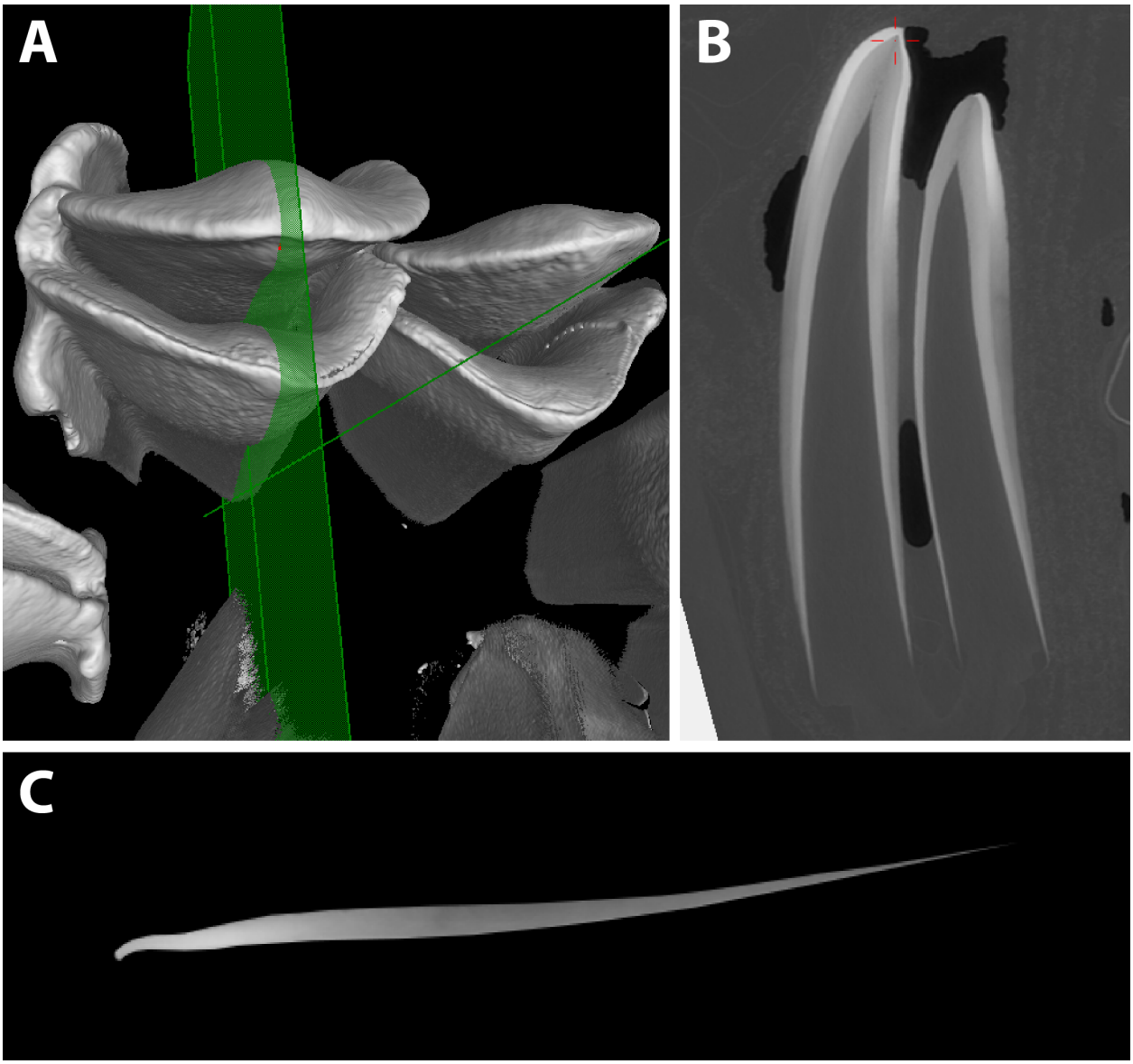

Figure 2.2 Virtual sectioning of sheep molars for model construction. **A**. A synchrotron-scanned virtual sheep tooth is sectioned along a buccal-lingual plane. **B**. The virtual section is shown in profile, with the cusp facing upward, the lingual loph to the left, and the buccal loph to the right. **C**. Buccal enamel digitally extracted, with denser mineral more brightly colored, and less mineralized enamel in grey.

coefficients were calculated in grams of hydroxyapatite per cubic centimeter following the protocol proposed by Nuzzo *et al.*, 2002 and adapted by Tafforeau *et al.*, 2007. In order to ensure measurement precision, hydroxyapatite phantoms of known densities were scanned using the

same protocol. A subset of 8 M1s were scanned on beamline ID19 with an isotropic voxel size of 13µm to better resolve the mineralization details of the innermost enamel. Beamline ID19 was used for higher resolution scans with a 13 meter propagation and a polychromatic beam with an average of 70 keV. The polychromatic beam in higher resolution scans did not allow for absolute quantitative analysis of mineral density.

We used 4998 projections of 0.5s exposure for each subscan, covering 6mm vertically, and duplicating projections with displacement to ensure homogeneous data quality and constant dynamic level. Tomographic data were reconstructed using the PyHST2 ESRF software and single distance phase retrieval, allowing density measurements from linear attenuation coefficients (Tafforeau *et al.*, 2007). Molar lophs were virtually sectioned mesio-distally with VGStudioMax 2.2 software and enamel virtually extracted from tooth sections using Photoshop 5.0 (Fig. 2.2).

2.3.2 Standardizing enamel coordinates and estimating extension. To quantitatively compare positions within different teeth, we standardized enamel spatial positions with a uniform coordinate system defined by two coordinates: distance from the dentin horn along the EDJ, and distance from the EDJ to the tooth surface (Fig. 2.3). For lightly-worn molars, the position of the dentin horn was estimated using unworn molars in the data set. HAp densities were calculated using synchrotron beam attenuation coefficients for each equivalent 46µm^2 pixel from all aligned molar sections. Due to light diffusion in the LuAG

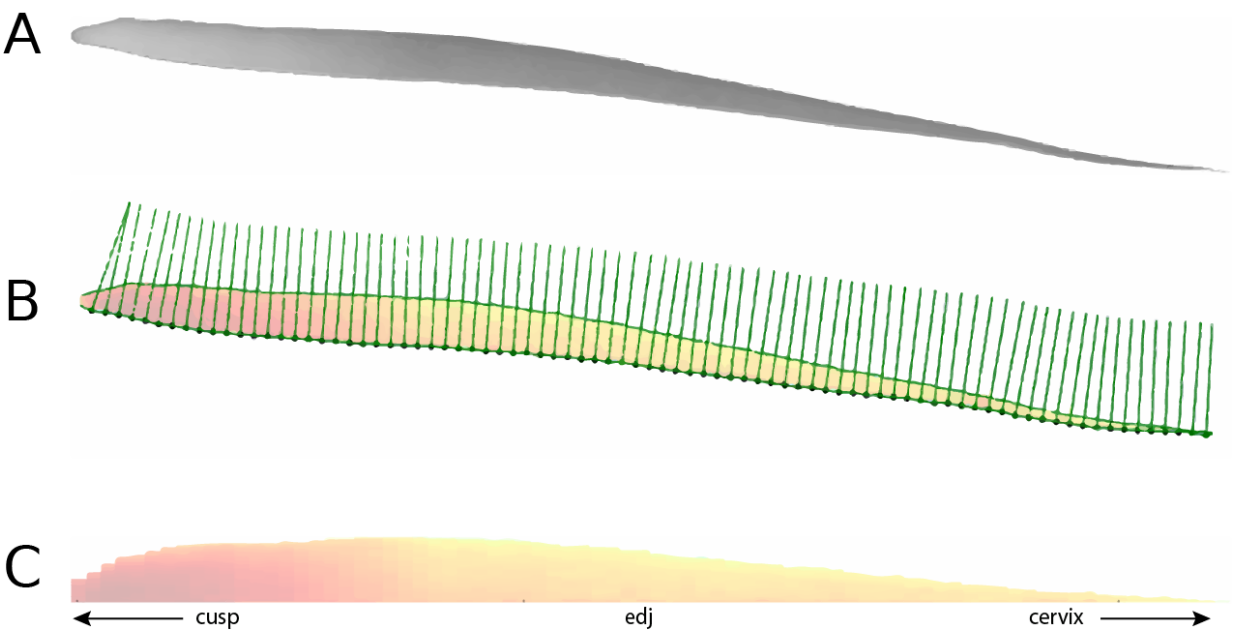

Figure 2.3 Tooth scans resampled along a coordinate system for quantitative comparison. **A.** Digital buccal enamel section virtually dissected from a M1, with dark gray representing less mineralized, and light gray more mineralized enamel. The cusp tip is leftward, EDJ is just below the lower enamel margin, and growing enamel front rightward. **B.** The section EDJ has been traced and landmarks (green circles) placed at regular intervals along it. Lines (green) along which enamel density may be sampled are drawn perpendicular to the EDJ from each landmark. Yellow represents less mineralized, and red more mineralized enamel. **C.** Resampled enamel flattened along the EDJ for comparison to other enamel sections.

and structured scintillating fiber scintillators used in the first scan, HAp density conversion attenuation coefficients were corrected to a beam energy of 119 keV instead of 100 keV, using density phantoms scanned with the same protocol. For the second set of scans, we used a powdered gadox screen scintillator better adapted for density quantification. A fit of the data of the first scans was calculated based on those of the second experiment to retrieve quantitative measurement for the whole dataset. Pixel grey values (Px) were converted to HAp densities (ρ) using the equations $\rho = 6.9 \times 10^{-5} Px + 1.54$ and $\rho = 2.8 \times 10^{-4} Px + 1.49$ for the first and second scans, respectively.

We used the length of each enamel section (extension length) and the age-at-death of each animal to calculate age as a sigmoid error function of enamel extension over time for the entire data set. When estimating extension curves, Gaussian rather than exponential or logistic functions were chosen based upon indications that highest extension rates are observed shortly after initiation (Jordana and Köhler, 2011; Zazzo *et al.*, 2012; Kierdorf *et al.*, 2013). Fitting parameters of amplitude *a*, slope *s* and offset *o*, we used this function to re-assign size-modeled ages t_m to each section as a function of its extension length e_l, according to the equation

$$t_m = \frac{erf^{-1}((a + e_l - e_{lmax})/a) + (o * s)}{s} \qquad \text{(eq. 2.1)}$$

where erf^{-1} is the inverse error function, and e_{lmax} is the maximum length of the tooth when mature. Fitting of *a*, *o* and *s* for extension, maturation onset and completion was conducted using the NLopt module for python, implementing the Multi-Level Single-Linkage (MLSL) and Constrained Optimization BY Linear Approximations (COBYLA) algorithms for global and local optimization, respectively (Powell 1998; Kucherenko and Sytsko, 2005). Similar fitting curves were used to describe the average progress of maturation onset and completion in the enamel crown. Onset and completion of maturation were defined as the estimated attainment of 40% and 85% HAp density midway between the EDJ and enamel surface, relative to the maximum measured density of 2.62g/cm^3 midway from the EDJ to the enamel surface. This is because mineralization data demonstrate that while trajectories are variable, all locations are either entering maturation phase with steep increases in mineral density (maturation onset), or leaving

it with declines in mineral addition rate (maturation completion), at approximately 40% and 85% densities.

We used the M1 of a sheep that died at 21 days of age to determine initiation timing. We sectioned the M1 using a Buehler Isomet Saw, polished the section to a thickness of 100 microns, and identified the birth line with light microscopy on a BX51 polarized light microscope. We measured 10.435mm of enamel extension from initiation to birth, and 4.415mm from birth until death 21 days later. Taking the 210μm/day average extension rate after birth and extrapolating over 10.435mm of prenatal extension, initiation was estimated at 50 days prior to birth. We independently estimated initiation from the same M1 by synchrotron scanning the thin section with phase contrast, and counting daily laminations in the resulting digital volume from initiation to birth, and from birth until death. Using this method, we estimated 48 laminations altogether prior to birth. We therefore choose an average M1 initiation value of 49 days prior to birth, between the two estimates. Second molar initiation was extrapolated from dissected M2 germs as approximately 86 days after birth, based on an examination of individuals near in age to the event of initial M2 calcification (Table 2.1).

Specimen	Age (days)	M2 present?
cxb11193	58	No
Finn3830	72	No
cxb10864	84	No
cxb11187	88	Yes
cxb10939	92	Yes
cxb10845	97	Yes

Table 2.1 Sheep second molar tooth germ presence or absence as determined by dissection of mandibles from animals that died at different ages (days after birth).

Incorporating histological estimates of -49 and 86 days relative to birth for M1 and M2 initiation as priors, we estimated most probable extension curve parameters by maximizing:

$$P\left(l_t^m \middle| l_t^d\right) = \frac{1}{\sqrt{2\pi\sigma^2}} \prod_t e^{\left(-\frac{\left(l_t^m - l_t^d\right)^2}{2\sigma_t^2}\right)} * \frac{1}{\sqrt{2\pi\sigma^2}} e^{\left(-\frac{\left(i^m - i^d\right)^2}{2\sigma^2}\right)} \qquad \text{(eq. 2.2)}$$

where l_t^m and l_t^d are the modeled and measured extension lengths, respectively, for all time points t, i^m and i^d are modeled and observed initiation times, respectively, and σ is estimated at 12 days.

2.3.3 Mineralization model construction using MCMC method. MCMC is a technique that allows unknown parameters (e.g. mineral density values over time, constituting a mineralization trajectory) to be sampled from their probability distribution given observations. Through the iterative proposal and evaluation of parameters using available data, MCMC is able to "step" towards more probable parameter values. In the Metropolis-Hastings MCMC algorithm, new parameters are proposed according to estimated error. Whenever proposed parameters are more probable given observations they are accepted. If they are less probable, they are rejected according to the ratio P_{new} / P_{old}, where P_{new} is the probability of the new proposals, and P_{old} is the probability of the old ones. The result is that given enough time, MCMC will sample parameters with a density proportional to their probability, and therefore estimate parameter probability distribution.

To estimate mineral density increases throughout the tooth crown, for each tooth coordinate location we used an MCMC technique to sample from the Gaussian of likely mineralization

histories given our observations. We assume that HAp mineral density may only increase (minimum 10^{-5} g/cm^3 per sample time interval) in developing enamel:

$$L\left(\rho_t^d \middle| \rho_t^m\right) = \prod_t e\left[-\frac{\left(\rho_t^m - \rho_t^d\right)^2}{2\sigma_t^2}\right] \qquad \text{(eq. 2.3)}$$

where ρ_t^d is the measured pixel HAp density at time interval t, ρ_t^m is the modeled density for the same interval, and σ_t is the estimated density error for each measurement. In these calculations we use a flat prior. Our model assumed that for a given pixel location density, measurements from each tooth were independent, and measurement error due to synchrotron imaging or natural biological variation amounted to 5% of all measurable HAp densities. In order to explore the posterior distribution of ρ_t^m, we used Metropolis-Hastings with four walkers and 150,000 samples per pixel, of which we stored 100 for our model of tooth mineralization. Final model resolution includes over 12,000 pixel locations, with density estimates calculated for 280 days per pixel, and 100 density estimates per pixel-day (336 million density estimates).

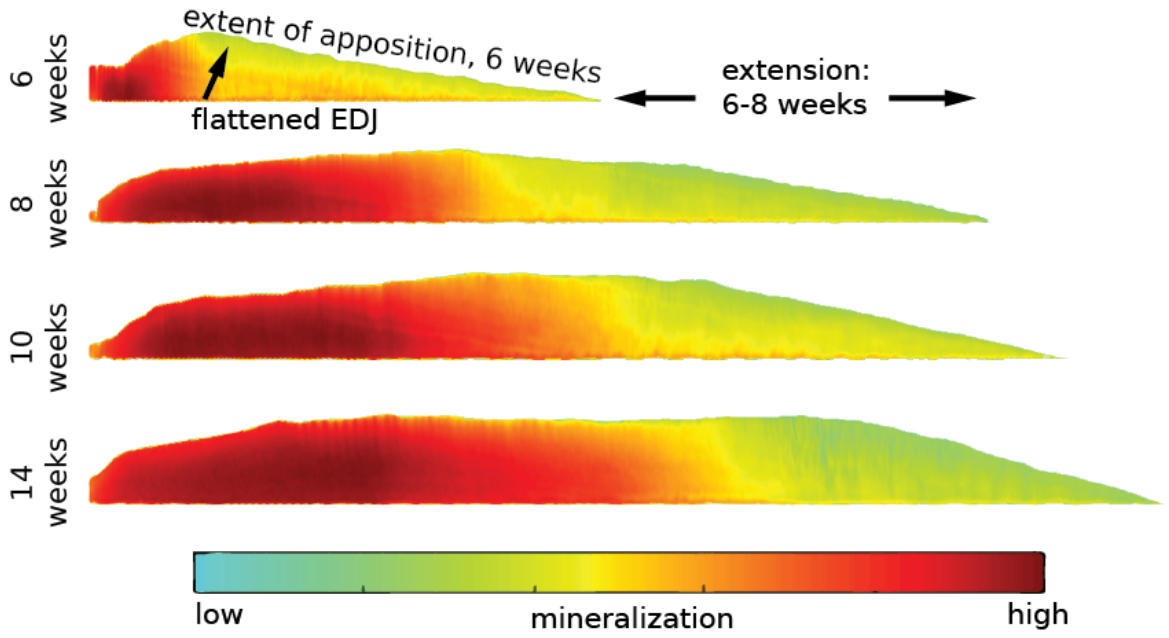

Figure 2.4 Shape-standardized mineralizing enamel. Colors indicate maturation extent from low (green) to high (red). To compare mineralization among molar crowns at different developmental stages, sections are flattened along their enamel-dentin junctions (EDJs) and aligned. Enamel structural features can be observed including Hunter-Schraeger Bands and isochronous bands revealing the ordered deposition of secretory enamel.

2.4 Results

2.4.1 Synchrotron μCT imaging. Virtual sections show that tooth shape is highly variable, even though all animals derive from a single research population of high-percentage dorset sheep (Appendix scanned enamel). Enamel growth and extension progress with age are also variable. Some of this variation is removed when a tooth coordinate system is used to standardize enamel shapes (Fig. 2.3; Fig. 2.4). At both low and high resolutions, flattened enamel scans clearly show separated secretion and maturation phases (Fig. 2.4). High resolution sections confirm that a thin layer adjacent to the EDJ is highly mineralized rapidly after

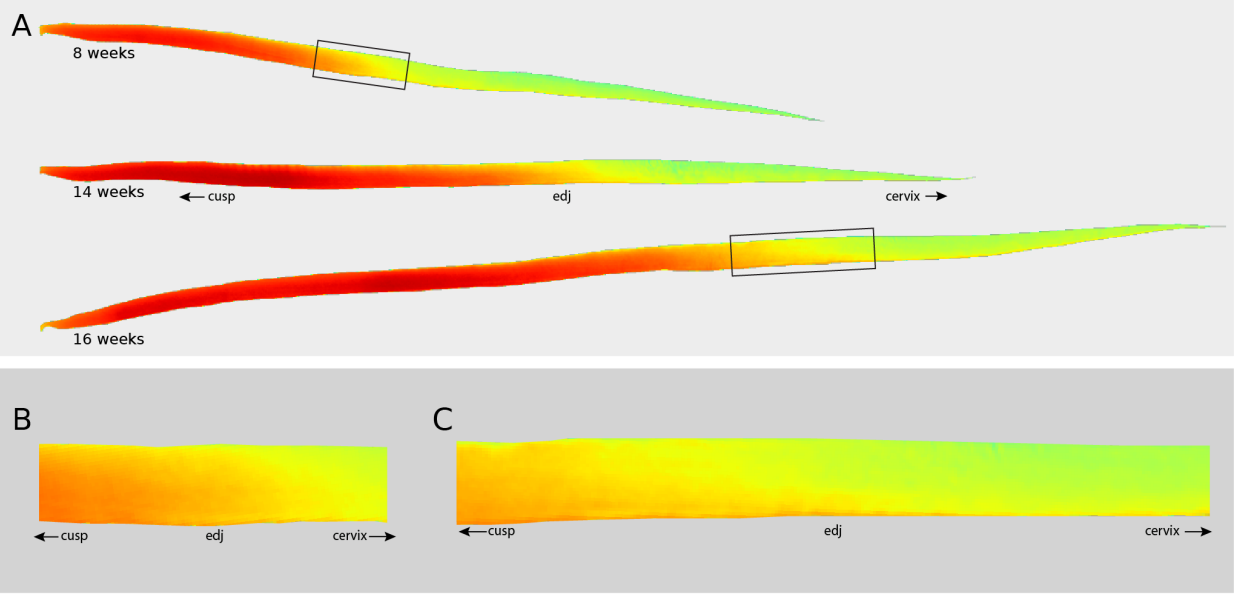

Figure 2.5 High-resolution (13 μm) synchrotron scans of developing teeth reveal density patterns in greater detail. **A.** Virtually dissected enamel crowns from molar scans of sheep that died at 8, 14 and 16 weeks of age. Green and red represent less and more HAp density, respectively. **B.** Detail of maturation onset for the 8 week-old molar. **C.** Detail of maturation onset for the 16 week-old molar, showing a more acute maturation geometry (orange and red boundary), with a highly mineralized innermost enamel layer cervically.

secretion, a finding useful for sequential sampling and seasonality reconstruction (Fig. 2.5a) (Blumenthal *et al.*, 2014; Smith and Tafforeau 2008; Suga 1982; Tafforeau *et al.*, 2007). Though the angle at which maturation advances down the mineralizing enamel crown appears generally intermediate between that of secretion and a line perpendicular to the EDJ, high resolution images show that maturation morphology differs among individuals. In some instances, maturation appears to advance perpendicularly to the EDJ, or even more quickly in the middle of the enamel crown (Fig. 2.5b), while in other cases inner enamel mineralizes more rapidly (Fig. 2.5c). Though some of this variation may be attributed to obliquity of virtual sections resulting from torsion in molar loph shape, these

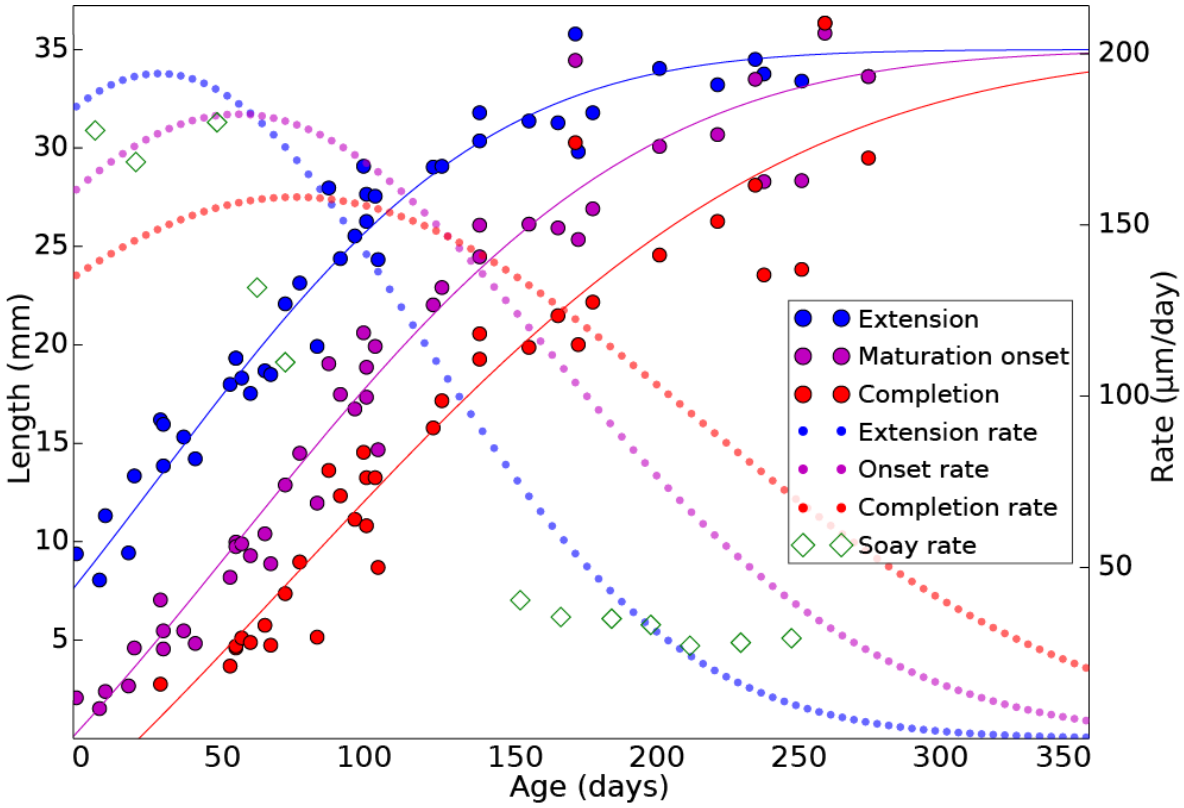

Figure 2.6: Gaussian modeling of extension and mineralization. Measurements of enamel extension (blue circles), maturation onset (purple circles) and completion (red circles) start at the dentin horn tip (cusp) and proceeding along the enamel-dentin junction (EDJ) from birth until the end of mineralization for an ontogenetic series of sheep M1s. Solid lines are fitted as integrated Gaussian functions. Maturation onset and completion are defined by the attainment of 40% and 85% mineral density, respectively, halfway between the EDJ and enamel surface. Rates of extension and maturation (dotted lines) are estimated as Gaussian functions, and compared to measured extension rates from a Soay sheep (green diamonds) (Kierforf *et al.*, 2013), a more primitive breed than the Dorset sheep used here.

data suggest that unlike secretion, maturation geometry is primarily driven by diffuse and possibly stochastic processes.

2.4.2 Gaussian model of mineralization. Gaussian modeling of mineral density maps reveal that sheep first molars (M1s) rapidly extend in size around birth, extension rates slow between 100-150 days, and molars are nearly complete by 200 days of age (Fig. 2.6). Decreasing postnatal extension rates are consistent with previous observations of sheep, bovid and equid M1s and M3s

(Longinelli and Padalino, 1980; Zazzo *et al.*, 2010; Jordana and Kohler, 2011; Kierdorf *et al.*, 2013; Bendrey *et al.*, 2015). We find that maturation onset and completion may also be modeled as a Gaussian process, and with variation comparable to that of extension until the very latest time points. While extension rate peaks prior to maturation onset or completion rates, and achieves a higher maximum velocity, sustained late stage maturation velocity allows maturation progress to converge with extension at the completion of mineralization.

A subset of scanned mineralizing M2 teeth, coupled with calcein labels recorded in the M2 of a dorset sheep (discussed further in Chapter 4), allow dorset M1 and M2 extension to be compared (Fig. 2.7). We derived parameters describing first and second molar extension over time within the framework of the Gaussian error function (Table 2.2).

	Amplitude (mm)	**Slope**	**Offset (days)**	**Max Height (mm)**
M1	21.8	.00789	29.12	35 (measured)
M2	68.0	.00335	-25.41	41 (measured)

Table 2.2: Parameters characterizing the Gaussian Error Function that describes enamel extension over time in M1 and M2 lower sheep molars.

The concordance of M1 and M2 extension patterns measured via virtual histology and calcein labeling, and their similarity with other fossil and extant taxa (Jordana and Köhler, 2011; Zazzo *et al.*, 2012; Kierdorf *et al.*, 2013; Bendry *et al.*, 2015), suggest that the Gaussian shape of modeled extension rate is conserved and, with extension data from light microscopy or virtual histology, could be calculated for a diverse set of teeth, taxa and contexts.

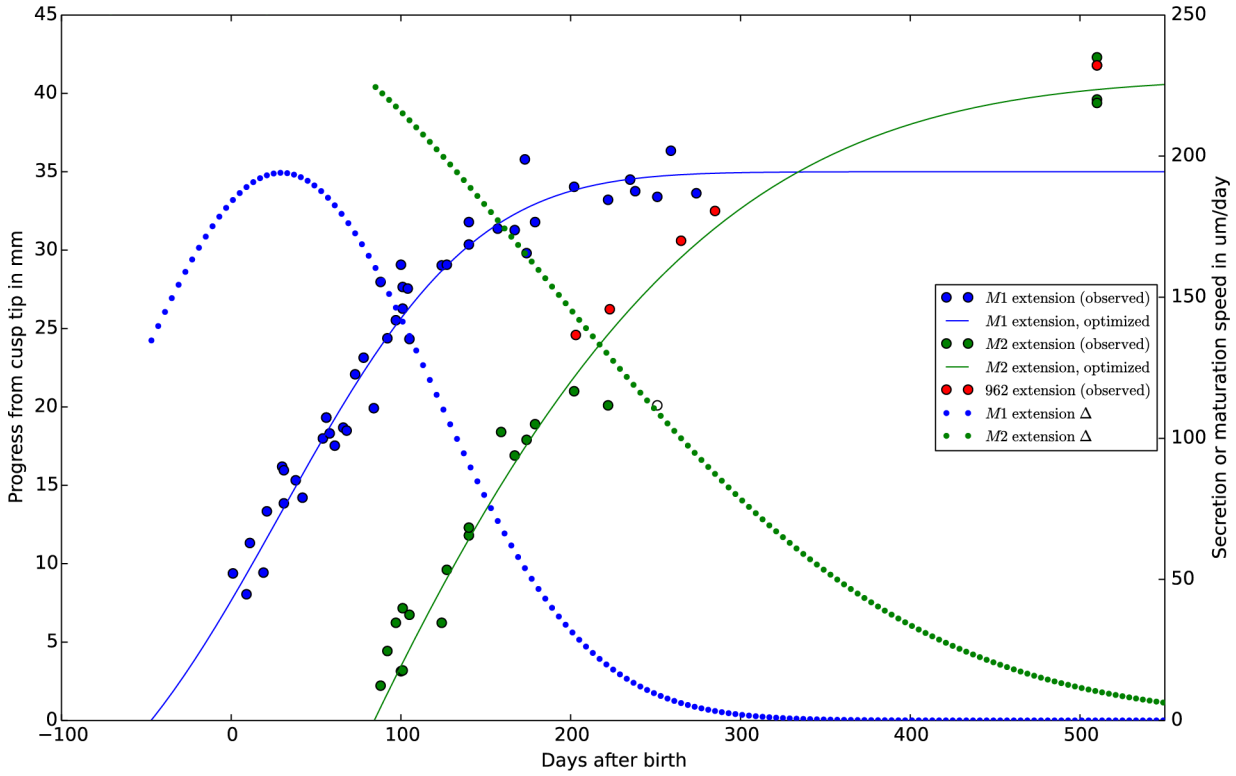

Figure 2.7. M1 and M2 extension trajectories (blue and green solid lines, respectively) estimated from enamel-dentine junction lengths of sheep that died at known ages (green and blue circles; open green circle is an outlier not used for analysis). Extension rates are shown as dotted lines. Lengths and ages for the experimental animal in Chapter 4 (sheep 962: red circles) match reasonably well with the M2 extension trajectory.

2.4.3 MCMC mineralization model. By standardizing variable M1 shapes and assembling mineralization trajectories from over 12,000 locations into a single dynamic mineralization model, we find that secretion and maturation proceed in two waves that are distinct in geometry and timing (Fig. 2.8; SI Video). Initial secretion occurs at a steep angle to the EDJ that becomes more oblique through time, while maturation occurs over a larger spatial area and longer time period, with a variable orientation largely perpendicular to the EDJ. Significant mineral density increase occurs only after ameloblasts have completed secretion from the EDJ to maturation. Thus the time averaging of environmental or body chemical input, depends on the precise

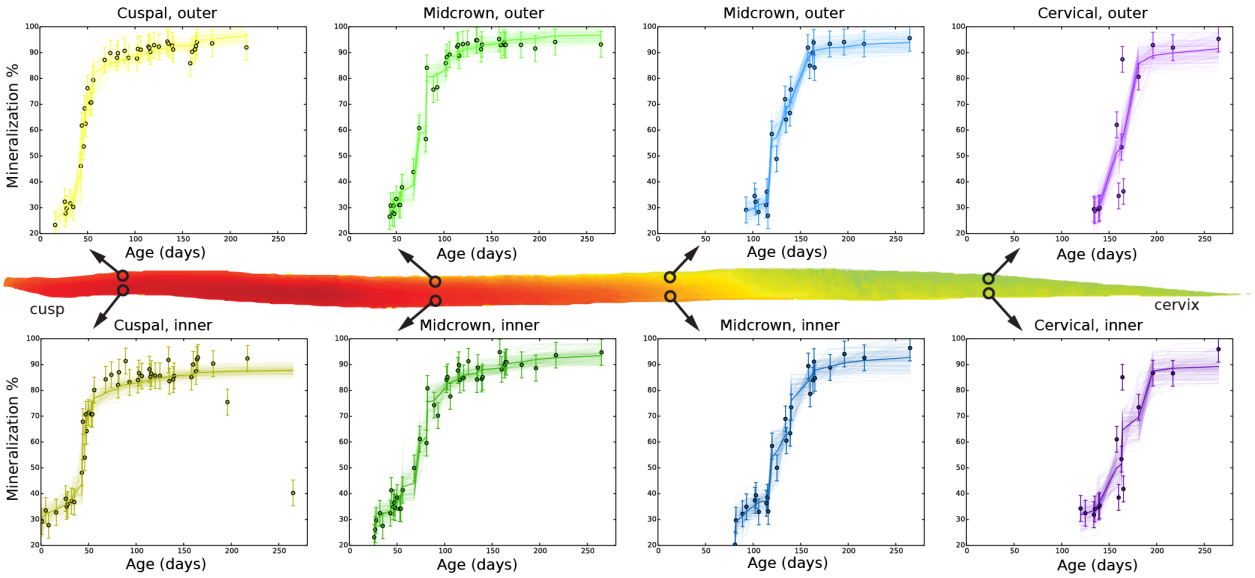

Figure 2.8. Mineralization percent over time (circles) determined from quantitative x-ray imaging. Mineralization trajectories (lines) may be sampled for over 12,000 locations, of which eight are shown here. These trajectories show that cuspal enamel begins mineralizing earlier and matures over a shorter time relative to cervical enamel. After secretion, inner enamel near the EDJ matures more slowly, while outer enamel farther from the EDJ proceeds from secretion to maturation more quickly and takes less time to mineralize overall.

location within the crown (Fig. 2.8). Above the innermost enamel layer, sharp increases of mineral density during maturation occur after a pause that follows secretion. The total time averaged during local mineralization is approximately 75-100 days. Near the enamel surface secretion occurs later, is quickly followed by maturation, and involves less time averaging (~55-75 days). The resolution of the model does not clearly reveal the mineralization of the innermost enamel visible in high-resolution scans.

2.5 Discussion

2.5.1 Relationship to previous models. These results do not specifically conform to either the Suga (1982) or Passey and Cerling (2002) models, but validate aspects of each. As proposed by

Suga (1982), maturation and secretion geometry are distinct, and there are multiple waves of mineralization. However, we do not find evidence for more than one wave of maturation. In this sense, Passey and Cerling's (2002) approximation is useful, especially if the model is modified to account for slowing growth in molar teeth. Characteristics of our results not present in either model, including the quantification of slowing growth, the internal spatial geometry of maturation, and its exact temporal relationship with secretion, would have been nearly impossible to reconstruct given the data collection methods and objectives of the former studies.

2.5.2 Implications beyond mineralization. An empirical model of density changes over space and time during mineralization can provide a valuable framework for interpreting multiple characteristics measured from mature teeth. This framework could be used to assess aspects of mineralization itself, where the discrete character of secretion and maturation might allow therapeutic treatments designed to target either phase. But a quantitative understanding of mineralization may also pave the way toward assessments of health beyond the tooth, including a quantitative measure of the "exposome:" the internal and external exposures experienced by an animal from the neonatal period onwards (Andra *et al.*, 2015). Measurements of lead or other potentially toxic compounds including phthalates, parabens, fluorinated compounds or pesticides can theoretically provide concrete estimates of blood concentration levels at the time of exposure, and of environmental risk to others similarly exposed (Andra *et al.*, 2015).

Estimates of the levels of non-toxic ingested constituents that transit the body are also possible through an understanding of the magnitudes and durations of secretion and maturation. These may become powerful tools for understanding the behaviors and diets of past organisms from

isotopic and elemental values measured from archaeological or fossil specimens. Strontium isotope ratios reflect geological provenance and can therefore provide a record of early life migratory patterns (Richards *et al.,* 2008, Britton *et al.*, 2009; Copeland *et al.*, 2016). Relative barium, strontium and calcium levels can indicate dietary transitions or weaning behavior, and in hominin teeth possibly identify life history traits unique among humans (Austin *et al.*, 2013; Humphrey 2014).

Repeated samples of tooth carbon stable isotopes are often used to infer dietary patterns over seasonal cycles, including grazing upon wet or arid adapted plants, or foraging of terrestrial or marine resources (Sponheimer *et al.*, 2006; Eerkens *et al.*, 2016; Ludecke *et al.*, 2016). Oxygen isotopes give an indication of seasonal changes in the evaporative state of ingested water or food sources, or of the heat or aridity stress of the subject (Gat 1996; Nelson 2007; Kirsanow *et al.*, 2008; Ludecke *et al.*, 2016). This mineralization model is accessible in an HDF5 data format that can be adapted to a variety of purposes (see electronic resources). An application explored in Chapter 4 is the reconstruction of individual dietary, behavioral or environmental history from tooth chemical constituents.

Our mineralization model uses mineral density measurements and cannot assess the possibility of mineral phase transitions that have been observed in a several taxa (Beniash *et al.*, 2009; Josephson *et al.*, 2010; Damkier *et al.*, 2014). Hydrated ferrous and α-chitin matrices evolve to magnetite during mollusk radula formation (Wang *et al.*, 2013), and amorphous calcium carbonate to aragonite and calcite transitions have been observed during the mineralization of sea urchin and mollusk shells (Gong *et al.*, 2012; DeVol *et al.*, 2015). Evidence of amorphous

calcium phosphate to HAp resetting has recently been found in developing *Mus* teeth (Beniash *et al.*, 2009), and with the addition of these findings, it is likely that mammalian enamel formation also depends upon HAp precipitation from amorphous precursors. If integrated with detailed knowledge of animal ingestion history this model can provide concrete tooth isotope values predictions, and prediction-data discrepancies could indicate phase transitions in sheep mineralization.

2.6 Conclusions. The dynamic model of mineralization presented here shows that sheep molars mineralize in two primary waves, each with distinct spatial orientation, and separated temporally until the end of the mineralization process. Synchrotron μCT density measurements presented here show that maturation is spatially and temporally variable, suggesting that it is driven by protein-mediated diffusion, and possibly by mineral phase transitions over a relatively large portion of the crown. Despite the heterogeneity of maturation among different teeth, data from individuals and tooth locations results in an overall model that is highly consistent in terms of secretory and maturation geometry and weight. This outcome has several implications. First, it supports the view that in overall form, and despite individual variation, mineralization is an ordered process that is conserved among a wide range of taxa. Second, it indicates that density characterization and MCMC sampling can be used to reconstruct a broad range of mineralization patterns in different skeletal and taxonomic contexts, including human tooth mineralization processes, and further illuminate the dynamic nature of biomineralization. Third, efforts to quantitatively reconstruct dietary or environmental histories using chemical measurements will be able to assess not only the relative contributions of secretory and maturation phases, but their expected distribution within mature, or even fossilized tissues.

2.7 References

Andra SS, Austin C, Wright RO, Arora M, 2015. Reconstructing pre-natal and early childhood exposure to multi-class organic chemicals using teeth: Towards a retrospective temporal exposome. Environment international, 83:137-145.

Antón SC, Potts R, Aiello LC (2014) Evolution of early Homo: An integrated biological perspective. *Science* 345:1236828.

Aubert M, Williams IS, Boljkovac K, Moffat I, Moncel MH, *et al.* (2012) In situ oxygen isotope micro-analysis of faunal material and human teeth using a SHRIMP II: a new tool for palaeo-ecology and archaeology. *J Arch Sci* 39:3184-3194.

Austin C, Smith TM, Bradman A, Hinde K, Joannes-Boyau R, Bishop D, Hare DJ, Doble P, Eskenazi B, Arora M (2013) Barium distributions in teeth reveal early-life dietary transitions in primates. Nature 498(7453):216-9.

Balasse M, Obein G, Ughetto-Monfrin J, Mainland I (2012) Investigating seasonality, birth in herds: a reference set of sheep enamel stable oxygen isotope ratios. *Archaeom* 54:349.

Bendrey R, Vella D, Zazzo A, Balasse M, Lepetz S (2015) Exponentially decreasing tooth growth rate in horse teeth: implications for isotopic analyses. Archaeometry.

Beniash E, Metzler RA, Lam RSK, Gilbert P (2009) Transient amorphous calcium phosphate in forming enamel. *J Struc Bio* 166:133-143.

Blumenthal S, Cerling T, Chritz K, Bromage T, Kozdon R, Valley J (2014) Stable isotope time-series in mammalian teeth: In situ δ18O from the innermost enamel layer. *Geochim Cosmochim Acta* 124:223236.

Bowen GJ, Revenaugh J (2003) Interpolating the isotopic composition of modern meteoric precipitation. *Water Resources Res* 39.

Boyde A (1989) Enamel. In *Teeth* 309-473. *Springer Berlin Heidelberg*.

Britton K, Grimes V, Dau J, Richards MP. (2009) Reconstructing faunal migrations using intra-tooth sampling and strontium and oxygen isotope analyses: a case study of modern caribou (Rangifer tarandus granti). Journal of Archaeological Science. 36(5):1163-72.

Copeland SR, Cawthra HC, Fisher EC, Lee-Thorp JA, Cowling RM, le Roux PJ, Hodgkins J, Marean CW, (2016) Strontium isotope investigation of ungulate movement patterns on the Pleistocene Paleo-Agulhas Plain of the Greater Cape Floristic Region, South Africa. Quaternary Science Reviews. 141:65-84.

Damkier HH, Josephsen K, Takano Y, Zahn D, Fejerskov O, Frische S (2014) Fluctuations in surface pH of maturing rat incisor enamel are a result of cycles of H(+)-secretion by ameloblasts and variations in enamel buffer characteristics. *Bone* 60:227-34.

De Yoreo JJ, Gilbert PUPA, Sommerdijk NAJM, Lee Penn R, *et al.* (2015) Crystallization by particle attachment in synthetic, biogenic, geologic environments. *Science* 349.

DeVol RT, Sun CY, Marcus MA, Coppersmith SN, Myneni SC, Gilbert PU (2015) Nanoscale transforming mineral phases in fresh nacre. Journal of the American Chemical Society. 137(41):13325-33.

Diekwisch TG (1998) Subunit compartments of secretory stage enamel matrix. *Connect Tissue Res* 38:101-11.

Driessens F, Verbeeck RK (1990) Biominerals. *CRC Press*.

Eerkens JW, Sullivan K, Greenwald AM (2016) Stable isotope analysis of serial samples of third molars as insight into inter-and intra-individual variation in ancient diet. Journal of Archaeological Science: Reports. 5:656-63.

Fricke H, O'Neil J (1996) Inter-and intra-tooth variation in the oxygen isotope composition of mammalian tooth enamel phosphate: implications for palaeoclimatological and palaeobiological research. *Palaeogeogr, Palaeoclim, Palaeoecology* 126:91–100.

Gat J (1996) Oxygen and hydrogen isotopes in the hydrologic cycle. *Ann. Rev. Earth Plan. Sci.* 24:225262.

Gong YU, Killian CE, Olson IC, Appathurai NP, Amasino AL, Martin MC, Holt LJ, Wilt FH, Gilbert PU (2012) Phase transitions in biogenic amorphous calcium carbonate. Proceedings of the National Academy of Sciences. 109(16):6088-93.

Hillson S. Teeth. Cambridge university press; 2005.

Hoppe KA, Stover SM, Pascoe JR, Amundson R (2004) Tooth biomineralization in horses: implications for isotopic microsampling. *Palaeogeogr, Palaeoclim, Palaeoecology* 206:355–365.

Huang TT, He LH, Darendeliler MA, Swain MV (2010) Correlation of mineral density and elastic modulus of natural enamel white spot lesions using X-ray microtomography and nanoindentation. Acta biomaterialia. 6(12):4553-9.

Humphrey LT (2014) Isotopic and trace element evidence of dietary transitions in early life. Annals of human biology. 41(4):348-57.

Jälevik B (2010) Prevalence and diagnosis of molar-incisor-hypomineralisation (MIH): a systematic review. European Archives of Paediatric Dentistry. 11(2):59-64.

Jordana X, Köhler M (2011) Enamel microstructure in the fossil bovid Myotragus balearicus (Majorca, Spain): implications for life-history evolution of dwarf mammals in insular ecosystems. *Palaeogeogr, Palaeoclim, Palaeoecology*, 300:59-66.

Josephsen K, Takano Y, Frische S, Praetorius J, Nielsen S, *et al.* (2010) Ion transporters in secretory and cyclically modulating ameloblasts: a new hypothesis for cellular control of preeruptive enamel maturation. *Am J Physiol Cell Physiol*. 299:C1299-307.

Kierdorf H, Kierdorf U, Frölich K, Witzel C (2013) Lines of Evidence–Incremental Markings in Molar Enamel of Soay Sheep Revealed by Fluorochrome Labeling, Backscattered Electron Imaging Study. *PLoS ONE* 8.9:e74597.

Kirsanow K, Makarewicz C, Tuross N (2008) Stable oxygen (δ18O) and hydrogen (δD) isotopes in ovicaprid dentinal collagen record seasonal variation. Journal of Archaeological Science. 35(12):3159-67.

Kucherenko S, Sytsko Y (2005) Application of deterministic low-discrepancy sequences in global optimization. *Computational Optimization and Applications*. 30:297-318.

Labiche J-C, Mathon O, Pascarelli S, Newton MA, Guilera Ferre G, Curfs C, Vaughan G, Homs A, Fernandez Carreiras D (2007) The fast readout low noise camera as a versatile X-ray detector for time resolved dispersive extended X-ray absorption fine structure and diffraction studies of dynamic problems in materials science, chemistry, and catalysis. *Review of Scientific Instruments* 78:091301-091311.

Longinelli A, Padalino AP (1980) Oxygen isotopic composition of water from mammal blood: first results. *Eur J Mass Spectrom Biochem Med Env Res* 1:135-139.

Marshall AJ, Wrangham RW (2007) Evolutionary consequences of fallback foods. *Int J Prim* 28:1219-1235.

Mirone A, Gouillart E, Brun E, Tafforeau P, Kieffer J, (2014). PyHST2: a hybrid distributed code for high speed tomographic reconstruction with iterative reconstruction and a priori knowledge capabilities. *Nuclear Instruments and Methods in Physics Research Section B: Beam Interactions with Materials and Atoms*. 324:41-48.

Nuzzo S, Peyrin F, Cloetens P, Baruchel J, Boivin G (2002) Quantification of the degree of mineralization of bone in three dimensions using synchrotron radiation microtomography. *Med Phys* 29:2672–2681.

Paganin D, Mayo SC, Gureyev TE, Miller PR, Wilkins SW (2002) Simultaneous phase and amplitude extraction from a single defocused image of a homogeneous object. *J Microscopy* 206:33-40.

Passey BH, Cerling TE (2002) Tooth enamel mineralization in ungulates: implications for recovering a primary isotopic time-series. *Geochim Cosmochim Acta* 66:3225-3234.

Passey B, Cerling T, Schuster G, Robinson T, Roeder B, Krueger S (2005) Inverse methods for estimating primary input signals from time-averaged isotope profiles. *Geochim Cosmochim Acta* 69:4101-4116.

Powell MJD (1998) Direct search algorithms for optimization calculations. *Acta Numerica* 7:287-336.

Richards M, Harvati K, Grimes V, Smith C, Smith T, Hublin JJ, Karkanas P, Panagopoulou E. Strontium isotope evidence of Neanderthal mobility at the site of Lakonis, Greece using laser-ablation PIMMS. Journal of Archaeological Science. 2008 May 31;35(5):1251-6.

Robinson C (2014) Enamel maturation: background, implications for enamel dysplasias. *Front Physiol* 5.

Sanchez S, Ahlberg PE, Trinajstic K, Mirone A, Tafforeau P (2012) Three dimensional synchrotron virtual paleohistology: a new insight into the world of fossil bone microstructures. *Microsc Microanalysis* 18:1095-1105.

Simmer J, Papagerakis P, Smith C, Fisher D, Rountrey A, *et al.* (2010) Regulation of dental enamel shape and hardness. *J Dent Res* 89:1024–38.

Simmer J, Richardson A, Hu Y-Y, Smith C, Hu J (2012) A post-classical theory of enamel biomineralization… and why we need one. *Int J Oral Sci* 4:129–134.

Smith CE (1998) Cellular and Chemical Events During Enamel Maturation. *Crit Rev Oral Bio Med* 9:128-161.

Smith TM (2006) Experimental determination of the periodicity of incremental features in enamel. *J Anat* 208: 99-113.

Smith T, Tafforeau P (2008) New visions of dental tissue research: Tooth development, chemistry, and structure. *Ev Anthro* 17:213–226.

Sponheimer M, Passey B H, de Ruiter D J, Guatelli-Steinberg D, *et al.* (2006) Isotopic Evidence for Dietary Variability in the Early Hominin P. robustus. *Science* 314:980-982.

Suga S 1982. Progressive mineralization pattern of developing enamel during the maturation stage. *J Dent Res* 1532-1542.

Tafforeau P, Bentaleb I, Jaeger JJ, Martin C (2007) Nature of laminations and mineralization in rhinoceros enamel using histology and X-ray synchrotron microtomography. *Palaeogeogr, Palaeoclim, Palaeoecology* 246:206-227.

Ungar PS. Mammal teeth: origin, evolution, and diversity. JHU Press; 2010.

Vincens A, Garcin Y, Buchet G (2007) Influence of rainfall seasonality on African vegetation in the Late Quaternary: pollen evidence, Lake Masoko, Tanzania. *J Biogeogr* 34:1274-1288.

Wang Q, Nemoto M, Li D, Weaver JC, Weden B, Stegemeier J, Bozhilov KN, Wood LR, Milliron GW, Kim CS, DiMasi E (2013) Phase transformations and structural developments in the radular teeth of Cryptochiton stelleri. Advanced Functional Materials. 23(23):2908-17.

Zazzo A, Balasse M, Passey B, Moloney A, Monahan F, Schmidt O (2010) The isotope record of short- and long-term dietary changes in sheep tooth enamel: Implications for quantitative reconstruction of paleodiets. *Geochim Cosmochim Acta* 74:3571-3586.

Zazzo A, Bendrey R, Vella D, Moloney A, Monahan F, Schmidt O (2012) Refined sampling strategy for intra-tooth stable isotope analysis of enamel. *Geochim Cosmochim Acta* 84:113.

3

Determinants of blood $\delta^{18}O$ turnover and variation in a population of experimental sheep

3.1 Abstract

Mammalian body, blood and hard tissue oxygen isotope ($\delta^{18}O$) compositions reflect environmental feed and water sources and important physiological processes. For this reason archaeological and fossil hard tissues are a valuable record of past physiology, behavior and climate. However, the physiological and environmental determinants of blood $\delta^{18}O$ composition have not been determined experimentally from large herbivores, the most abundant fauna in terrestrial fossil assemblages from the Cenozoic. Furthermore, existing models predicting blood $\delta^{18}O$ values from environmental sources have been evaluated on gross timescales, but not employed to track seasonal variation. Here we report how water, feed, and physiology determine blood $\delta^{18}O$ values in experimental sheep (*Ovis aries*) subjected to controlled water switches. We find that blood $\delta^{18}O$ reaches steady state with environmental drinking water rapidly and records transient climatic events, including snowstorms. Behavioral and physiological variation within a single genetically homogenous population of herbivores results in significant inter-animal variation in blood $\delta^{18}O$ compositions at single collection times (σ=0.1-1.4‰, range=3.5‰) and reveals a range of water flux rates ($T_{1/2}$=2.2-2.9 days) within the population. We find that extant models predict average observed sheep blood $\delta^{18}O$ with striking fidelity, but predict a pattern of seasonal variation exactly opposite of that observed in our population. We introduce an

environmental temperature-sensitive evaporative loss function that behaves nearly identically in different models, and brings 100% of predicted values to within 1.0‰ of observations. These results increase the applicability of available physiological models for paleoseasonality reconstructions from stable isotope measurements. However, blood $\delta^{18}O$ variation in this experimentally controlled population should promote caution when interpreting isotopic variation in the archaeological and paleontological record.

3.2 Introduction

3.1.1 Oxygen isotopes in the environment and body. The chemistry of the environment and the body are intimately linked, and fossil and archaeological remains are a potentially rich source of information about past environments. One aspect of the environment, hydrology, is reflected in animal bodies through oxygen from water, which is incorporated into animal hard tissues that are often preserved after death. Spatial and temporal variations in hydrological systems are reflected by $\delta^{18}O$ values in precipitation and surface waters, and in the blood and body water of animals that consume them (Gat 1996; Kirsanow and Tuross 2011). For this reason, $\delta^{18}O$ measurements from animal tissues can be used to infer origins or movement across continents, latitudes, and elevations, and to describe hydrological patterns of precipitation source, aridity or seasonality (Levin *et al.*, 2006; Bowen 2010; Kirsanow and Tuross 2011). In general terms, precipitation $\delta^{18}O$ values decrease with distance from coastal waters, increased elevation or latitude, and at colder temperatures (Bowen 2010). In the tropics, $\delta^{18}O$ further correlates with atmospheric moisture content, rainfall origin and amount, and evaporation; lowest and highest values are typically recorded during wet and dry seasons, respectively (Gat, 1996; Levin *et al.*,

2009). Because animal body $\delta^{18}O$ composition reflects these hydrological dynamics, and because hard tissues record $\delta^{18}O$ composition, modeling the environmental and physiological determinants of body water $\delta^{18}O$ facilitates the reconstruction of paleoclimate and its role in shaping evolution.

Complexity in local environmental hydrology, animal behavior and physiology contributes to variability in the relationship between blood $\delta^{18}O$ and meteoric water (rainfall) values. Blood and precipitation $\delta^{18}O$ data from disparate geographic regions and taxa have established varying meteoric water-blood correlations (Longinelli and Padalino 1980; Longinelli 1984):

$$\delta_{bw} = m * \delta_{dw} + b \qquad \text{(eq. 3.1)}$$

where blood $\delta^{18}O$ composition (here used as a proxy for body water, δ_{bw}) is a function of drinking water δ_{dw}, which is presumably linked to meteoric water, slope x and offset b (Longinelli 1984; Luz *et al.*, 1984; Kohn 1996). Across both broad and restricted geographic regions however, these parameters demonstrate remarkable variability. Among terrestrial mammals the slope m typically ranges from 0.5-1.0 $\delta^{18}O$ δ_{bw}/δ_{dw}, where higher slopes reflect greater, and lower slopes less physiological dependence upon meteoric water intake (Longinelli and Padalino 1980; Kohn 1996; Wang *et al.*, 2008). Frequently, the slope and offset have been estimated using measurements of nearby meteoric water $\delta^{18}O$ and animal bone or tooth hydroxyapatite $\delta^{18}O$ values that are not directly linked (Longinelli 1984; D'Angelo and Longinelli 1990; Longinelli *et al.*, 2003; Longinelli and Selmo 2011). These estimates relating environmental water and blood $\delta^{18}O$ values typically rely upon yet another link: that between blood and bone or tooth phosphate $\delta^{18}O$ (Longinelli and Nuti 1973; Pucéat *et al.*, 2010; Lécuyer *et al.*, 2013; Chang and Blake, 2015).

Because of uncertainty in the general relationships that link environmental water $\delta^{18}O$ to blood $\delta^{18}O$, and blood to skeletal $\delta^{18}O$, a series of more sophisticated models have been developed that attempt to predict these relationships using animal behavior, physiology, and properties of the environment.

Many animals do not consume meteoric water directly (Kohn 1996), obtaining drinking water from a range of surface water sources that include streams, rivers, lakes, and pools. Each of these sources have different turnover and evaporative regimes (Gat 1996). In addition to drinking water, herbivores acquire water from plant tissues with their own complex isotopic dynamics and variable water contents. These are typically enriched compared to surface water (Ellis *et al.*, 1995; Dawson *et al.*, 2002). Some animals are capable of acquiring most or all of their body water from ingested food, relying not only on food water content, but also on water produced during metabolism (Nagy 1987). Physiological reliance on drinking water varies with animal mass, adaptation to aridity, and predator avoidance behavior (Taylor 1970; Bryant *et al.*, 1996; Cain *et al.*, 2006). Lastly, animals regulate transpiration and evaporation for thermoregulation and water conservation differently depending on their location, diet, mass, and physiological and behavioral capability (Bryant and Froelich 1995; Ellis *et al.*, 1995; Kohn 1996). The diversity of animal water inputs, metabolic processing of food, and evaporative loss characteristics lend themselves to a variety of approaches to estimate blood $\delta^{18}O$ from environmental sources.

3.1.2 Modeling body water $\delta^{18}O$ steady-state: inputs and outputs. The $\delta^{18}O$ composition of an animal's blood, δ_{bw}, is in steady-state with input and output water $\delta^{18}O$ values. In general terms, tracking blood $\delta^{18}O$ means accounting for the masses of oxygen entering and leaving the body,

and the $\delta^{18}O$ composition of each mass. A steady-state is calculated, instead of an equilibrium, because oxygen continues to flow into and out of an animal's body even as δ_{bw} may remain constant. Steady state calculation requires one additional parameter, the fractionation (or unequal partitioning) of isotopes in the masses that enter and leave the body. Steady-state for δ_{bw} can therefore be approximated by the input and output masses, the input values, and the input and output factors that partition isotopes unequally as they transit the body (Gretebeck *et al.*, 1997). Body input $\delta^{18}O$ values include drinking water oxygen δ_{dw}, and air and food oxygen δ_{O2} and δ_{fd}. The $\delta^{18}O$ of metabolic water δ_{mw} also adds to the pool of body water and blood $\delta^{18}O$. Metabolic water is produced by inspired molecular oxygen, and ingested carbohydrate, lipid and protein values as they are catabolized for energy to produce CO_2 and water. Important oxygen outputs from the body include liquid water (urine and sweat), vapor, and CO_2, with the magnitude of these inputs and outputs determined by drinking water, metabolic activity and evaporative loss. A variety of models have been developed that can calculate δ_{bw} from the balance of δ_{dw}, δ_{O2} and δ_{fd}, and are reviewed below.

3.2.3 Luz *et al.* (1984) model. One approach to modeling oxygen flux relies upon measurement of ingested carbohydrate, fat and protein, and the overall metabolic output of the organism in terms of heat or CO_2. This approach is advantageous because it does not require a precise accounting of the mass and stoichiometry of each unknown step in the diverse paths of microbial and host metabolism. It is also advantageous because the composition of feed input and final CO_2 output can be estimated more easily than the *in vivo* metabolic derivatives of ingested food. Luz *et al.*, (1984) adopt this approach by modeling δ_{bw} as a function of drinking water, metabolic water production, food, and evaporative water loss:

$$\delta_{bw} = \frac{F_{dw}}{F_{dw} + F_{mw} + F_{CO2}}\delta_{dw} + \frac{8(1-x)(F_{dw} + F_{mw}) + 23F_{O2} - 38F_{CO2} + F_{fd}\delta_{fd}}{F_{dw} + F_{mw} + F_{CO2}}$$

(eq. 3.2)

where F_{CO2} is the molar fraction of oxygen leaving the body as CO_2 gas, x is the fraction of water lost as liquid without fractionation, 1 - x the fraction of water lost to evaporation with fractionation, F_{O2} is the fraction of oxygen that enters the body during respiration as O_2 gas, and δ_{fd} and F_{fd} are the isotopic composition and molar fraction of oxygen metabolized from food, respectively. In this model food water amount and composition must be accounted for through incorporation with drinking water input. In this system the isotopic compositions of gaseous oxygen entering and leaving the body via O_2 and CO_2 are set to +23 and δ_{bw} + 38‰, values consistent with measurements in a wide variety of contexts. The fractionation of body water lost to evaporation is estimated at δ_{bw} - 8‰ (for an extended discussion of this term, see Kohn 1996). While δ_{bw} is positively correlated with δ_{dw} and δ_{fd}, the slope of this relationship is proportional to the magnitude of metabolic water production. The implication is that animals whose body water composition best reflect environmental changes are those with relatively high drinking water consumption and low metabolic activity. Luz *et al.* (1984) find that this system predicts the δ_{bw} of experimental rats raised with controlled δ_{dw} and δ_{fw}, using estimates of mass fluxes derived from previous experiments (Lee and Lifson, 1960).

3.2.4 Gretebeck *et al.* (1997) and Podlesak *et al.* (2008) models. Nearly identical approaches are adopted by Gretebeck *et al.* (1997) and Podlesak *et al.* (2008), who instead of using δ_{bw} delta

notation, solve for the ratio of heavy to light isotopes ($^{18}O/^{16}O$) in body water, or R_{bw}, as contingent upon the ratios of inputs and outputs:

$$R_{bw} = \frac{(R_{dw} * F_{dw}) + (R_{O2} * F_{O2} * \alpha_{O2}) + (R_{fd} * F_{fd})}{F_{H2O-un} + (F_{H2O-fr} * \alpha_{H2O-fr}) + (F_{CO2} * \alpha_{CO2})} \qquad \text{(eq. 3.3)}$$

where R_{dw} is the isotope ratio drinking water, R_{O2} is that for inspired oxygen, α_{O2} is the fractionation factor altering that ratio at the gas-liquid boundary in the lungs, and R_{fd} is the ratio of feed. F_{H2O-un} is the fraction of water oxygen leaving the body in water without fractionation, F_{H2O-fr} is that fraction of water oxygen leaving the body in water that fractionates according to the factor α_{H2O-fr}, and F_{CO2} is the fraction of body water oxygen leaving as CO_2, fractionated by the factor α_{CO2} Gretebeck *et al.* (1997) estimates and measures of food and air O influx, and CO_2 efflux in humans, imply mixed carbohydrate, protein and fat metabolism. Podlesak *et al.*, (2008) instead set the relative fractions of air and food oxygen to metabolic water production according to pure carbohydrate metabolism.

$$\frac{1}{3}F_{fd} + \frac{2}{3}F_{O2} = \frac{2}{3}F_{CO2} + \frac{1}{3}F_{H2O} \qquad \text{(eq. 3.4)}$$

This assumption is more feasible in an experimental context of consistent, carbohydrate-rich dry feed.

3.2.5 Kohn (1996) A more comprehensive approach to understanding body water $\delta^{18}O$ and its relationship to environmental sources is developed by Kohn (1996) for application beyond

controlled environments to diverse animals and contexts. This approach is necessary for ecological or paleontological studies where $\delta^{18}O$ measurements from tissues are used to make inferences about animal diet, physiology or environmental $\delta^{18}O$ sources. Because various food $\delta^{18}O$ sources may be unknown but are dependent upon surface water (for consistency here we continue to use the term drinking water, δ_{dw}), Kohn (1996) estimates δ_{bw} primarily in terms of δ_{dw} fractionations between δ_{dw} and δ_{dw}-dependent input sources, the fractionation of oxygen leaving the body, and the masses of oxygen entering and exiting the body:

$$\delta_{bw} = \frac{(M_{O2} * \delta_{O2}) + (\Sigma M_{in} * \Delta_{in}) - (\Sigma M_{out} * \Delta_{out})}{\Sigma M_{out}} + \frac{\Sigma M_{in} * \delta_{dw}}{\Sigma M_{out}}$$

(eq. 3.5)

where M_{O2} are the moles of oxygen entering the body via inspiration, ΣM_{in} are the moles of other input oxygen sources, Δ_{in} are the isotopic offsets between each source and drinking water, ΣM_{out} are the moles of output oxygen sources, and Δ_{out} are the isotopic offsets between each output and δ_{bw}. Kohn (1996) implements this calculation for a variety of taxa by estimating oxygen inputs from environmental temperature and relative humidity, metabolic scaling laws, and physiological drought and heat tolerance. Kohn also models the general composition of feed, which includes C3/C4 plants composition, and the carbohydrate, fat and protein components with associated metabolic stoichiometry.

Kohn (1996)'s model successfully replicates phosphate $\delta^{18}O$ trends from a variety of wild taxa. Importantly, measured $\delta^{18}O$ variation in North American deer, Australian Red Kangaroos, and several herbivorous taxa in Turkana, northern Kenya is as high as 4‰, with model-data

mismatch equally high in some cases. To contextualize this discrepancy: 4‰ is higher than total annual rainfall $\delta^{18}O$ variation at many arid sites throughout the east African Rift Valley (Bowen 2010). It is therefore possible that in some cases, model error is greater than the largest signal that might be expected from animal blood $\delta^{18}O$ values. Kohn proposes that evaporative loss is likely one important source of uncertainty when examining model-data fits, and demonstrates that altering evaporative loss terms can account for some model-data discrepancies.

The Luz *et al.* (1973), Kohn (1996) and Podelsak *et al.* (2008) models provide an important framework within which to approach as yet unresolved difficulties associated with modeling blood $\delta^{18}O$ compositions from environmental sources. These include the following questions: 1) What are expected levels of variation in a single, homogeneous population of animals? 2) How do physiological changes in mass, energy and water flux during growth change values over time? 3) Which variables are most important when accounting for seasonal changes in environmental conditions? To answer these questions we raise a population of sheep under controlled conditions, and experimentally alter their drinking water sources. We measure input drinking water and feed $\delta^{18}O$ values, and blood $\delta^{18}O$ values, while animals are transitioning between water sources, and while they are at steady state. Lastly, using model-data residuals we propose a number of simple procedures that can improve the performances of all models, and better characterize seasonal $\delta^{18}O$ compositions.

3.3 Methods

3.3.1 Sheep experiment. We raised ten sheep (five male wethers, five females) at the Concord Field Station in Bedford, MA following weaning at two months of age. All sheep were born on

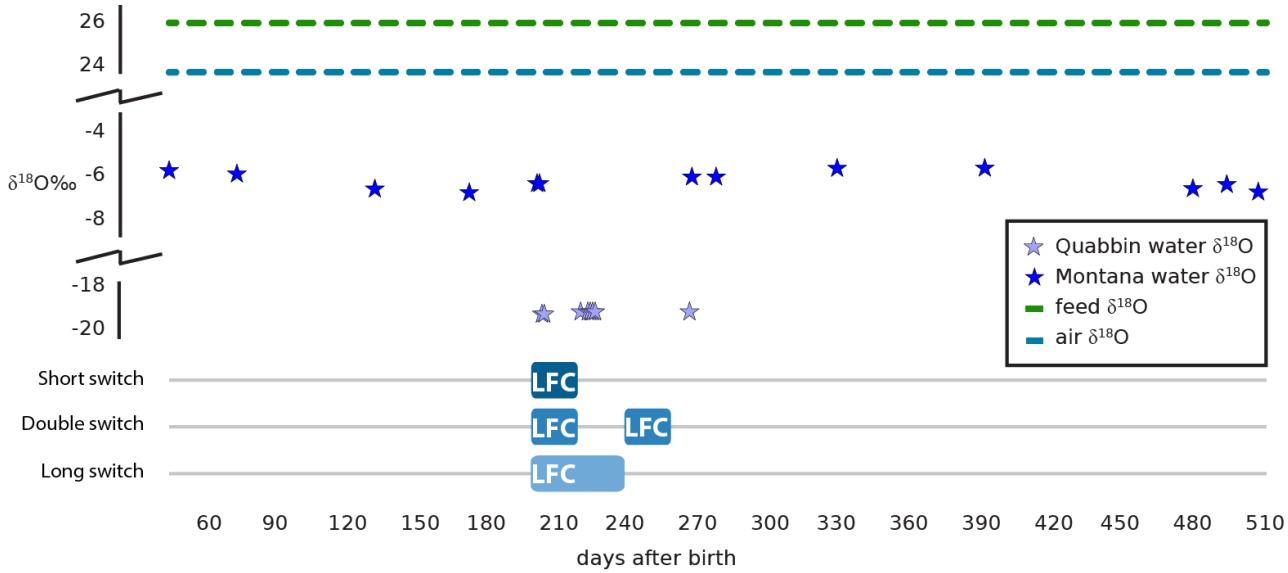

Figure 3.1 Experimental design. Sheep arrived in Bedford, MA 60 days after birth, and remained on constant feed (+25.3‰) and nearby Quabbin Reservoir water (dark blue stars, -6.53 ±0.46‰) for 16 months, except for 20-62 day intervals where some consumed LFC water from Montana (light blue stars, -19.38 ±0.05‰), marked "LCF" below. Control animals remain on Quabbin water for the entire period.

known dates between January 1st and 15th, 2013. After weaning they were fed from a single batch of dry feed stored at -20°C and thawed in monthly aliquots. The animals were provided Lexington, MA drinking water originating from the 1.5km^3 Quabbin Reservoir (-6.44‰, σ=0.35‰ and ranging from -7.4 to -5.9 δ^{18}O‰ throughout the experiment). Beginning August 2nd, when the animals were 199-213 days of age, we provided six individuals with glacial melt water from Lake Fork Creek (LFC) in the Beartooth Mountains near Red Lodge, MT (Fig. 3.1) (-19.38 δ^{18}O‰, σ=0.05 over the duration of the experiment). The six sheep were divided into three treatment groups of two individuals each. The first group drank LFC water for 20 days, then returned to Quabbin water. The second group did the same, but drank LFC water a second time for 20 days beginning October 3rd. The third group drank LFC water for 62 days beginning August 2nd, then returned to Quabbin water. The remaining four control animals drank only

Quabbin water. Jugular intravenous (IV) blood samples were collected at regular intervals prior to, during and after the water switch. At 1.4 years of age we sacrificed the sheep by 180mg/kg IV sodium pentobarbital injection. Animal care and data collection protocols were approved by the Harvard University Faculty of Arts and Sciences Institutional Animal Care and Use Committee.

3.3.2 Stable isotope analyses. Sheep blood and drinking water samples were analyzed for oxygen isotope composition at the Colman laboratory in Chicago using standard CO_2-H_2O equilibrations performed at 26 °C on a Thermo GasBench II, followed by headspace sampling and analysis using the GasBench II and Delta V Plus isotope ratio mass spectrometer (IRMS). Sheep blood (300µl) and drinking water samples (100µl) were aliquoted into He-flushed exetainer tubes. The exetainers receiving water standards and samples contained 0.3% CO_2 in He for standard CO_2-H_2O equilibrations. Blood samples were allowed to outgas and equilibrate endogenous CO_2. Equilibration incubations were conducted for 24 hours at 26 °C on a Thermo GasBench II, followed by headspace sampling and analysis using the GasBench II and Delta V Plus IRMS. Samples were referenced to lab standards (HH and HL), which are stored in flame-sealed glass ampoules and processed and analyzed in parallel with samples. The HH and HL standards have $d^{18}O$ values of +1.59 and -23.8 ‰ Vienna Standard Mean Ocean Water (VSMOW) as determined through repeated analysis against VSMOW, GISP, and SLAP2 standards. The precision of replicate analyses was better than 0.03 ‰ (1 s.d.), and accuracy for water samples is better than 0.1 ‰ (1 s.d.) based on repeat analyses on different days and participation in international laboratory intercalibration exercises.

Aliquots of the feed were dried at 60 °C and analyzed for oxygen isotopes on the TCEA-Conflo IV-Delta V Plus IRMS system. The $\delta^{18}O$ was measured to be +25.3 (+/- 0.8 1 s.d.) ‰. Results were assessed relative to standards IAEA-601 benzoic acid (+23.14 ‰) and IAEA-CH-6 sucrose (+36.20 ‰; also referred to as "ANU sucrose") in addition to the encapsulated waters. The larger scatter for organic $\delta^{18}O$ may represent variable contributions of a small amount of residual moisture in the feed to the oxygen (O) intrinsic to organic molecules in the feed.

3.3.3 Weight, VO2, feed and temperature parameterization. We model weight by fitting a polynomial to average weights at birth, weaning and maturity for Lin, Sd and Merino sheep for which published records were available (Karihaloo and Combs 1971; Butterfield 1988), and to weight measurements of our Dorset sheep that we conducted in April and October, 2013. We estimate atmospheric O2 consumption using a variety of metrics. Adult sheep oxygen consumption at rest has been measured at 3 – 7 ml/min/kg in Dorsets, though VO2 may rise to 15 ml/min/kg during walking, and over 20 during trotting (Cross *et al.*, 1959; Lotgering *et al.*, 1983; Entin *et al.*, 1999). Here we adopt a value of 6 ml/min/kg as broadly representative of Dorset measured VO2, yielding an average inspired air O daily intake of 50.2 mols through the duration of the experiment. We acknowledge that this value may be higher for lambs in the context of growth, activity or high feed consumption. Employing generalized mammalian scaling relationships, Kohn (1996) would estimate average sheep air O intake at 79 mols, with 101 mols inspired at peak mass.

Calculating oxygen throughput from feed in this experiment yields higher estimates, resulting from the growth-oriented, calorie-rich composition of feed provided to our animals. Throughout

the duration of the experiment each animal consumed 2.5kg of dry feed daily, of which 80.3% was digestible dry matter, most of this being carbohydrate, with a remaining 14.9% crude protein, and 2.4% ether extract, as determined by the Cornell STAR Sheep Management Program. The stoichiometry of metabolic processes oxidizing these compounds can be approximated as follows:

$$CH_2O + O_2 = CO_2 + H_2O \quad \text{(eq. 3.7)}$$

$$CH_4 + 2O_2 = CO_2 + 2H_2O \quad \text{(eq. 3.8)}$$

$$NH_2CHCH_3COOH + 3O_2 = 3CO_2 + 2H_2O + NH_3 \quad \text{(eq. 3.9)}$$

$$NH_2CHCH_3COOH + 3O_2 = 2.5CO_2 + 1.5H_2O + 0.5CO(NH_2)_2 \quad \text{(eq. 3.10)}$$

During these reactions, $\delta^{18}O$ is therefore determined by the stoichiometry and magnitude of each reaction. In monogastric animals feed energy yield is estimated to be 4 Kcal/g for protein and carbohydrate, and 9 Kcal/g for fat. The complex transformation of digested materials into volatile fatty acids lowers these returns in ruminants. Accounting for indigestible material, overall feed caloric content is estimated to be 2,930 kcal/kg, which at 2.5 kg/day yields a daily caloric intake of 7,330 kcal. This number is consistent with a 6.3 – 8.8 Mcal range of potential metabolizable energy intake estimates from feed digestible energy that are available for growth and maintenance given 2.5 kg ingested feed (Freer *et al.*, 2007). Based on feed composition we estimate that for every mol O of food consumed, 2.30 mol of air O are inspired, 1.05 mol metabolic water O produced, and 2.25 mol CO2 O exhaled. Consuming 2.5 kg feed, of which 80% is digestible, sheep would be expected to inspire 156 mol air O daily.

We measured sheep rectal temperature on several occasions to monitor animal health, finding average healthy temperatures of 39.6°C (+/- 0.4°C) and sick temperatures of 40.1 (+/- 0.3°C), higher than the average large herbivore temperature of 38°C estimated by Kohn (1996). Our measurements are consistent with the 39.2 °C (+/- 0.4°C 1s.d.) mean reported daytime rectal temperature for a population of 35 sheep in Goodwin (1998), and with higher average summer temperatures (Refinetti & Menaker 1992; daSilva & Minomo 1995). We adopt a value of 39.0°C (+/- 0.5°C) as being broadly representative of mean sheep temperature over a diurnal cycle. External ambient temperatures, relative humidity and dew point used in our calculations are taken from Hanscom Air Force Base, two miles from the Concord Field Station. We use these measures to calculate vapor pressure deficit (VPD), the saturation vapor pressure – actual vapor pressure, to aid in estimation of animal evaporative water loss (Seager *et al.*, 2015).

We compared observed blood $\delta^{18}O$ compositions to steady-state expectations derived from models of Luz *et al.* (1984), Kohn (1996) and Podlesak *et al.*, (2008) using a least-squares metric.

3.3.4 Water flux modeling. Change in environmental oxygen sources over time and the speed of oxygen transit within the body further complicate characterization of δ_{bw}. Determination of water flux was among the first applications of experimental isotope work after the discovery of oxygen isotopes by Giauque and Johnston (1929). Only five years later Hevesy and Hofer (1934) used heavy water as a tracer, finding that the water half-life in humans is $t_{1/2}$ = 9 days, a figure consistent with later experiments (Richmond *et al.*, 1962; Leiper *et al.*, 2001). Water fluxes have been measured in a great number of organisms, and observations in a subset of large mammals are presented here (Table 1). Water half-lives tend to increase with increasing body size, and are

lower for aquatic animals. Among terrestrial animals, half-lives are lower for those who live near aquatic or mesic environments (Streit *et al.*, 1982). However, even within genera or species water flux times can vary substantially. Measurements of water half-lives in rats have ranged from 1.4-3.6 days, and in sheep, from 2.6-9.0 days (Lee and Lifson, (1960); Richmond *et al.*, (1962); MacFarlane *et al.*, (1971); Longinelli and Padalino, (1980); Luz *et al.*, (1984) Podlesak *et al.*, (2008). Experiments with deuterated water in humans demonstrate that flux times may vary substantially with activity level Leiper *et al.*, (2001).

Species	$T_{1/2}$ **(days)**	**Reference**
Rattus sp.	1.4-3.6	Lee and Lifson, (1960); Richmond *et al.*, (1962); Longinelli and Padalino, (1980); Luz *et al.*, (1984) Podlesak *et al.*, (2008)
Ovis aries	2.4 – 9.0	MacFarlane *et al.*, (1971); Dawson (1977)
Bos taurus	2.9 – 3.3	Roubicek (1969); MacFarlane *et al.*, (1971)
Rangifer tarandus	3.0 – 5.0	MacFarlane *et al.*, (1971)
Capra aegagrus	3.8 – 7.7	MacFarlane *et al.*, (1971) ; Dawson (1977)
Alces alces	4.5	MacFarlane *et al.*, (1971)
Canus familiaris	5.1	Richmond *et al.*, (1962)
Camelus dromedarius	5.3 – 6.1	MacFarlane *et al.*, (1971)
Taurotragus oryx	5.5 – 8.2	MacFarlane *et al.*, (1971)
Bos indicus	5.9 – 6.8	MacFarlane *et al.*, (1971)
Equus caballus	8.4	MacFarlane *et al.*, (1971)
Homo sapiens	8.4 – 13.0	Hevesy and Hofer (1934); Richmond *et al.*, (1962); Leiper *et al.*, (2001)
Connochaetes taurinus	9.1	MacFarlane *et al.*, (1971)
Alcelaphus buselaphus	10.6	MacFarlane *et al.*, (1971)
Ovibus moschatus	12.9	MacFarlane *et al.*, (1971)

Table 3.1 Measured half-lives, in days, of water in the bodies of several large herbivores and omnivores, made via deuterated or tritiated water dosing.

As reviewed in Podlesak *et al.*, (2008), $t_{1/2}$ can be calculated experimentally as an animal's body water isotope composition at time t, δ_t, transitions from an initial value δ_{init} towards a new steady state δ_{eq}:

$$t_{1/2} = \frac{t * ln(2)}{ln\left(\frac{\delta_{init} - \delta_{eq}}{\delta_t - \delta_{eq}}\right)} \quad \text{(eq. 3.11)}$$

In the event that multiple water stores turn over at different rates due to incomplete or partial mixing within the body, following Cerling *et al.*, (2007) these combine to determine δ_{bw} during equilibration:

$$\left(\frac{\delta_t - \delta_{eq}}{\delta_{init} - \delta_{eq}}\right) = \sum_{j}^{n} f_j \, e^{-\left(ln(2)/t_{1/2}\right)*t} \quad \text{(eq. 3.12)}$$

where f and $t_{1/2}$ are the fractional oxygen contribution and half-life of each pool j out of n pools altogether. Detection of secondary or tertiary turnover pools requires an experimental design that includes a prolonged sampling period following a drinking water switch. In our calculations we estimate that from August – November 2013 sheep consumed 8.4 liters of water (480 moles of oxygen) per day, based upon the provision of 11.5 liters per day, and an estimate of as much as 25% remaining in the trough or lost. This consumption rate is consistent with observations that sheep may consume anywhere from 4-15 liters of water daily, depending on their size, the moisture content of their food, and environmental conditions.

3.4 Results

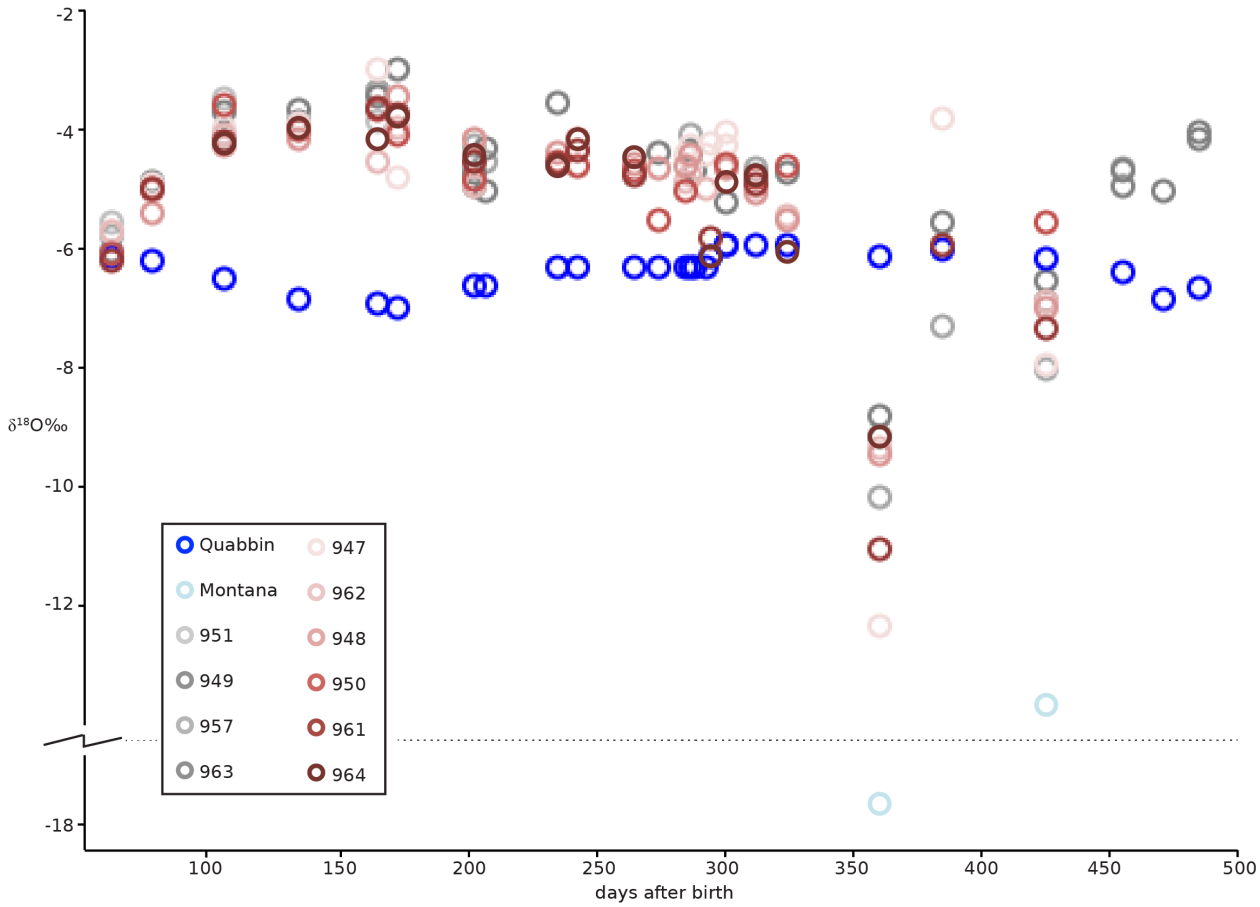

Figure 3.2 Blood measurements from control (gray) and experimental (red) sheep while at steady-state with Quabbin reservoir water (blue). Not every sample day includes measurements from all animals. Blood values from experimental animals during or after drinking Montana LFC water, and LFC water values, are excluded. The overall pattern of blood $\delta^{18}O$ is anticorrelated with drinking water except during major snowstorms when sheep consumed snow (light blue).

3.4.1 Blood values, turnover and variance. Average sheep blood $\delta^{18}O$ values are -5.86‰ (±0.24) when they arrive in Bedford following weaning, and increase to -3.95‰ within their first 6 weeks drinking Quabbin water and dry feed consumption (Fig. 3.2). Values are most enriched at the end of June (-3.60‰, ±0.46). For measurements made from control animals and switch animals at steady state with Quabbin water, values decreasd with some fluctuation to a low of -5.08‰ (±0.60) in December. During a series of snowstorms average blood values drop significantly (as

low as -9.93‰, ±1.20) Average blood $\delta^{18}O$ values begin to rise again in May (Fig. 3.2). For animals appearing to be at steady state with LFC water, average blood $\delta^{18}O$ is measure at -12.63‰ (±0.55) over a 66 day period.

During periods of steady-state with Quabbin reservoir control water or LFC water, and excluding periods of heavy snow, average blood $\delta^{18}O$ standard error for the entire population is 0.40‰, with standard error ranging from 0.18-1.44 through the duration of the experiment. Blood $\delta^{18}O$ population minimum and maximum differences among individuals average 0.96‰, and range from 0.30-3.48. During snowstorms, standard error increases substantially to 2.57‰, and minimum and maximum measurement range increase to 8.80‰. Through the duration of the entire experiment individual sheep blood $\delta^{18}O$ varied seasonally, with average within-individual variation at σ=0.72‰ (from 0.51-1.12‰), and average measurement range 2.52‰ (from 1.76-3.92‰). Including snowstorms, within-individual measures of variance double: average σ is 1.54‰ (from 1.32-2.16) and average range is 6.04‰ (from 2.48-9.34‰).

We find that fitted water oxygen half-lives vary from 2.2 – 2.9 days assuming a single oxygen pool, with no apparent dependence upon sex or weight (Fig. 3.3). In the two individuals subject to a longer switch, we are not able to detect a second turnover pool.

3.4.2 Model performances. Under conditions where feed $\delta^{18}O$ is constant, we find that blood values are determined by two factors: the ratio of drinking water to metabolic (feed and air) oxygen inputs (D:M), and the percentage of water output lost to evaporation and therefore fractionated (F%). We use the simplified framework of the Luz *et al.*, (1984) and Podlesak *et al.*,

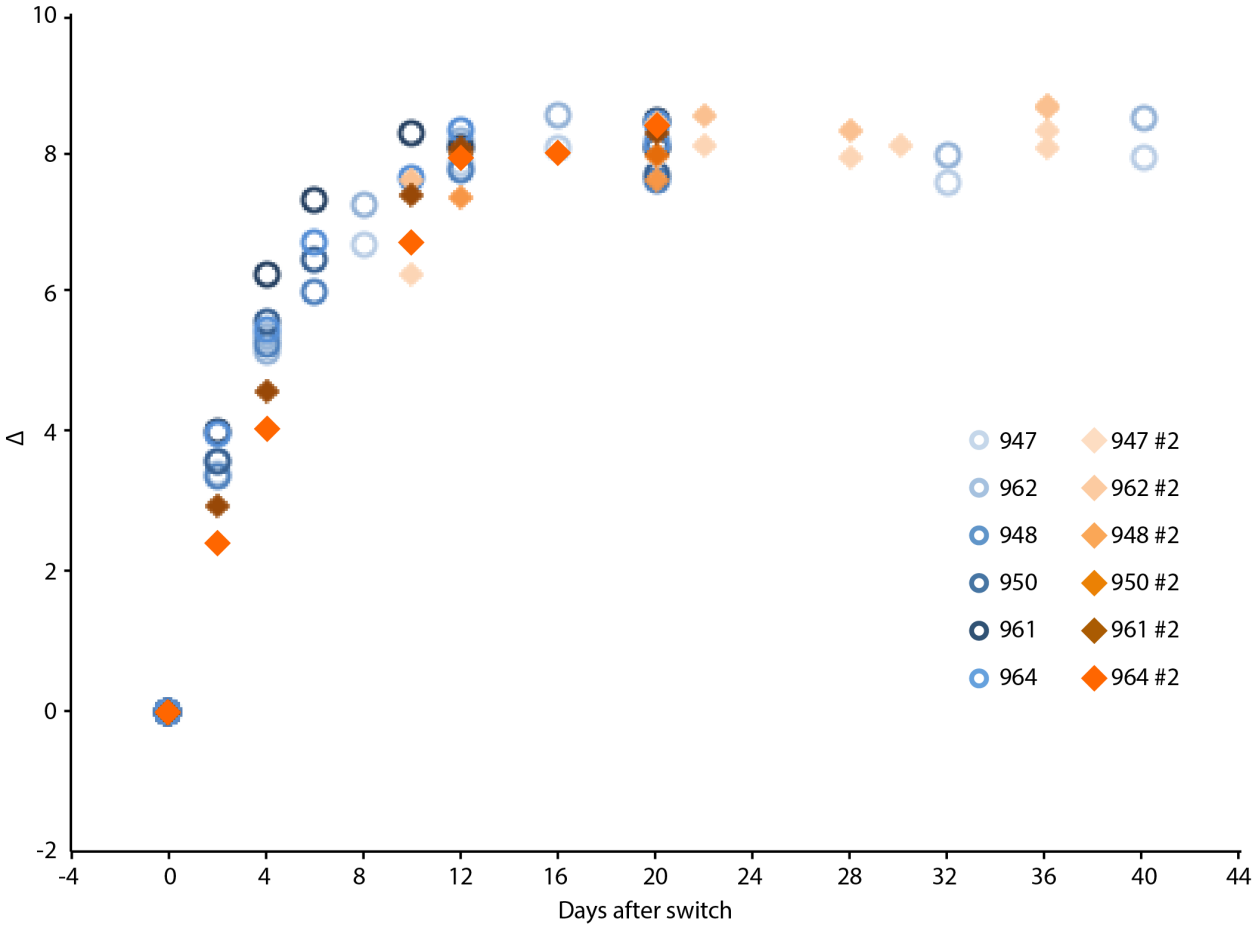

Figure 3.3 Sheep blood $\delta^{18}O$ reaches steady state with new water source while feed remains constant. Data are plotted as divergence from the initial value for each animal, set to 0; animals transitioning towards LFC water are shown in blue circles, and animals transitioning away from LFC water are shown orange diamonds. Two animals given a longer water switch to LFC water, 947 and 962, show no sign of a secondary turnover pool.

(2008) model (both return identical results, and are hereafter referred to only as Luz *et al.*, 1984) to determine most likely drink:metabolic oxygen input, and evaporative loss %, in our population. This is accomplished by evaluating model-data mismatch from August-November for all animals while they consume either Quabbin or LFC water, and through mean squared error (MSE) measures. We find that D:M oxygen input ratios may vary from approximately 1.2-2.5 with strong model performance, but that F% is generally constrained to 35-45 (Fig. 3.4).

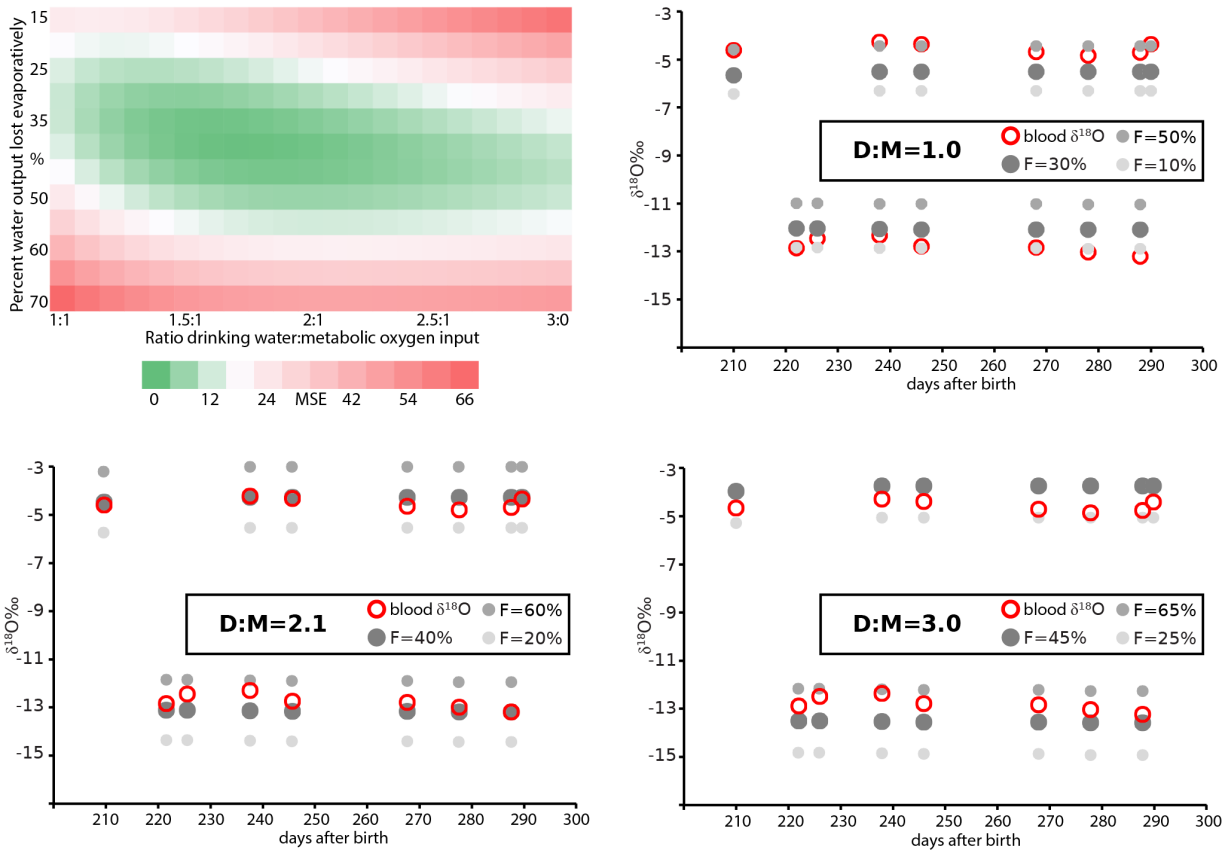

Figure 3.4 Model-data comparisons of D:M input oxygen ratios and water output F%. **Top left**, MSE from Luz *et al.*, (1984) predicted and observed $\delta^{18}O$ from August-October while sheep are at steady-state either Quabbin or LFC water, given different M:D and F% values. Best fits are green, poor fits are red. **Top right**, observed (red open circles) and modeled (gray closed circles) blood $\delta^{18}O$ values when modeled D:M = 1; modeled F% at 30 is shown in dark gray, with higher and lower modeled evaporative loss shown as lighter gray. **Bottom left**, modeled D:M = 2.1, and **Bottom right,** modeled D:M = 3. Higher modeled D:M values exaggerate drinking water $\delta^{18}O$ changes, while increasing modeled F% raises blood $\delta^{18}O$ values.

Drinking water $\delta^{18}O$ fluctuations are exaggerated in the model when D:M is overestimated, and are dampened when it is underestimated. Similarly, the model predictions are low relative to data when F% is too low, and high when F% is too high. We estimate that from August-November, D:M is likely 2.1 and F% likely 40%. This estimate is close to the D:M and F% values that minimize model-data MSE, but does not require that animals consumed above their daily feed or

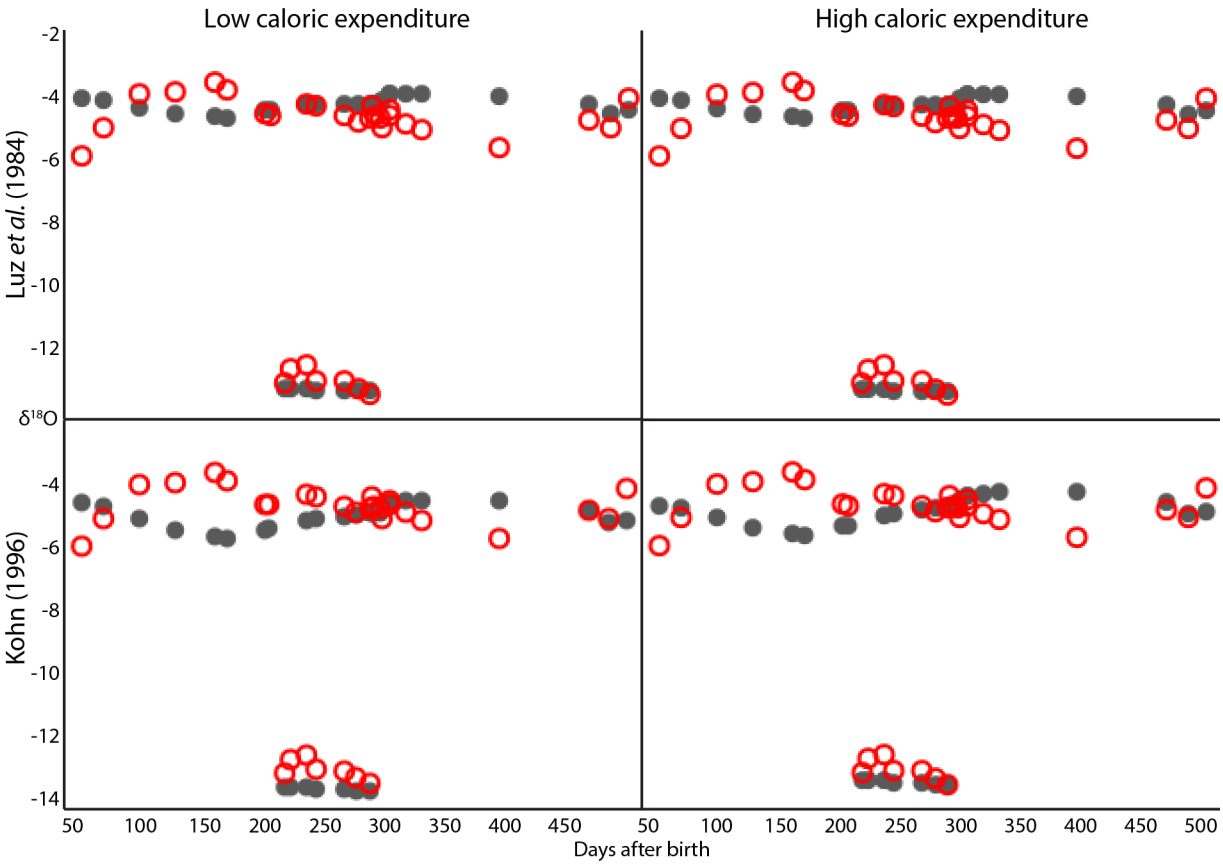

Figure 3.5 Data and model predictions for Luz *et al.* (1984) and Kohn (1996) at different calorie and oxygen flux magnitudes. Measured (red open circles) and modeled (solid gray circles) average sheep blood $\delta^{18}O$ values over time are shown over time for periods where sheep are at apparent steady state with their drinking water source. Luz *et al.*, (1984) model predictions are shown above, and Kohn (1996) predictions shown below, with low O flux (50-80 mol air O input for Luz *et al.* (1984) and Kohn (1996) on the left, respectively), and high flux (156 mol O) on the right.

water intake. It also is consistent with likely water consumption per calorie expenditure values of c. 18 – 25 g/KJ (Nagy 1987; Kohn 1996; Lane *et al.*, 1997). We test the Luz *et al.*, (1984) model using D:M=2.1 and F%=40 at a variety of caloric expenditures and oxygen flux magnitudes. Model results are identical when assuming a low average air O flux of 50 mol/day measured in adult Dorset sheep at rest (Entin *et al.*, 1999), which increases over time as sheep grow, or a fixed high air O flux of 156 mol/day based upon feed consumption (Fig. 3.5). We find that the Kohn (1996) model performs similarly, whether employed directly as described in the manuscript

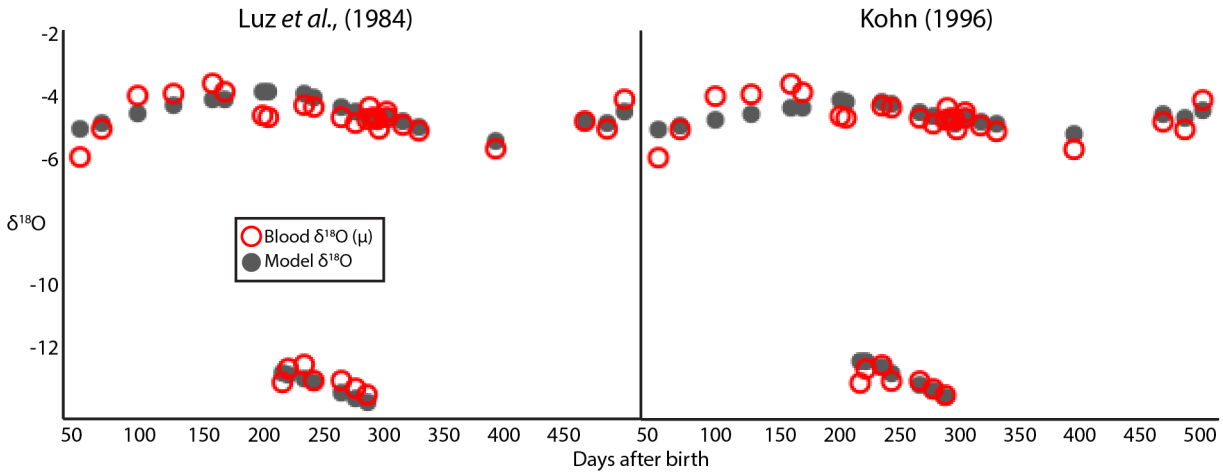
Luz et al., (1984)
Kohn (1996)
δ18O
Blood δ18O (μ)
Model δ18O
Days after birth

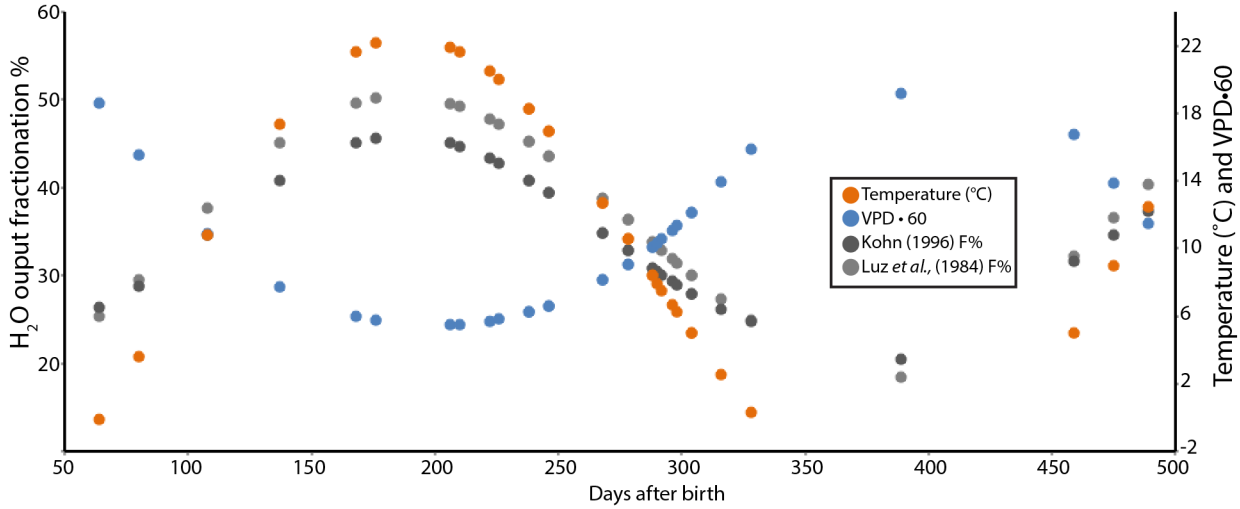
H2O ouput fractionation %
Temperature (°C) and VPD•60
Temperature (°C)
VPD • 60
Kohn (1996) F%
Luz et al., (1984) F%
Days after birth

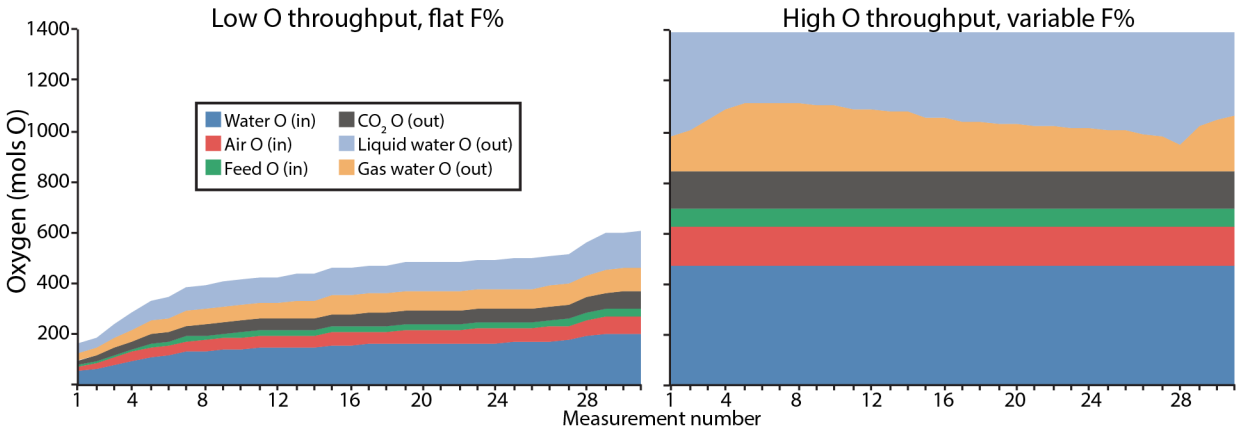
Low O throughput, flat F%
High O throughput, variable F%
Oxygen (mols O)
Water O (in)
Air O (in)
Feed O (in)
CO2 O (out)
Liquid water O (out)
Gas water O (out)
Measurement number

Figure 3.6: Modeling fractionated water loss. **Above**: Luz *et al.* (1984) and Kohn (1996) model predictions (filled gray circles) and observed blood $\delta^{18}O$ (open red circles) when F% is modeled as a function of ambient temperature. **Middle**: best-fit modeling (gray) of F% as function of ambient temperature (orange) from both Luz *et al.* (1984) and Kohn (1996), where evaporative loss is highest at highest temperatures; humidity is shown in blue. **Below**: total input and output daily oxygen fluxes (mol) assuming an average air O intake of 50 mol, linked to body weight (left) or a constant air O intake of 156 mol (right) calculated from feed composition. Right, variable F% is also shown (orange). Note: measurement number denotes an irregular scale, reflecting the n^{th} sample collected from animal blood or drinking water. Apparently rapid changes in measurement numbers 1-6 and 24-28 result from infrequent sample collection, so that long term changes are graphically condensed.

(average of 80 mol air O/day, increasing over time with mass), or assuming 156 mol/day based on feed composition. In all cases, both models perform strikingly well, with 28% and 34% of predicted values falling within measurement error (0.3‰) of measurements for the Luz and Kohn models, respectively. The Kohn (1996) model predicts slightly lower blood $\delta^{18}O$ (0.6‰ on average), due to an atmospheric water vapor input term. Both models produce a pattern of seasonal variation that closely tracks Quabbin drinking water, where values are higher in the winter, and lower in the summer, a result of the Quabbin Reservoir's utilization rate in Lexington and Bedford. Model predictions are however anticorrelated with measured blood $\delta^{18}O$ seasonal variation. This phenomenon is slightly amplified in the Kohn model, as a result of higher predicted atmospheric vapor intake during humid summer months.

We adapt both models by proposing that F% is a linear function of ambient temperature and VPD, and optimize function parameters by comparing model predictions to the data. Both models predict nearly identical F%-temperature relationships and closely replicate observed blood $\delta^{18}O$ (Fig. 3.6). In the Luz *et al.*, (1984) model, 28% of predicted values are within measurement error (0.3‰) of data prior to fitting. Introducing temperature-sensitive evaporative loss increases this number to 47%. In the Kohn (1996) model, predictions within measurement error rise from 34% to 66% with evaporative fitting. Using temperature-sensitive evaporation, both models render 100% of predictions within 1‰ of observations.

3.5 Discussion

In our population some observed blood $\delta^{18}O$ variation is undoubtedly due to minor behavioral differences between animals. For instance during summer months, animals may have foraged

minimal quantities of grass at the margins of their pen; in the autumn falling oak leaves were also available. Grass or leaf consumption would have tended to increase blood $\delta^{18}O$ values of animals investing greater effort in consuming them, and may explain elevated variability in late June and early July (peak insolation) and in late October and early November. Similarly, animals likely consumed snow at different rates during snowstorms. The lowest blood values measured in this study, when animals were not drinking LFC water, derive from one animal (947) that was observed eating snow.

It is also possible that some observed variation results from physiological differences in water flux. Water turnover rates are high, with $T_{1/2}$ values at and below those previously reported. These rates are consistent with estimates of normal water consumption given the quantity of dry feed consumed: 3-5 liters/kg depending upon ambient temperatures between 0-25°C (Roubicek 1969). Furthermore, these $T_{1/2}$ values are consistent with the elevated water consumption rates measured in our animals, and sheep % total water mass of 45-55% (Roubicek 1969; Oberbauer *et al.*, 1994). Given animal masses of 60-75kg measured during the experimental switches, and estimated water intake rates (470-640 mol), predicted $T_{1/2}$ is 1.8-3.4 days. These predicted values exactly bracket observed turnover times, and are simply derived from $T_{1/2} = \ln(2) / \lambda$, where the total water oxygen pool $N = -\lambda(dN / dt)$, and dN / dt is daily water oxygen turnover (Cerling *et al.*, 2007). It is possible that large overall oxygen fluxes and caloric expenditure are consistent with insulin resistance and metabolic disorder, driven by a calorie-rich, processed diet, and the absence of roughage (O'Grady *et al.*, 2010). It is also possible that fluxes are somewhat lower than estimated, which would be consistent with rapid, observed turnover if body fat % is high, and water pools are correspondingly lower (Roubicek 1969; Oberbauer *et al.*, 1994).

While model-data optimization suggests that efficiency of water use per calorie may vary with relatively little impact on blood $\delta^{18}O$, blood values are by contrast more sensitive to fractionated water loss. This result is consistent with Kohn (1996)'s sensitivity testing, and appears further bolstered by the extent to which temperature-sensitive evaporative loss closely aligns both models with observations. Slight variations in preferred temperature, panting behavior, or peripheral vasodilation to increase heat loss might also contribute to observed variation between individuals within the population. As discussed by Kohn (1996), the extent to which an animal loses water to panting, and the fractionation factor of water lost transcutaneously, are difficult to estimate. Further study to characterize these parameters would improve models predicting blood $\delta^{18}O$ from environmental conditions.

The performance of both Luz *et al.*, (1984) and Kohn (1996) models suggests that both may be employed with confidence, provided that D:M and F% are appropriately estimated. The extent to which both models predict even minor features of observed data when F% is linked to temperature is remarkable. This predictive power is especially important for understanding temporal variation in blood $\delta^{18}O$ in response to environmental seasonality, and associated changes in evaporative loss across wet and dry regimes. In the tropics, where temperature variation is limited, rainfall $\delta^{18}O$ variation is also low, typically on the order of 2-8‰ intra-annually (Bowen 2011). Both rainfall and temperature contribute to seasonal landscape aridity, which is notoriously complex in East Africa (Herrmann and Mohr, 2011). One application of appropriately quantifying evaporative loss over time is the reconstruction of blood $\delta^{18}O$ from serial tooth samples that form over changing seasons. While serial sampling is an increasingly

common technique, variation in enamel $\delta^{18}O$ may reflect half or less of the original variation in animal blood $\delta^{18}O$, depending upon the scale of discrete samples, the duration of mineralization processes, and the complexity of the environmental and blood record (Chapter 4).

In the context of ecological and paleontological study, this dataset may be viewed as a baseline for the minimum variation that can be expected within any single, homogeneous population with the same feed and water sources. Hypotheses regarding niche separation and ecological function should anticipate that for large herbivores, σ may rise above 1‰ and range increase above 2‰ even if all animals are closely related and interact with nearly identical environmental inputs. High baseline variation will influence the interpretation of $\delta^{18}O$ values from herbivore teeth at paleontological sites relevant to human origins. Ludecke *et al.*, (2016) report that serial enamel carbonate $\delta^{18}O$ values from three Pliocene Malawi rift *Alcelaphus* individuals, identified as belonging to different genera, are 26.2 (σ=0.98‰, range=3.20‰), 27.98 (σ=0.34‰, range=0.80‰) and 24.93 (σ=0.70‰, range=2.20‰). While carbon isotope measurements help demonstrate foraging pattern differentiation among these taxa, $\delta^{18}O$ measurements cannot clearly distinguish *Alcelaphus* genera. In the Turkana Basin, the differences between average Hippopotamus, Elephant and Cercopithecoid enamel carbonate $\delta^{18}O$ values are 4.0‰, 3.5‰ and 2.6‰ in the present, early Pleistocene and early Pliocene, respectively (Quinn, 2015). In Turkana today, rainfall has been measured at -0.3‰ with relatively minimal variation (σ=2.3‰, range=5.6‰), though by including a greater diversity of available water sources including Lake Turkana, the Omo River, watering holes, springs and streams, water $\delta^{18}O$ sources vary by as much as 11‰ (Quinn 2015). These results suggest that while oxygen isotope measurements may be potent tools for reconstructing landscape hydrology and animal interaction with the

environment, additional sources of information, including carbon isotope ratios, dental morphology, skeletal adaption, assemblage composition and other environmental contexts are necessary for adequately interpreting $\delta^{18}O$ values from fossil data.

3.6 Conclusions

Oxygen isotope values of sheep raised under controlled conditions provide a useful framework for interpreting variation observed in large herbivores from wild, archaeological, and paleontological contexts. We find that variation in blood $\delta^{18}O$ σ at any given point in time among the population of sheep varies from c. 0.2-1.0‰ (1 σ) throughout the experiment. This rises to 2.8‰ following snowstorms, during which behavioral observations and blood measurements both reveal differences among the animals in their propensity to eat snow. This shift along with population level variation in midsummer and late fall, suggest that blood $\delta^{18}O$ may also record slight differences in behavior or physiological response to water stress. We find that available models predict average blood $\delta^{18}O$ from environmental sources well, and that model performance is driven primarily by two factors: drinking water to metabolic oxygen intake ratios, and evaporative water loss. By linking evaporative water loss magnitude to ambient temperature, we improve model performance substantially, making this more applicable to seasonality reconstruction. The expected variation in population baseline presented here will help with continued efforts to reconstruct past climatic and seasonal environments from animal tissues, using models that relate animal and environmental $\delta^{18}O$.

3.7 References

Bowen GJ (2010) Isoscapes: Spatial Pattern in Isotopic Biogeochemistry. *Annual Reviews in Earth and Planetary Sciences* **38**:161-87.

Bryant JD, Froelich PN (1995) A model of oxygen isotope fractionation in body water of large mammals. Geochimica et Cosmochimica Acta. 59(21):4523-37.

Bryant JD, Koch PL, Froelich PN, Showers WJ, Genna BJ (1996) Oxygen isotope partitioning between phosphate and carbonate in mammalian apatite. Geochimica et Cosmochimica Acta. 60(24):5145-8.

Cain JW, Krausman PR, Rosenstock SS, Turner JC (2006) Mechanisms of thermoregulation and water balance in desert ungulates. Wildlife Society Bulletin. 34(3):570-81.

Cerling TE, Ayliffe LK, Dearing MD, Ehleringer JR, Passey BH, Podlesak DW, Torregrossa AM, West AG (2007) Determining biological tissue turnover using stable isotopes: the reaction progress variable. Oecologia. 151(2):175-89.

Chang SJ, Blake RE (2015) Precise calibration of equilibrium oxygen isotope fractionations between dissolved phosphate and water from 3 to 37 C. Geochimica et Cosmochimica Acta. 150:314-29.

Dawson TE, Mambelli S, Plamboeck AH, Templer PH, Tu KP (2002) Stable isotopes in plant ecology. Annual review of ecology and systematics. 507-59.

Ellis WA, Melzer A, Green B, Newgrain K, Hindell MA, Carrick FN (1995) Seasonal-Variation in Water Flux, Field Metabolic-Rate and Food-Consumption of Free-Ranging Koalas (Phascolarctos-Cinereus). Australian Journal of Zoology. 43(1):59-68.

Entin PL, Robertshaw D, Rawson RE (1999) Effect of locomotor respiratory coupling on respiratory evaporative heat loss in the sheep. Journal of Applied Physiology. 87(5):1887-93.

Gat J. (1996) Oxygen and hydrogen isotopes in the hydrologic cycle. *Annual Review of Earth and Planetary Sciences* **24**:225262.

Gretebeck RJ, Schoeller DA, Socki RA, Davis-Street J, Gibson EK, Schulz LO, Lane HW (1997) Adaptation of the doubly labeled water method for subjects consuming isotopically enriched water. Journal of Applied Physiology. 82(2):563-70.

Karihaloo AK, Combs W (1971) Some maternal effects on growth in lambs produced by reciprocal crossbreeding between Lincoln and Southdown sheep. Canadian Journal of Animal Science. 51(2):511-22.

Kirsanow K., and Tuross N. (2011) Oxygen and hydrogen isotopes in rodent tissues: Impact of diet, water and ontogeny. *Palaeogeography, Palaeoclimatology, Palaeoecology* 310(1):9-16.

Kohn MJ, Schoeninger MJ, Valley JW (1998) Variability in oxygen isotope compositions of herbivore teeth: reflections of seasonality or developmental physiology? *Chem Geo* 152:97.

Lane HW, Gretebeck RJ, Schoeller DA, Davis-Street J, Socki RA, Gibson EK (1997) Comparison of ground-based and space flight energy expenditure and water turnover in middle-aged healthy male US astronauts. The American journal of clinical nutrition. 65(1):4-12.

Leiper JB, Pitsiladis Y, Maughan RJ (2001) Comparison of Water Turnover Rates in Men Undertaking Prolonged Cycling Exercise and Sedentary Men. Int J Sports Med; 22(3): 181-185.

Kirsanow K, Tuross N (2011) Oxygen and hydrogen isotopes in rodent tissues: Impact of diet, water and ontogeny. *Palaeogeogr, Palaeoclim, Palaeoecology* 310:9-16.

Kohn MJ (1996) Predicting animal δ18O: accounting for diet and physiological adaptation. *Geochimica et Cosmochimica Acta.* 60(23):4811-29.

Lécuyer C, Amiot R, Touzeau A, Trotter J. Calibration of the phosphate δ18O thermometer with carbonate–water oxygen isotope fractionation equations (2013) Chemical Geology. 347:217-26.

Levin NE, Cerling TE, Passey BH, Harris JM, Ehleringer JR (2006) A stable isotope aridity index for terrestrial environments. Proceedings of the National Academy of Sciences. 103(30):11201-5.

Levin NE, Zipser EJ, and Cerling TE (2009) Isotopic composition of waters from Ethiopia and Kenya: Insights into moisture sources for eastern Africa. *Journal of Geophysical Research* **114**:D23306.

Longinelli A, Nuti S. Revised phosphate-water isotopic temperature scale (1973) Earth and Planetary Science Letters. 19(3):373-6.

Longinelli A, Padalino AP (1980) Oxygen isotopic composition of water from mammal blood: first results. *Eur J Mass Spectrom Biochem Med Env Res* 1:135-139.

Longinelli A (1984) Oxygen isotopes in mammal bone phosphate: a new tool for paleohydrological and paleoclimatological research? *Geochim Cosmochim Acta* 48:385-390.

Longinelli A, Iacumin P, Davanzo S, Nikolaev V (2003) Modern reindeer and mice: revised phosphate–water isotope equations. Earth and Planetary Science Letters. (3):491-8.

Longinelli A, Selmo E (2011) δ18O values of Sus scrofa blood water and bone phosphate; a marked discrepancy between domestic and wild specimens. Rapid Communications in Mass Spectrometry. 24:3732-4.

Lüdecke T, Mulch A, Kullmer O, Sandrock O, Thiemeyer H, Fiebig J, Schrenk F (2016) Stable isotope dietary reconstructions of herbivore enamel reveal heterogeneous savanna ecosystems in the Plio-Pleistocene Malawi Rift. Palaeogeography, Palaeoclimatology, Palaeoecology. 459:170-81.

Luz B, Kolodny Y, and Horowitz M (1984) Fractionation of oxygen isotopes between mammalian bone-phosphate and environmental drinking water. *Geochimica et Cosmochimica Acta*. 48:1689-93.

Nagy KA (1987) Field metabolic rate and food requirement scaling in mammals and birds. Ecological monographs. 57(2):111-28.

Oberbauer AM, Arnold AM, Thonney ML (1994) Genetically size-scaled growth and composition of Dorset and Suffolk rams. Animal Production. 59(02):223-34.

O'Grady SP, Wende AR, Remien CH, Valenzuela LO, Enright LE, Chesson LA, Abel ED, Cerling TE, Ehleringer JR (2010) Aberrant water homeostasis detected by stable isotope analysis. PLoS One. 5(7):e11699.

Podlesak DW, Torregrossa AM, Ehleringer JR, Dearing MD, Passey BH, Cerling TE (2008) Turnover of oxygen and hydrogen isotopes in the body water, CO 2, hair, and enamel of a small mammal. *Geochim Cosmochim Acta*, *72*:19-35.

Pucéat E, Joachimski MM, Bouilloux A, Monna F, Bonin A, Motreuil S, Morinière P, Hénard S, Mourin J, Dera G, Quesne D (2010) Revised phosphate–water fractionation equation reassessing paleotemperatures derived from biogenic apatite. Earth and Planetary Science Letters. 298(1):135-42.

Quinn RL (2015) Influence of Plio-Pleistocene basin hydrology on the Turkana hominin enamel carbonate δ18O values. Journal of human evolution. 86:13-31.

Roubicek CB (1969) Water metabolism. Animal Growth and Nutrition. Lea & Febiger, Philadelphia. 353-73.

Streit, B (1982) Water turnover rates and half-life in animals studied by use of labeled and non-labeled water. *Comparative Biochemistry and Physiology*, 72A(3):445-454.

Taylor CR (1970) Dehydration and heat effects on temperature East African ungulates. American Journal of Physiology. 219(4)1136-9.

Wang Y, Kromhout E, Zhang C, Xu Y, Parker W, Deng T, Qiu Z (2008) Stable isotopic variations in modern herbivore tooth enamel, plants and water on the Tibetan Plateau: Implications for paleoclimate and paleoelevation reconstructions. Palaeogeography, Palaeoclimatology, Palaeoecology. 260(3):359-74.

Wiedemann-Bidlack FB, Colman AS, Fogel ML (2008) Phosphate oxygen isotope analysis on microsamples of bioapatite: removal of organic contamination and minimization of sample size. *Rapid Comm Mass Spectrom* 22:1807-1816.

4

High-resolution stable isotope analyses reveal tooth mineralization patterns for climate reconstruction

4.1 Abstract

Seasonal climate patterns impact ecosystem productivity, and are hypothesized to have influenced early human subsistence and technological development. Rainfall patterns are reflected by oxygen isotope ratios ($\delta^{18}O$ values) in mammalian tooth enamel, which records environmental chemistry during mineralization. Seasonal variation in landscape hydrology results in spatial variation in tooth phosphate $\delta^{18}O$, and fossilized herbivore molars are commonly used for climate reconstruction. However, this approach has been hampered by incomplete knowledge of isotope incorporation during tooth mineralization. Here we integrate a new synchrotron-based mineralization model with blood oxygen isotope turnover to produce high-resolution isomap predictions. First, we devise a method to test these predictions with fine-scaled phosphate $\delta^{18}O$ measurements in a sheep subjected to a controlled water switch. Isotopic measurements demonstrate that enamel secretion and maturation waves advance at nonlinear rates with distinct geometries, and include isotopic shifts during enamel maturation from amorphous precursors. Next, we combine these discoveries to produce an inverse modeling system for reconstructing water $\delta^{18}O$ inputs from tooth isotopic measurements. Modeling suggests that this system reconstructs precipitation histories at different latitudes with striking fidelity, and it accurately reproduces the controlled switch of the experimental sheep. By

accounting for nonlinear growth with our model, even simple conventional sampling approaches may yield accurate reconstructions. Last, we use model-data discrepancies from additional sheep to further refine our mineralization model, and constrain the phosphate-water $\delta^{18}O$ offset, a parameter critical to paleoenvironmental research. Tooth isotopic measurements facilitate quantitative reconstructions of seasonal water input patterns, aiding in paleoclimate research and further exploration of the relationships between climate, behavior and human evolution.

4.2 Introduction

4.2.1 Seasonality, evolution and adaptation. Seasonal climate patterns in water and resource availability influence human and primate behavior, adaptation and evolution (Marshall and Wrangham 2007; Potts 2013; Isler and Van Schaik 2014; Melin *et al.*, 2014). Human subsistence, health and conflict are all sensitive to ecosystem stability, and changes in the seasonality of precipitation are recognized as an important consequence of contemporary climate change (Sellen 2000; Hsiang *et al.*, 2013; Kumar 2013; Morin and Comrie 2010; Watson *et al.*, 2013; Garcia *et al.*, 2014). More broadly, seasonal precipitation regimes are major determinants of ecosystem structure, regulating grassland, savannah and forest plant communities (Vincens *et al.*, 2007; Good and Caylor 2011; Mayer and Khalyani 2011; Hoetzel *et al.*, 2013). Seasonal rainfall cycles can be inferred from spatial variation in the mineral composition of teeth, because the stable oxygen isotope composition ($\delta^{18}O$ value) of precipitation exhibits characteristic variation that is recorded in teeth as they grow over time (Bryant *et al.*, 1996; Gat 1996; Bowen and Revenaugh 2003; Balasse *et al.*, 2012). The $\delta^{18}O$ of body water and blood of animals drinking surface waters reflects the $\delta^{18}O$ of precipitation, alongside food, air and physiological processes

(Longinelli and Padalino 1980; Kohn *et al.*, 1998; Podlesak *et al.*, 2008). Oxygen in blood plasma phosphate, carbonate, and hydroxyl ions equilibrates isotopically with blood water, and these ions retain their isotopic composition as they are incorporated into tooth enamel hydroxyapatite (HAp) (Cerling and Sharp 1996). Thus, tooth $\delta^{18}O$ values provide an important record of recent and ancient seasonal climatic patterns, bearing in mind that animal behavior, physiology, and local hydrology can also influence the relationship between environmental and individual isotopic compositions.

4.2.2 Documenting seasonality in teeth. Tooth $\delta^{18}O$ can be measured to make inferences about past seasonal water sources using several techniques. While enamel and dentin are both viable tissues for isotope analysis, enamel is favored for fossil specimens because it is more resistant to diagenetic modification over geological timescales (Kohn and Cerling 2002; Kirsanow *et al.*, 2008). Enamel carbonate $\delta^{18}O$ is sampled in bulk or through microdrilling, which also allows an estimate of the dietary incorporation of arid-adapted C4 plants from carbon isotopes ($\delta^{13}C$) (Pellegrini *et al.*, 2011). Laser or ion-based ablative techniques can sample enamel $\delta^{18}O$ or $\delta^{13}C$ in much smaller quantities, but cannot distinguish between oxygen in phosphate, carbonate and hydroxyl ions. This lack of discrimination is problematic because these ions have different susceptibilities to diagenetic alteration (Passey and Cerling 2006; Sponheimer *et al.*, 2006; Aubert *et al.*, 2012; Blumenthal *et al.*, 2014), and the processes determining their incorporation into mineral may vary. Enamel phosphate is particularly useful for the study of hydrology as bulk phosphate oxygen fractionation from water into teeth is well understood, and substitution after death and burial is limited (Kohn and Cerling 2002; Pellegrini *et al.*, 2011; Longinelli 1984; Daux *et al.*, 2008; Gehler *et al.*, 2011; Kirsanow and Tuross 2011). Importantly, accurate $\delta^{18}O$

measurements can be made from very small enamel samples, which facilitates high-resolution intra-tooth sequential sampling, or repeated isotope measurements across a single tooth (Sponheimer *et al.*, 2006; Wiedemann-Bidlack *et al.*, 2008; Fricke and O'Neil 1996). Conventional bulk sampling approaches are limited by the problem of time-averaging, where a single low-resolution sample may include enamel secreted and mineralized over months or even years.

Because of their large size and abundance in the fossil record, ungulate teeth are regularly sampled for $\delta^{18}O$ to reconstruct seasonal pastoralist practices, hydrology, feeding and migratory behaviors (Longinelli and Padalino 1980; Zazzo *et al.*, 2010; Stevens *et al.*, 2011). Despite these efforts, the significance of intra-tooth $\delta^{18}O$ fluctuations is difficult to evaluate because ungulate tooth mineralization remains poorly understood. In particular, it is unknown how mineralization integrates and dampens seasonal $\delta^{18}O$ shifts in drinking water during incorporation into blood and ultimately enamel (Passey and Cerling 2002; Passey *et al.*, 2005). Efforts to infer aspects of past climate or diet from sequential isotope sampling rely on models of mineralization developed for ever-growing canines and incisors. It is unclear if these models are appropriate for ungulates, which form their large molars at variable rates over a fixed period (Zazzo *et al.*, 2010; Passey and Cerling 2002; Passey *et al.*, 2005; Kohn 2004; Zazzo *et al*, 2012), or how developments in the understanding of HAp mineralization affect interpretations of isotopic patterns (Beniash *et al.*, 2009; De Yoreo *et al.*, 2015). Furthermore, enamel mineral $\delta^{18}O$ values are offset from blood by a factor known as $\Delta_{PO4\text{-}H2O}$ that remains unconstrained, with different models producing uncertainty as high as 3‰ (Longinelli and Nuti, 1973; Lecuyer 2013; Pucéat *et al.*, 2010; Chang

and Blake 2015). An accurate understanding of mineralization in ungulates is critical to efforts linking seasonal patterns to $\delta^{18}O$ values in teeth.

4.2.3 Tooth mineralization and inverse method reconstruction. Tooth enamel mineralization is traditionally conceptualized in two stages: secretion and maturation (Simmer *et al.*, 2012). During secretion, enamel-forming cells (ameloblasts) secrete a proteinaceous matrix that controls the formation of amorphous calcium phosphate (ACP) and its transformation into HAp (Beniash *et al.*, 2009; Simmer *et al.*, 2012; Diekwisch 1998; Smith 1998). Through extension, secretion advances towards the future enamel cervix and root, adding organic matrix and mineral lattice from the enamel-dentin junction (EDJ) towards the enamel surface. Secreted enamel accounts for only 20-30% of mature mineral weight (Passey and Cerling 2002; Simmer *et al.*, 2012). The majority of mineral is added during maturation, a diffuse process that begins with delay once ameloblasts complete secretion and full enamel thickness is reached (Smith 1998; Driessens and Verbeeck 1990; Chapter 2).

Two principle models have been proposed to explain maturation phase geometry and timing during mineralization (Passey and Cerling 2002; Suga 1982; Hoppe *et al.*, 2004). One of these, designed for ever-growing teeth (Passey and Cerling 2002), has subsequently been deployed to solve for original body fluid carbon isotope composition in an experimentally manipulated rabbit and in sheep (Passey *et al.*, 2005; Zazzo *et al.*, 2010). The process by which original body fluid compositions are estimated from tooth isotopic compositions, using both physiological and mineralization models, is described as an "inverse" method (Passey *et al.*, 2005). However, a recent empirical and synchrotron-based mineralization model demonstrates that both secretion

and maturation advance with differing geometries and at nonlinear rates (Chapter 2). Here, we conduct an experiment to test the power of this model to predict large herbivore tooth isotope distributions. Our results confirm that the timing and geometry of tooth $\delta^{18}O$ values are determined, in part, by phosphate oxygen exchange during mineralization. We then develop an inverse method that uses nonlinear optimization to estimate original drinking water inputs, facilitating comparisons of our high-resolution (2D) samples with conventional (1D) samples. This method reconstructs specific seasonal patterns from tooth isotope measurements during simulations, and accurately reconstructs the drinking water history of an experimental animal.

4.3 Methods

4.3.1 Experimental water switch and dicing. To test the accuracy and capacity of the new synchrotron-based mineralization model to link environmental $\delta^{18}O$ history with tooth isomaps, we raised 10 sheep at the Concord Field Station in Bedford, MA following weaning at two months of age. All sheep were fed from a single batch of dry feed, and provided Lexington, MA drinking water (ranging from -7.4 to -5.9 $\delta^{18}O$‰ throughout the experiment) originating from the 1.5km^3 Quabbin Reservoir. At different times in the experiment we provided certain sheep with glacial melt water (-19.38 $\delta^{18}O$‰, 1 s.d.=0.05 over the duration of the switch) collected from Lake Fork Creek (LFC) in the Beartooth Mountains near Red Lodge, MT (Chapter 3). This chapter primarily analyzes data from sheep 962, which received LFC water for a "long switch" between 201 and 263 days of age. Additional animals received either control (949), short switch (950), double switch (964), or long switch (947) LFC water doses (Chapter 3). At 201, 221, 263 and 283 days of age subcutaneous calcein injections (8mg/kg) were given. Jugular IV blood

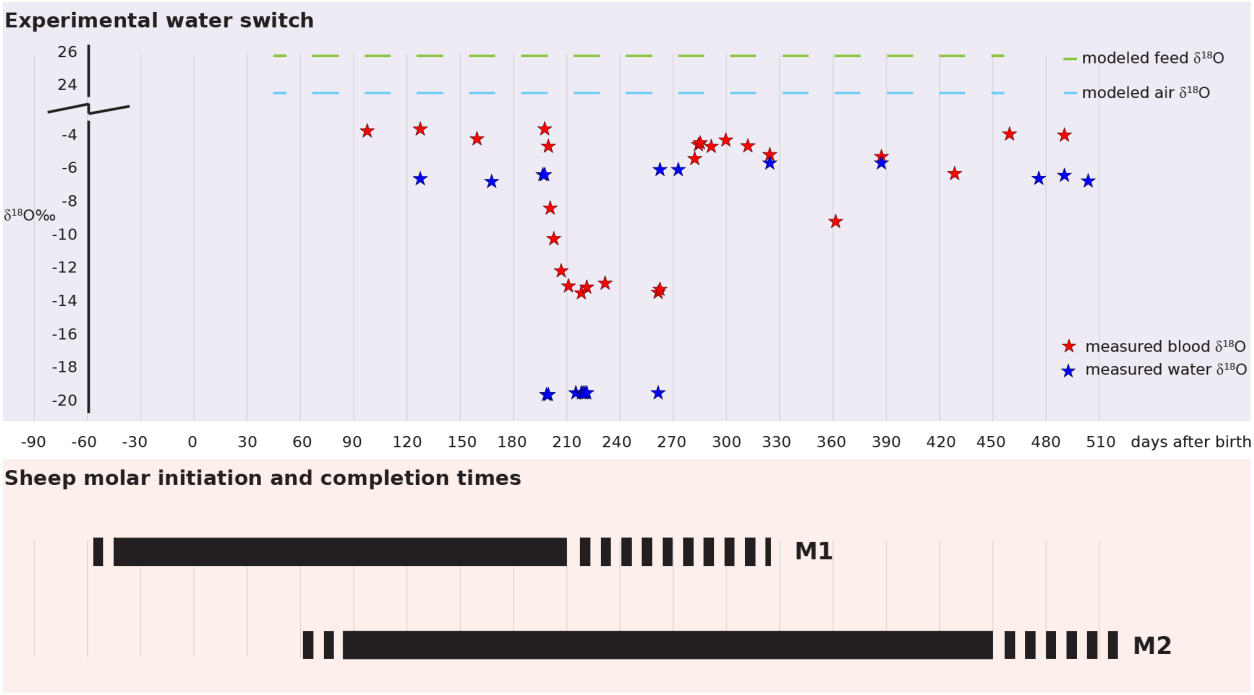

Figure 4.1 Experimental set-up for the sheep water switch experiment, which holds feed (green line) and inspired air (light blue line) $\delta^{18}O$ constant, while switching measured drinking water (sheep 962, blue stars) and blood (sheep 962, red stars) to an isotopically lighter source from 201-263 days. Estimated first (M1) and second (M2) molar mineralization initiation and completion times are shown below, with dashed lines representing uncertainty in initiation and completion timing. The experimental water switch was planned to occur during the middle of M2 formation.

samples were collected at regular intervals prior to, during and after the water switch. At 1.4 years of age we sacrificed all sheep by 180mg/kg IV sodium pentobarbital injection. Animal care and data collection protocols were approved by the Harvard University Faculty of Arts and Sciences Institutional Animal Care and Use Committee.

The lower left M2s were manually extracted from sheep 962 and four other animals, soft tissues removed, and embedded in methymethacrylate. The mesial lophs were sectioned with a Buehler Isomet saw to produce two 1mm-thick sections at the maximum buccal-lingual loph breadth. For each tooth, one section was glued onto a silica wafer and diced using a Disco DAD3240 dicing

saw and zinc alloy blade (DZAD1150 Z09-SD2000-Y1-60, Disco). The teeth were diced at 1.530mm x 0.180mm increments, with long axis cuts (1.530mm) proceeding from the cusp tip to root, and short axis cuts proceeding from the EDJ to the enamel surface. Cut depth was 0.600mm, and blade advance and water jet speeds were reduced to minimize sample loss. This method yields 3-6 rows and 23-26 columns of blocks for analysis, 80 – 130 individual blocks and on average 260 samples for analysis (because of sample replicates from individual blocks) per tooth section. This represents the highest spatial resolution tooth phosphate oxygen isotope measurements of which we are aware.

4.3.2 Oxygen isotope measurements. After dicing, each block was removed under a microscope using fine forceps and placed in a separate 2ml microcentrifuge tube. The resultant enamel samples were 0.4-0.6mg. Following the Colman (2002) and Wiedemann-Bidlack *et al.* (2008) protocols for silver phosphate microprecipitation, samples were pre-treated overnight with a 2.5% NaOCl solution to remove trace organics, centrifuged and rinsed in DI water five times, and dissolved overnight in 100µl 2M HNO_3 (s34-s35). For 962 samples, dissolved Ca^{2+} was removed by adding 100µl 2M HF and 150µl 2M NaOH to each sample for 1-4 hours to precipitate CaF_2. The resultant suspension was centrifuged to pellet CaF_2, and the supernatant transferred to a pipette bulb. The solution was reacted at 50°C with 750µl silver-ammine solution (0.067M $AgNO_3$, 0.12M NH_4NO_3, 0.43M NH_4OH), 450µl 1.25M NH_4NO_3 buffer and 90µl 1:1 NH_4OH until solution volume was brought below 250µl (ca. 12 hours). For the additional four animals, Ag_3PO_4 samples were produced using a crash precipitation technique that is similar to that described above, but generates higher yields (Mine *et al.*, 2017). Ag_3PO_4 precipitates were then

rinsed six times with 1000μl DI to remove silver nitrate solution, dried, and weighed into silver foil capsules. A single apatite sample yielded sufficient Ag_3PO_4 for one to three x 250-300 mg aliquots of Ag_3PO_4 for analysis.

The oxygen isotope analysis was completed using a ThermoFisher (Bremen, Germany) TCEA system operated at 1450°C to thermally decompose the phosphate and produce CO from reaction between the released O and the graphite and glassy carbon reactor. The CO was entrained in a He carrier gas, and conveyed to a Delta V Plus isotope ratio mass spectrometer (irms) via a Conflo IV open split. Isotopic compositions are reported using standard $\delta^{18}O$ notation in units of ‰ on the Vienna Standard Mean Ocean Water (VSMOW) scale, and precision was 0.15‰ (1 s.d.) for within-sample replicates. Samples were analyzed relative to lab internal standards, which were reagent Ag_3PO_4 from Strem Chemicals (Newburyport, MA, USA), Aldrich (Sigma-Aldrich, St. Louis, MO, USA), and Elemental Microanalysis (Okehampton, UK). The $\delta^{18}O$ values of the Strem, Aldrich, and Elemental lab standards have been determined as 8.2, 10.8, and 21.87 ‰ through repeat evaluation against YR-1, YR-2, and YR3-1 Ag_3PO_4 standards (Vennemann *et al.*, 2002) and checked against VSMOW, SLAP2, UC03, and UC04 silver-tube encapsulated waters (USGS, Reston, VA, USA). All reagents were from Fisher Chemical (Fairlawn, NJ, USA) or Sigma Aldrich (St. Louis, MO, USA) and were ACS grade or higher. Laboratory deionized (DI) water was 18.2 MΩ, produced by a Thermo Barnstead Nanopure system.

Four sample apatite blocks from column 22 in sheep 962 were lost during extraction; thus $\delta^{18}O$ values shown represent adjacent measurement averages. For columns 2-6 (15 blocks), several Ag_3PO_4 samples were lost prior to measurement; the remaining Ag_3PO_4 from all blocks within a column were combined for columns 2-4, and for 3/4 blocks in columns 5-6.

Sheep blood (300µl) and drinking water samples (100µl) were aliquoted into He-flushed exetainer tubes. The exetainers receiving water standards and samples contained 0.3% CO_2 in He for standard CO_2-H_2O equilibrations; blood samples were allowed to outgas and equilibrate endogenous CO_2. Equilibration incubations were conducted for 24 hours at 26 °C on a Thermo GasBench II, followed by headspace sampling and analysis using the GasBench II and Delta V Plus irms. Samples were referenced to lab standards (HH and HL), which are stored in flame-sealed glass ampoules and processed and analyzed in parallel with samples. The HH and HL standards have $d^{18}O$ values of +1.59 and -23.8 ‰ as determined through repeat analysis against VSMOW, GISP, and SLAP2 standards. The precision of replicate analyses was better than 0.03 ‰ (1 s.d.), and accuracy for water samples is better than 0.1 ‰ (1 s.d.) based on repeat analyses on different days and participation in international laboratory intercalibration exercises.

Aliquots of the feed were dried at 60 °C and analyzed for oxygen isotope analysis on the TCEA-Conflo IV-Delta V Plus irms system. The $\delta^{18}O$ was measured to be +25.3 (+/- 0.8 1 s.d.) ‰. Results were assessed relative to standards IAEA-601 benzoic acid (+23.14 ‰) and IAEA-CH-6 sucrose (+36.20 ‰; also referred to as "ANU sucrose") in addition to the encapsulated waters.

The larger scatter for organic $d^{18}O$ may represent variable contributions of a small amount of residual moisture in the feed to the O intrinsic to organic molecules in the feed.

4.3.3 Blood-water $\delta^{18}O$ modeling. Blood turnover models were adapted to predict sheep blood $\delta^{18}O$ changes given known water and feed ingestion histories (Podlesak *et al.*, 2008). Changing blood $\delta^{18}O$ values over time are defined by:

$$\frac{d\delta_b}{dt} = -\lambda\left[\delta_b(t) - \delta_{eq}(t)\right] \qquad \text{(eq. 4.1)}$$

where λ is the isotope decay constant, $\delta_b(t)$ is the blood $\delta^{18}O$ value at time t, and $\delta_{eq}(t)$ is the theoretical blood $\delta^{18}O$ steady state at that same time, determined by physiological parameters and feed and air $\delta^{18}O$ values. Following Gretebeck *et al. (*1997) and Podlesak *et al.* (2008), we modeled the steady-state ratio of heavy to light isotopes ($^{18}O/^{16}O$) in body water, or R_{bw}, as contingent upon the ratios of inputs and outputs:

$$R_{bw} = \frac{(R_{dw} * F_{dw}) + (R_{O2} * F_{O2} * \alpha_{O2}) + (R_{fd} * F_{fd})}{F_{H2O-un} + (F_{H2O-fr} * \alpha_{H2O-fr}) + (F_{CO2} * \alpha_{CO2})} \qquad \text{(eq. 4.2)}$$

where in the numerator, R_{dw} and F_{dw} are the isotope ratio and fractional contribution of drinking water to body water oxygen, R_{O2} and F_{O2} are those for inspired oxygen and α_{O2} is the fractionation factor altering that ratio at the gas-liquid boundary in the lungs, and R_{fd} and F_{fd} are the ratio and fractional contribution of feed. In the denominator, $F_{H2O\text{-}un}$ is the fraction of water oxygen leaving the body in water without fractionation, $F_{H2O\text{-}fr}$ is that fraction of water oxygen leaving the body in

water that fractionates according to the factor $\alpha_{H2O\text{-}fr}$, and F_{CO2} is the fraction of body water oxygen leaving as CO_2, fractionated by the factor α_{CO2} (Gretebeck *et al.*, 1997; Podlesak *et al.*, 2008; Chapter 3). We fit these parameters simultaneously with MSLS and COBYLA algorithms (Powell 1998; Kucherenko and Sytsko 2005) using observed blood, drinking water and feed $\delta^{18}O$ for sheep 962. Following Podlesak *et al.* (2008) we set F_{dw} and $F_{H2O\text{-}un}$, F_{O2} and F_{CO2}, F_{fd} and $F_{H2O\text{-}fr}$, and α_{O2} and $\alpha_{H2O\text{-}fr}$ pairs equal to one another, though liquid water input and output fractions may be uncoupled (Table 1; Chapter 3).

	Fraction	**alpha**
Drinking water influx	.690	
O_2 influx	.181	.990
Feed influx	.129	
O efflux (unfractionated)	.690	
O efflux (fractionated)	.129	.990
CO_2 O efflux	.181	1.040

Table 4.1: oxygen water and metabolic input and out fractions (masses) and alphas (fractionation factors).

4.3.4 $\delta^{18}O$ integration with tooth mineralization. Tooth isotope maps integrating tooth mineralization with water history were produced by combining daily mineral density increases with daily blood $\delta^{18}O$ at all locations within the tooth crown. On any day *d*, newly added mineral at pixel location $px_{x,y}$ would be in equilibrium with blood $\delta^{18}O$ on that day. In our model the $d^{18}O$ value of the cumulative mineral phosphate on that day was therefore:

$$\delta^{18}O_{px,d} = \Delta_{PO4-H20} + \sum_{i=init}^{d} \delta^{18}O_i * \rho_i^{\Delta}/\rho_d^t \quad \text{(eq. 4.3)}$$

where *init* was the first day of mineral density increase for that pixel, $\delta^{18}O_i$ was the blood $\delta^{18}O$ value for each of *i* days since mineralization began, ρ_i^{Δ} was the density increase for each day, and ρ_d^t was the total cumulative mineral density through day *d* over that same period. $\Delta_{PO4\text{-}H2O}$ represents the equilibrium offset between phosphate and water $\delta^{18}O$. This offset is a function of temperature and was originally established by Longinelli and Nuti (1973).

Uncertainty in our parameterization of $\Delta_{PO4\text{-}H2O}$ arises in part from uncertainty in sheep oral temperature. Our measurements were consistent with the 39.2 °C (+/- 0.4°C 1s.d.) mean reported daytime rectal temperature for a population of 35 sheep in Goodwin (1998). In humans, oral temperatures are roughly midway between rectal and tympanic, can rise by up to half a degree during exposure to warm ambient conditions (Zehner and Terndrup 1991) and may be affected by activity levels (Weinert and Waterhouse 2007). Mammalian body temperatures fluctuate following circadian rhythms: in sheep, typical maximum amplitude of diurnal variation for rectal temperature has been reported as 0.6 and 1.0°C (Refinetti and Menaker 1992). We adopt a value of 39.0°C (+/- 0.5°C) as being broadly representative of mean sheep molar formation temperature over a diurnal cycle; the temperature uncertainty converts to an uncertainty in $\Delta_{PO4\text{-}H2O}$, and by extension, to $\delta^{18}O_{px,d}$, of approximately +/- 0.13‰.

A greater source of uncertainty in $\Delta_{PO4\text{-}H2O}$ stems from a number of recent studies that suggest different temperature-dependent phosphate-water offsets. The Longinelli and Nuti (1973) offset

was calibrated on minor phosphate extracted from calcium carbonate shells that grew at mean temperatures ranging from 3.5 - 27.3 °C. Puceat *et al.* (2010) analyzed biogenic apatite from the teeth of fish raised at temperatures from 8 – 28 °C, and Lecuyer *et al.* (2013) report on biogenic apatite from modern lingulids and shark teeth from 12 – 28 °C. Chang and Blake (2015) conducted laboratory equilibrations of dissolved orthophosphate using pyrophosphatase mediated exchange of oxygen between phosphate and water over a temperature range from 3 – 37 °C. Mammalian oral temperatures are higher than the calibration range for all of these thermometers, and enamel hydroxyapatite is different from the phosphate phases examined in most of these studies. Nevertheless, the calculated $\Delta_{PO4\text{-}H2O}$ obtained using a temperature of 39.0°C is 16.8, 17.4, 18.9, and 19.7‰ for the thermometers advocated by Longinelli and Nuti (1973), Lecuyer *et al.* (2013), Puceat *et al.* (2010) and Chang and Blake (2015), respectively. A further complexity in estimating offset stems from the possibility of evolving water flux throughout the course of the experiment (O'Grady *et al.*, 2010). We tested values ranging from 16.5 – 20‰ by using these offsets in our forward model, and comparing resulting model isomaps with our data from 962 using a likelihood score. Best fit offsets were sensitive to spatial uncertainty at the model perimeter and showed a range of possible values from 18.8 – 19.4‰. Through a least squares metric we found a most likely value for $\Delta_{PO4\text{-}H2O}$ to be 18.8‰ in 962, and used this offset for most modeling with this animal (but see discussion below in "PO4 resetting optimization").

We conduct a water switch experiment during the middle of M2 formation, and use the results to test a model produced with density scans of mineralizing M1s. Second molar and M3 teeth are considered better targets for study of environmental seasonality because they form after birth

and largely after weaning, containing little maternal signal. They may also contain more temporal information, because they form over longer periods of time, and are less worn than M1s until late in life. The spatial pattern of isotopes in a tooth results from the interaction between the timing of mineralization, and a drinking and feeding history influencing body chemistry during mineralization. To predict M2 isomaps resulting from a specific drinking water histo

ry, we used M1 and M2 extension curves derived in Chapter 2 to estimate the drinking water history timing in an M1 that would produce the same isomap in an M2. For a given drinking water event occurring on day t_{m2} during the mineralization of the second molar,

$$m2_l = A_{m2} * erf\left(s_{m2} * (t_{m2} - o_{m2}) * (l_{maxm2} - A_{m2})\right) \qquad \text{(eq. 4.4)}$$

where *erf* represents the Gaussian error function, $m2_l$ is the EDJ length of the M2 at time t_{m2}, and A_{m2}, s_{m2}, o_{m2} and l_{maxm2} are the amplitude, slope, offset and maximum extension rate describing M2 extension. The percent completion of the M2 at t_{m2} is calculated using $m2_l$ / l_{maxm2}, and this same percent is multiplied by the maximum EDJ length of the M1 l_{maxm1} to return the EDJ length of the M1 $m1_l$ at the equivalent stage of mineralization. We derived an equivalent day in M1 mineralization, t_{m1}, with

$$t_{m1} = \frac{erf^{-1}((a_{m1} + m1_l - l_{maxm1})/a_{m1}) + (o_{m1} * s_{m1})}{s_{m1}} \qquad \text{(eq. 4.5)}$$

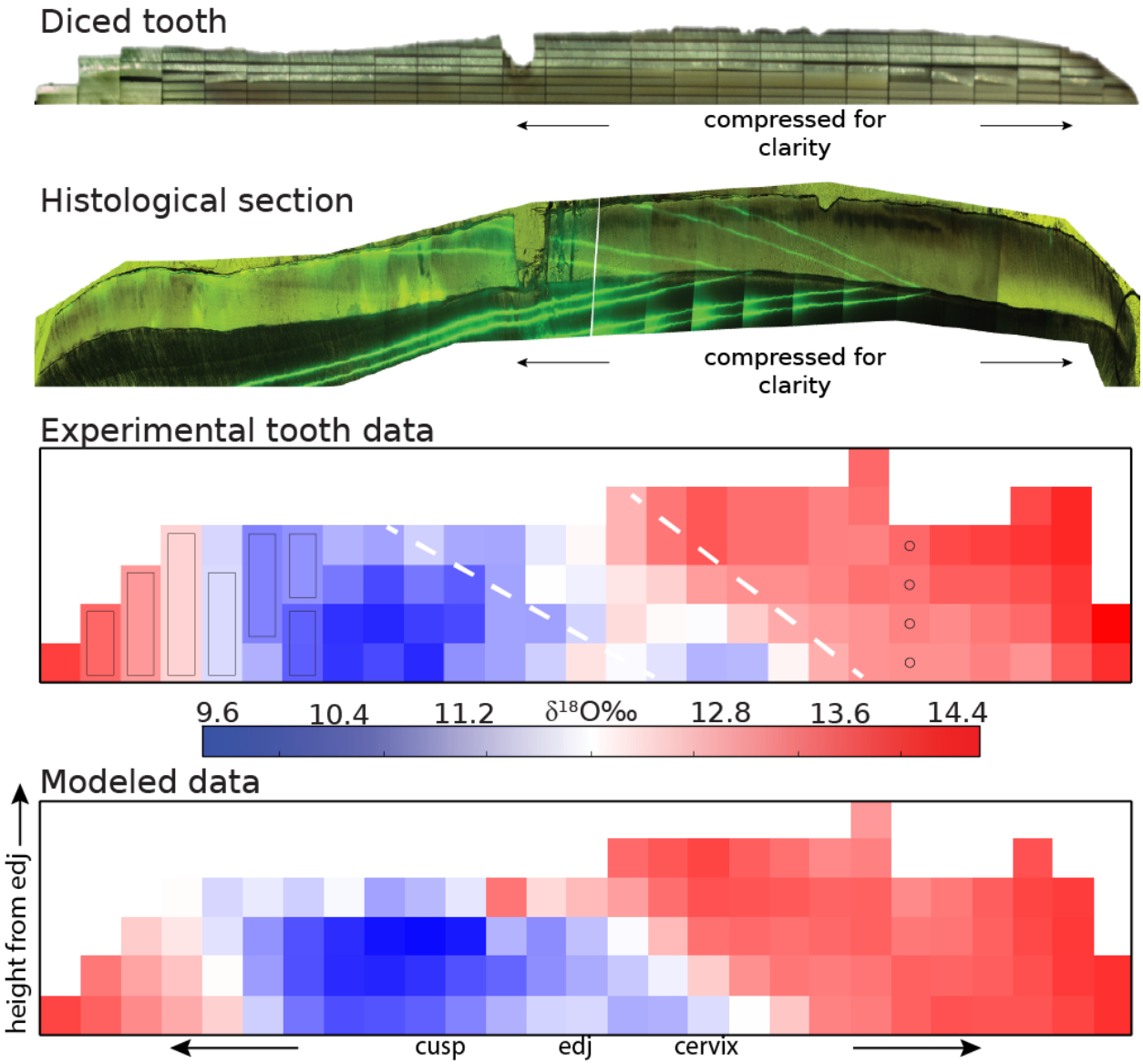

Figure 4.2 Validation of mineralization model using the buccal enamel of sheep 962 M2 diced into 1.50 x 1.00 x 0.15 mm blocks. Both the physical sample and histological section are compressed along the cuspal-cervical axis for ease of visualization. Calcein labels (bright green lines in the histological section) were given to the sheep at 201, 221, 263 and 283 days of age from left to right. Experimental tooth data shows phosphate $\delta^{18}O$ values measured from the diced tooth blocks. White dotted lines indicate the positions of calcein labels and the extent of extension at the start (201 days) and end (263 days) of the experimental water switch. Black squares show where multiple blocks were combined for a single measurement, and black circles where $\delta^{18}O$ was calculated from adjacent blocks due to sample loss. Modeled data represents the predicted $\delta^{18}O$ isomap from the mineralization model, initial estimates of oxygen exchange during mineralization, and conditions replicating our experimental water switch.

in this case using parameters that describe first molar extension (Chapter 2). These equations allow the M1 mineralization model to be adapted to predict spatial isotope patterns in an M2 or any other tooth where extension has been characterized.

4.4 Results and Discussion

4.4.1 Experimental validation of mineralization model. Blood $\delta^{18}O$ measurements (Fig. 4.1) for 962 yield an overall single-pool blood water oxygen half-life of 2.6 days, at the low end of 2.4-9.0 day variation previously observed in sheep (MacFarlane *et al.*, 1971; Dawson 1977; Chapter 3). Relatively rapid blood oxygen turnover shows that body water time averaging of environmental drinking water has only a minor impact on the magnitude of $\delta^{18}O$ values. The geometry and values of our predicted tooth isomap accord reasonably well with the measured M2 phosphate $\delta^{18}O$ from our experimental animal (Fig. 4.2). Important features are predicted by the synchrotron-based mineralization model are observed in our sheep, including an initial secretory front deposited at a steep angle to the EDJ, a pause between secretion and maturation, and a large maturation wave in which the bulk of depleted values from the experimental switch are deposited in the tooth. Importantly, while secretory enamel records the switch, most of the signal is preserved in maturational enamel, where the secretory front was formed 2-3 months earlier.

4.4.2 Hydroxyapatite PO_4 resetting. While the predicted and actual (measured) isomaps show a similar range of $\delta^{18}O$ magnitudes, the experimental animal shows more depleted $\delta^{18}O$ values in the cuspal region, which return to enriched $\delta^{18}O$ values more gradually than in the predicted isomap. These observations cannot be accounted for by varying estimated mineralization timing

within the variance observed in Dorset sheep. We hypothesize that a portion of measured HAp $\delta^{18}O$ reflects isotopic equilibration with blood $\delta^{18}O$ after initial deposition, leading to these minor differences. This may be due to phosphate exchange during the secretory transformation of amorphous precursors to HAp, and dissolution-reprecipitation during maturation (Beniash *et al.*, 2009; Josephson *et al.*, 2010; Damkier *et al.*, 2014). We estimate this $\delta^{18}O$ exchange during maturation quantitatively based on three variables: 1) the delay between phosphate oxygen deposition and exchange, 2) the proportion of phosphate that exchanges, and 3) the rate of exchange.

Phosphate exchange begins after mineral deposition, causing isotopic compositions in a fraction f of already laid-down mineral to move towards re-equilibration with blood. The pause between deposition and the beginning of phosphate exchange is given as Δt_{ex}, and the decay constant for this exchange is given as λ_{PO4}. In order to model phosphate oxygen exchange after mineral deposition, we use the blood isotope history in our calculation so that the effective PO_4 $\delta^{18}O$ equilibration history δ_{PO4} at time t is influenced by the blood history over time after Δt_{ex}. The δ_{PO4} history of the mineral fraction that equilibrates with later phosphate is described by:

$$\frac{d\delta_{PO4}}{dt} = -\lambda_{PO4}[\delta_{PO4}(t) - (\delta_b + \Delta_{PO4-H20}) * (t + \Delta t_{ex})], \qquad \text{(eq. 4.6)}$$

where $\Delta_{PO4\text{-}H20}$ is the mineral-water phosphate $\delta^{18}O$ offset. Because only a fraction of deposited mineral resets, the phosphate $\delta^{18}O$ equilibration history we use in our calculations of mineral isotopic composition is $\delta_{PO4}(t) + (1 - f)\delta_b(t)$ (eq. 4.7).

To approximate the effect of PO_4 oxygen exchange during enamel mineralization, we assume that the transition from ACP to HAp in secretion, or the onset of dissolution-reprecipitation in maturation, might follow a pause approximating the delay between secretion and maturation throughout the enamel crown. To measure the extent of this delay we average initiation to maturation delays from mineralization trajectories at ten locations in the enamel crown. We estimate delay timings by identifying steep increases in mineral density around 40% maximum density. We choose this value because, despite variation in mineralization trajectories throughout the enamel crown, all locations show that mineralization is occurring rapidly when 40% maximum density has been reached. Using this metric we derived an average delay between secretion and maturation onset of approximately 35 days throughout the enamel crown. We furthermore expect that only some proportion of ACP PO_4 would be available for exchange with matrix fluid (either oxygen exchange between phosphate and water, or replacement of phosphate ions from the ACP with equilibrated phosphate in the matrix fluid) during evolution to HAp. Beniash *et al.* (2009) suggested that this transition would occur *in vivo* within hours to days in a mouse (Beniash *et al.*, 2009). We first estimated resetting half-life at 3 days, and phosphate available for isotopic resetting at 30%, representing the approximate amount of mineral deposited during secretion. Incorporating resetting modeling, the new predicted tooth isomap matches experimental observations more closely (Fig. 4.2), and the $\delta^{18}O$ water switch appears more cuspally, as in the measured values.

4.4.3 Development of inverse procedure to estimate $\delta^{18}O$ inputs. The tooth mineralization model described above is a potentially powerful tool for reconstructing original seasonal

environmental signals with inverse methods from measured $\delta^{18}O$ values. We approach reconstruction by iteratively generating hypothetical drinking water histories and resulting forward tooth $\delta^{18}O$ isomaps. This method proposes water histories using a nonlinear Quasi-Monte Carlo search routine (Powell 1998; Kucherenko and Systsko 2005), evaluates their goodness of fit under a likelihood framework, and simulates forward-inverse mineralization model mismatch as would be expected in nature.

Forward synthetic tooth isomaps are produced from drinking water $\delta^{18}O$ histories composed of sine waves with 360 and 90 day, and 180 and 45 day periods. We also produce synthetic tooth isomaps resulting from precipitation $\delta^{18}O$ histories measured in Entebbe, Uganda; Mulu, Borneo and North Platte, Nebraska. To simulate likely natural variation in real mineralization processes compared to our model, synthetic tooth isomaps are produced from a ten mineralization trajectory sample randomly drawn from the 100 mineralization trajectories available for each tooth location in our larger model. For each inverse optimization run, forward isomaps are also generated by a ten mineralization trajectory sample randomly drawn from the full model. This subsampling procedure allows for discrepancy between modeled "inverse" and synthetic "forward" mineralization processes, therefore mimicking the possibility that the isotopically sampled tooth mineralized differently than predicted by our models.

Inverse model reconstruction of synthetic and measured tooth isomaps is achieved by iteratively proposing $\delta^{18}O$ drinking water histories, and generating associated forward isomaps until these closely matched the target synthetic or measured tooth isomaps. Proposed drinking water histories are composed of linearly interpolated 14-day $\delta^{18}O$ value parameters spanning the

duration of tooth formation. For each proposed drinking water history, resulting blood and PO_4 $\delta^{18}O$ values are also calculated, and used to generate forward tooth isomaps. We estimated 14-day drinking water parameters using a likelihood method that minimized the likelihood estimator *L*:

$$L\left(\delta^{m}_{x,y}\middle|\delta^{d}_{x,y}\right) = \prod_{i}^{n_{px}} e^{\left(-\frac{\left(\delta^{m}_{i}-\delta^{d}_{i}\right)^{2}}{2\sigma_{i}^{2}}\right)} \qquad \text{(eq. 4.8)}$$

where $\delta^{m}_{x,y}$ and $\delta^{d}_{x,y}$ describe model and target (either synthetic or measured) $\delta^{18}O$ values for all of i to n_{px} pixel locations x,y within the tooth crown. Total modeled ‰ error per pixel σ_{px} is estimated as the root of the sum of squared error sources:

$$\sigma_{px} = \sqrt{(\sigma_m)^2 + (\sigma_\delta)^2 + (\sigma_z)^2} \qquad \text{(eq. 4.9)}$$

where σ_δ is the overall PO_4 $\delta^{18}O$ irms measurement error, and σ_z is a minimum error set to 0.05. Parameter σ_m is the single-pixel error derived from 30 samples, ten of each drawn from three forward mineralization model isomaps produced using three separate extension curves that approximate mean, rapid and slow extension curves that could be observed in sheep lower M2s (Chapter 2). Rapid and slow extension curve amplitudes, slopes and offsets in this case are 62.00, .0037, 0.00, and 74.00, .0031, -48.00, respectively.

Inverse drinking water $\delta^{18}O$ reconstructions from synthetic tooth isomaps tend to result in "spiky" reconstructions with rapid, high-amplitude oscillations. To address this, we introduce a dampening measure during inverse modeling that penalizes high rates of $\delta^{18}O$ while evaluating water history solutions, modifying the likelihood estimator:

$$P\left(\delta_d^w \middle| \delta_{x,y}^d, d_{rate}\right) = \prod_i^{n_{px}} e^{\left(-\frac{\left(\delta_i^m - \delta_i^d\right)^2}{2\sigma_i^2}\right)} * \prod_i^{n_{days}} e^{\left(-\frac{\left(\delta_i^w - \delta_{i+1}^w\right)^2}{d_{rate}^2}\right)} \qquad \text{(eq. 4.10)}$$

where $\delta^w{}_d$ is the $\delta^{18}O$ of proposed drinking water for each of i to n days, and d_{rate} is an expected rate of $\delta^{18}O$ change/day that modifies the rate change penalization. Where inverse model drinking water reconstructions are conducted with 1D sampling, pixel likelihood score is increased proportional to the decreased number of evaluated pixels (n_{pix1D} / n_{pix2D}). Lower d_{rate} values produce more dampened reconstructed drinking water histories, whereas higher d_{rate} values produce less dampened histories. To shorten search times and capture input signal detail, for all reconstructions, optimizations are run in series of three, with d_{rate} progressively relaxed for each optimization, using values of d_{rate} = $^1/_5$, ½ and 1. Within a series, results of each optimization are used as first guesses for each subsequent optimization. This routine may be characterized as a reverse-simulated annealing technique, because simulated annealing is an optimization heuristic where search constraints are progressively increased. Our routine has the advantage of dramatically reducing search times, while guaranteeing that even short searches produce inversion results broadly consistent with inputs. While the fidelity of input reconstruction from low-resolution sampling is striking, the Shannon-Nyquist sampling theorem holds that perfect signal reconstruction is possible at the highest signal frequency with only two samples per period. Our results show that samples from ungulate molars growing at nonlinear rates over the course of a year can broadly reconstruct the timing and amplitude of seasonal climates characterized by two annual rain and dry seasons, despite the fact that weather patterns include complex signals, and the process of tooth mineralization is not simple.

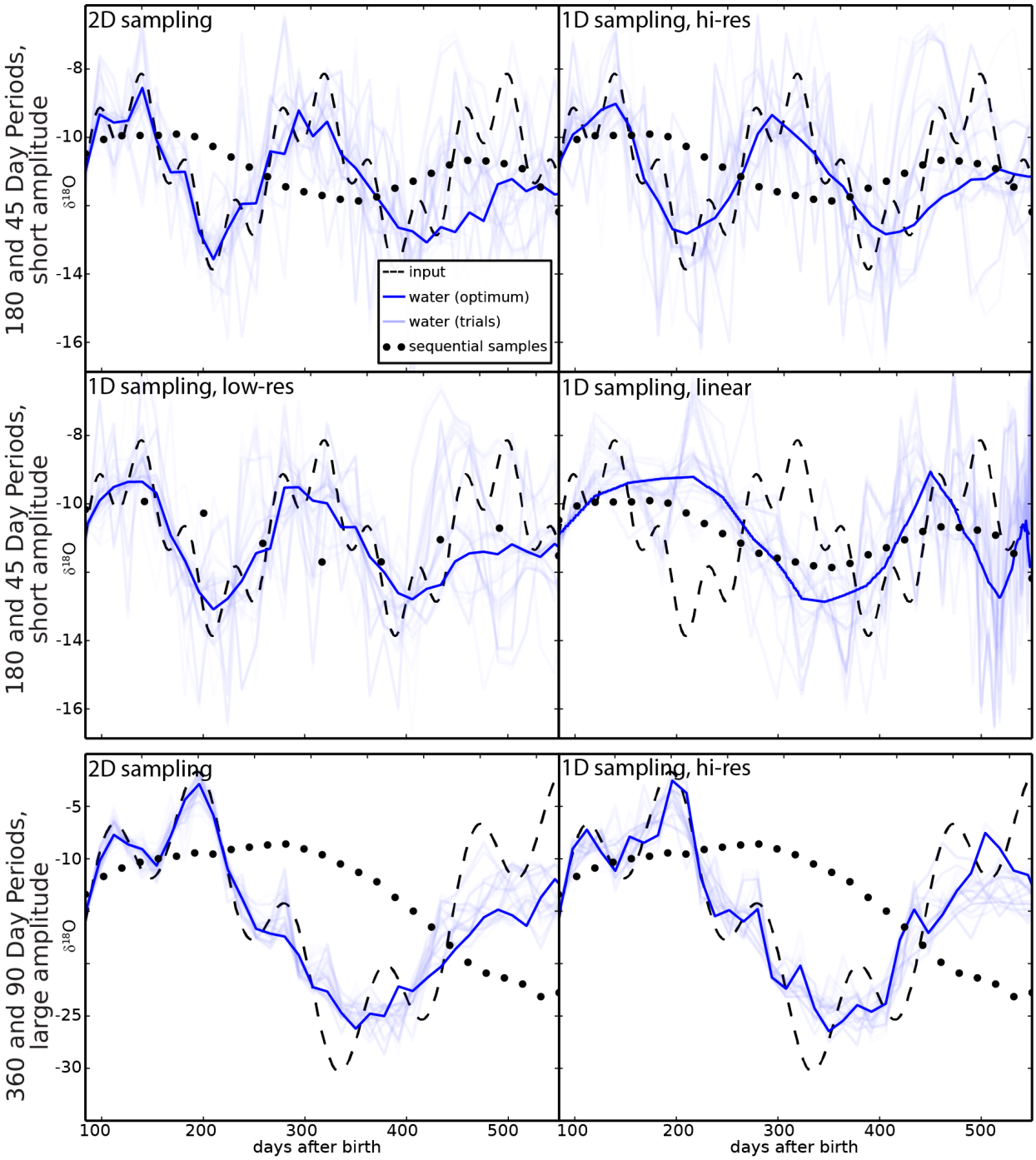
2D sampling
1D sampling, hi-res
1D sampling, low-res
1D sampling, linear
2D sampling
1D sampling, hi-res
180 and 45 Day Periods, short amplitude
360 and 90 Day Periods, large amplitude
δ18O
input
water (optimum)
water (trials)
sequential samples
-8
-10
-14
-16
-5
-25
-30
100
200
300
400
500
days after birth

Figure 4.3 Inverse method reconstructions of sine wave rainfall functions at different frequencies, amplitudes, with variable sampling rates. Upper four plots: seasonally variable, sinusoidal input drinking water $\delta^{18}O$ histories (black dashed line) with 180 and 45 day periods are used to predict spatial $\delta^{18}O$ tooth isotope patterns (Conventional 1D samples shown as black dots; 2D tooth isotope patterns are not shown). Then, inverse reconstruction attempts to estimate original drinking water inputs from 2D, high-resolution sampling (upper left), 1D high resolution sampling (upper right), 1D low resolution sampling (middle left), or 1D high resolution sampling under the assumption that tooth extension is linear (middle right). Best-fit, optimum reconstructed drinking water history (dark blue) and a subset of the best 30% of all reconstructed histories (light blue) perform well at all sample resolutions when nonlinear extension is accounted for, and best when sample resolution is high. Reconstructions can be especially detailed early in tooth formation, but degrade towards the end of the input signal. This is because slowing tooth growth incorporates longer drinking water $\delta^{18}O$ histories into progressively smaller tooth spatial dimensions at the end of enamel formation. Below, reconstruction performance is shown for a sinusoidal input signal with 360 and 90 day periods. Combined 180 and 45, and 360 and 90 day sinusoidal inputs are used to demonstrate reconstruction performance under unimodal or bimodal monsoon seasonality regimes with additional, smaller scale rainfall variation disrupting the dominant pattern.

In the special case of drinking water reconstruction from the tooth of our experimental animal, water histories are fitted using an additional three parameters that allow for an experimental switch in water sources: the day of switch onset, the length of switch onset, and the $\delta^{18}O$ value of the switch water. Rate of change penalization is employed with $d_{rate} = {}^{1}/_{5}$, ${}^{1}/_{3}$ and ½, penalization does not include the days of switch onset and conclusion, and drinking water $\delta^{18}O$ does not change during the switch.

4.4.4 Inverse reconstruction results. We reconstruct input $\delta^{18}O$ histories from sinusoidal inputs at varying frequencies (45, 90, 180 and 360 days) to first test our inverse method. When nonlinear extension and growth processes are accounted for, inverse reconstruction of high frequency (45 and 90 day) inputs is possible using both 1D and 2D sampling regimes (Fig. 4.3). These reconstructions are most accurate early in tooth growth, where temporal signals are reflected in larger spatial scales due to rapid extension rates. Reconstruction of water inputs degrades later in tooth formation, and this degradation is faster with lower sampling resolution (few samples). Lower frequencies (180 and 360 day) require the implementation of dampening priors to filter out implausibly noisy solutions, as demonstrated previously (Passey *et al.*, 2005). Overall we find that both 2D and 1D sampling regimes are able to faithfully reconstruct the original water $\delta^{18}O$ inputs over the majority of tooth formation time. Though not inconsistent with sampling theory, the fidelity of low-resolution 1D sampling is an unexpected result that underscores the value of the information gained from detailed study of tooth mineralization.

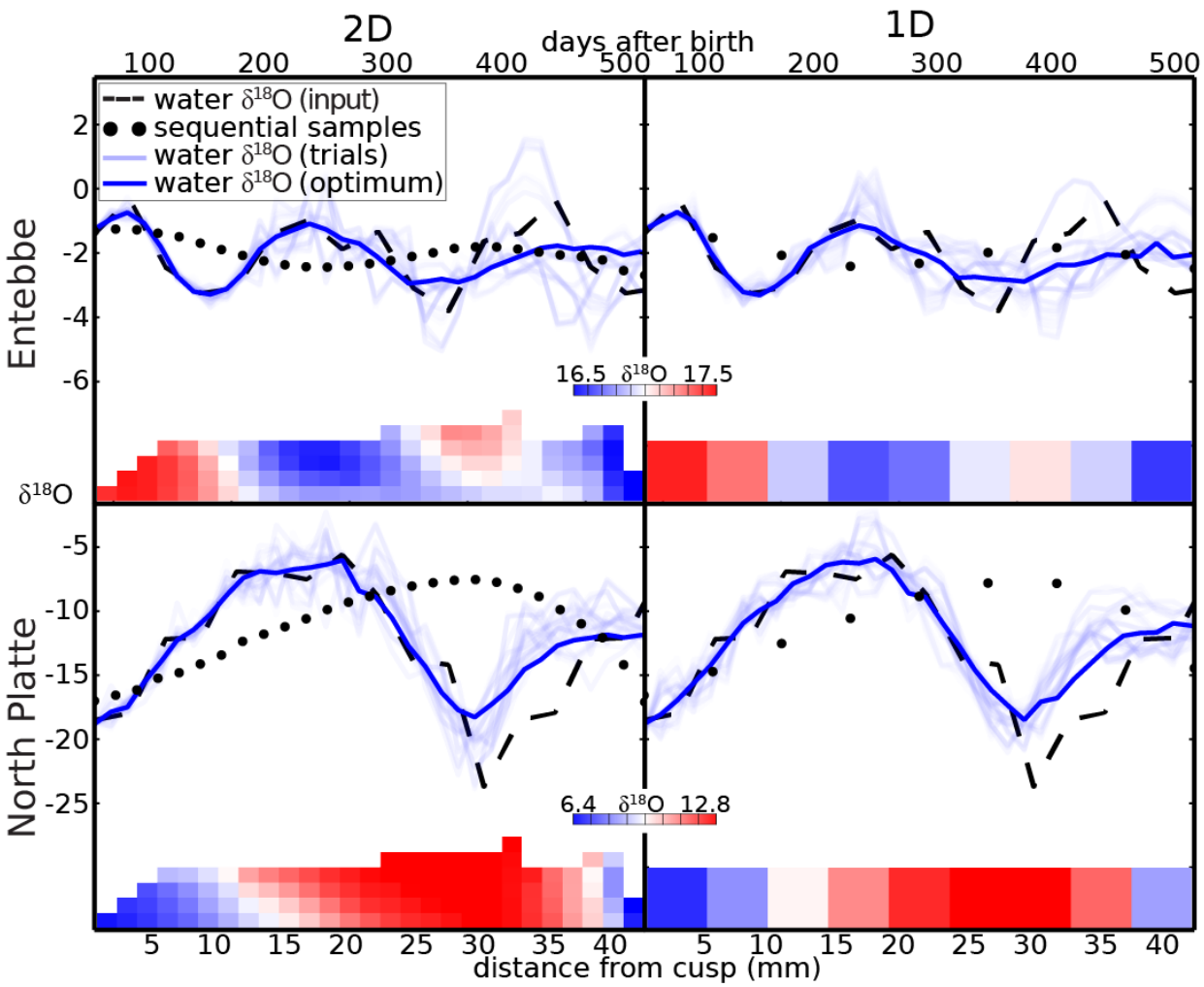

Figure 4.4 Inverse method reconstructions of drinking water $\delta^{18}O$ history (black, dashed) using 2D high-resolution (left) or 1D low-resolution (right) forward model isomaps derived from precipitation $\delta^{18}O$ records in Entebbe, Central Uganda and North Platte, Nebraska. The reconstructed optimum drinking water inputs (blue) and a sample of the most likely 30% of discovered solutions (light blue) are estimated at 14-day intervals. The 2D and 1D tooth $\delta^{18}O$ data used for reconstructions are shown at the bottom of each panel. Drinking water estimation from conventional serial sampling using finely spaced (1.5mm, left) or coarsely spaced (5mm, right) enamel samples yields the precipitation history represented by black dots.

We further test the inverse method by reconstructing water inputs from forward maps generated using published and open-access $\delta^{18}O$ precipitation records at high and low latitude sites. Inverse reconstructions with 2D and 1D sampling are fairly accurate, and their accuracy decreases only marginally with lowered sample resolution (Fig. 4.4). Importantly, the spatial distribution of conventionally-sampled tooth $\delta^{18}O$ measurements do not closely correspond to original input

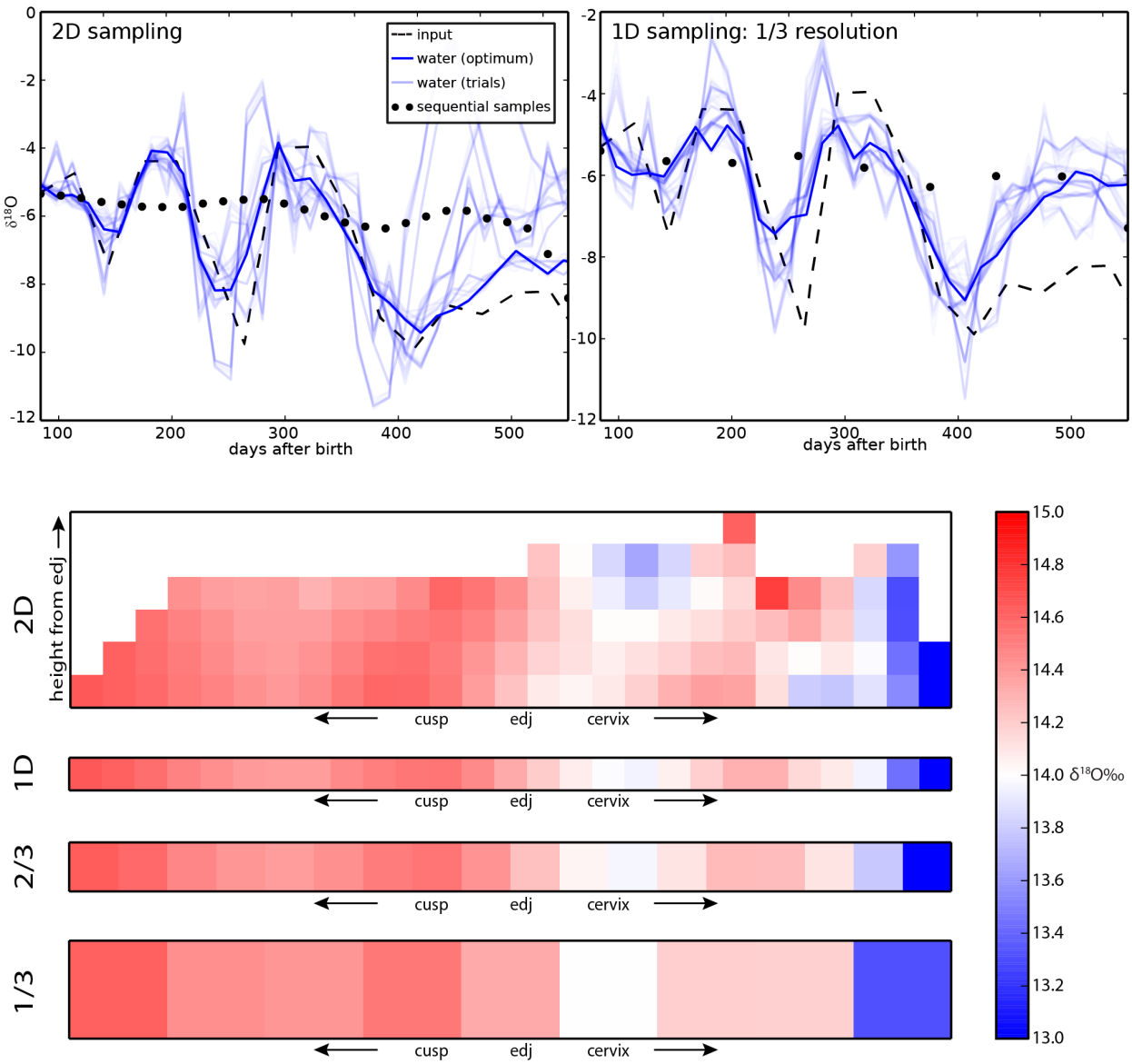

Figure 4.5 Reconstructing a Borneo $\delta^{18}O$ record at high and low sampling resolution. Above, monthly rainfall records from Mulu, Borneo (dashed black line) generate forward tooth isomaps (below), which estimate best fit (blue line) and a sample of most likely trials (light blue lines) via optimization. Above left, optimization with 2D, high $\delta^{18}O$ sample resolution; above right, with reduced 1D sample resolution. Below, the forward tooth isomaps shown at 2D, 1D, 2/3 and 1/3 (both 1D) sample resolutions. Monthly precipitation $\delta^{18}O$ data taken from Moermanetal (2013).

signal timing without an inverse method that incorporates nonlinear growth. Conventional 1D sampling substantially underestimates the amplitude of input signal variability at low latitude

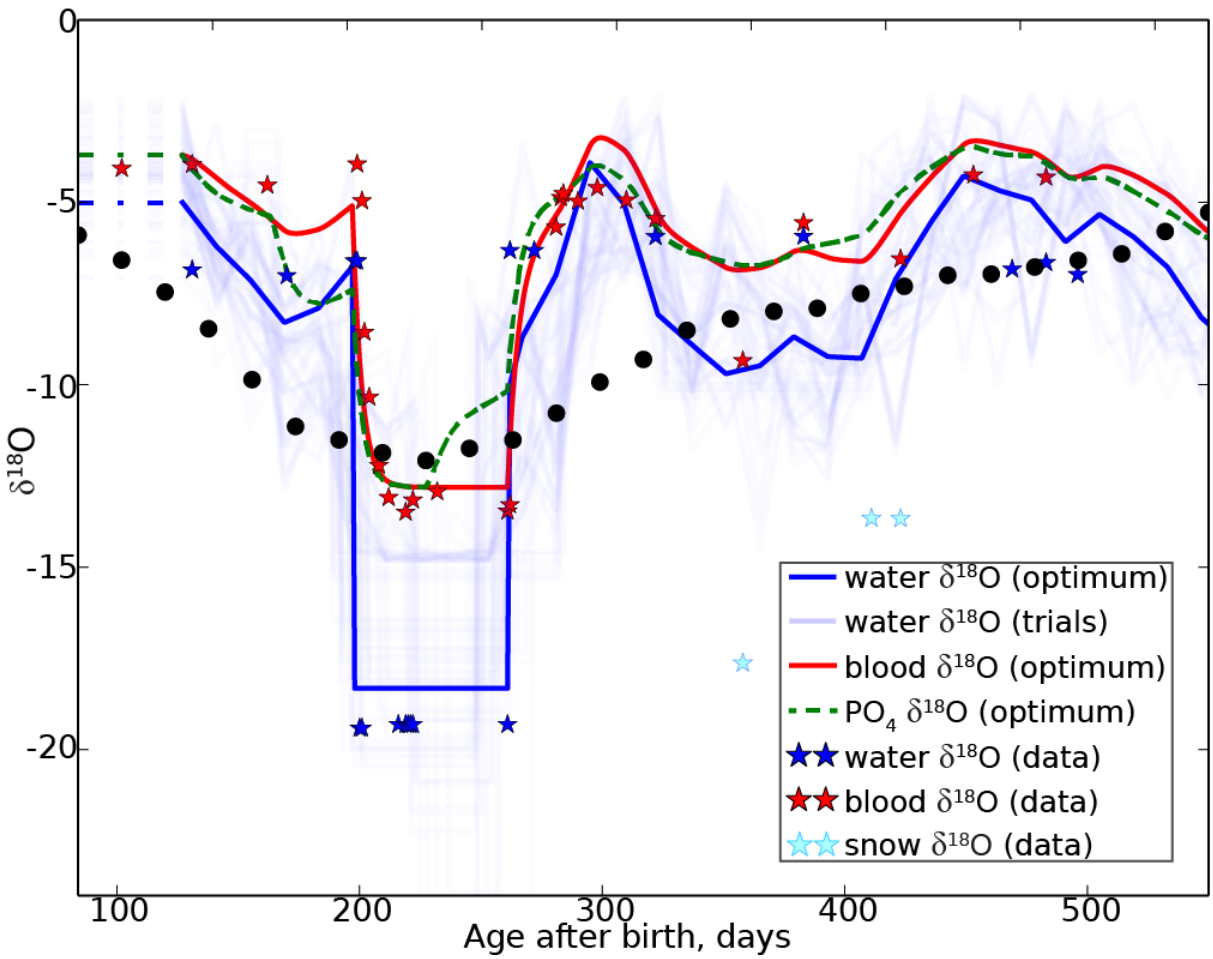

Figure 4.6 Inverse method reconstruction of drinking water $\delta^{18}O$ for sheep 962 subject to a water switch experiment. Optimum drinking water predictions (blue), most likely 30% of associated solutions (light blue), and optimum blood (red) and PO_4^{eq} (green) predictions are shown alongside measurements of drinking water, snowfall and blood (blue, light blue and red stars). Tooth $\delta^{18}O$ measurements as they would have been sampled conventionally are shown above as black dots, with dots representing column averages, and $\delta^{18}O$ values converted to drinking water inputs based on known feed and air values. This solution employs dampening priors d_{rate} = $^1/_5$, $^1/_3$ and ½.

sites where $\delta^{18}O$ variations are relatively small and transient. At some low latitude sites, inverse results reconstruct input signal amplitudes more fully through the use of higher sample resolution (Fig. 4.5). Increased resolution sampling may therefore be important for reconstructing seasonal patterns from some low-latitude ecosystems, but even reduced sampling

resolution can quantitatively reconstruct the timing and magnitude of isotopic inputs from a wide range of locations, provided that nonlinear extension is accounted for.

Finally, we test this inverse method by reconstructing drinking water $\delta^{18}O$ from the tooth phosphate $\delta^{18}O$ measurements of our experimental animal, and compare the results with measured drinking water, feed, and air $\delta^{18}O$ inputs in addition to blood $\delta^{18}O$ composition. Inversion trials reconstruct the approximate location and magnitude of the experimental switch (Fig. 4.6), although many solutions propose variable switch morphologies that preserve the integrated weight of the switch history. Interestingly, many inverse trials estimate depleted $\delta^{18}O$ input values following the experimental water switch. These excursions appear to track unanticipated local storms and observed consumption of snow following the switch, which is supported by blood and snow $\delta^{18}O$ measurements (Fig. 4.1).

4.4.5 Resetting optimization. We make use of these additional blood $\delta^{18}O$ measurements to better constrain our estimate of phosphate resetting parameters by employing the optimization architecture used for inversion. We estimate these parameters using a likelihood method that minimizes differences between our forward model and measured enamel $\delta^{18}O$ values from our experimental animal, by minimizing the likelihood estimator as described previously. This method returns two classes of results depending upon whether PO4 resetting delay was constrained to values below 45 days, or unconstrained (Fig. 4.7). Unconstrained optimizations resulted in a delay of 71 days, which we consider implausible within the context of secretory and maturation histories. When delay is constrained, we estimated PO_4 turnover half-life per on average to be 5.9 days, and the PO_4 oxygen available for exchange to be 36%. Using this method,

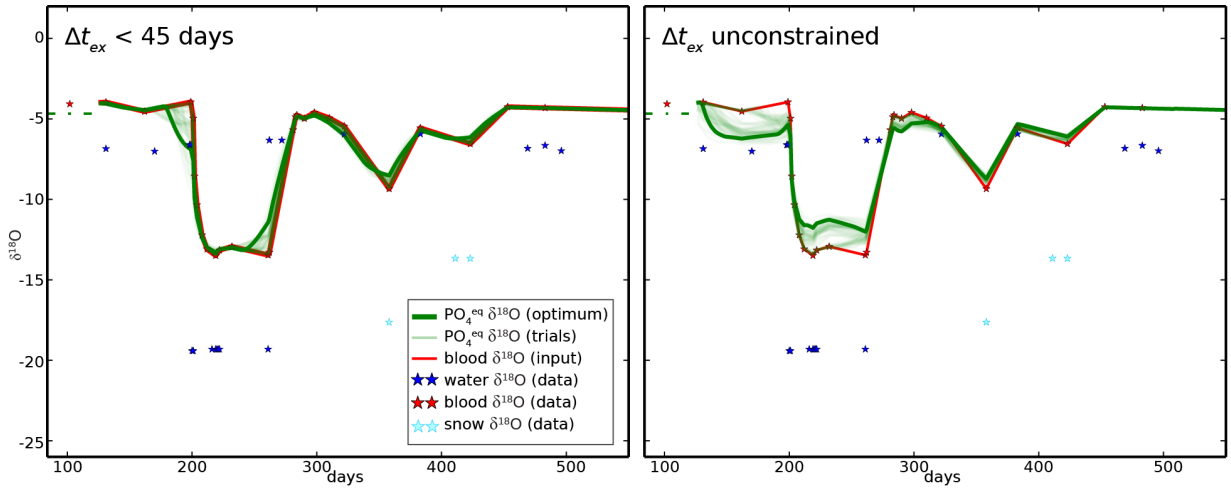

Figure 4.7 Phosphate resetting optimization, with resetting delay constrained or unconstrained, in 962. The optimum estimated $\delta^{18}O$ of mature tooth HAp originally deposited at a given time (days) after it has experienced partial resetting (dark green), alongside less likely trial values (light green). Reset PO_4^{eq} values are a function of known blood $\delta^{18}O$ (red stars) over time as it continues to determine evolving HAp $\delta^{18}O$ composition. They are here determined via an optimization procedure minimizing model-data tooth isomap discrepancy when PO_4^{eq} parameters are varied, while known blood composition is held constant. Measured water and snow $\delta^{18}O$ are shown as dark and light blue stars, respectively. On the left, best fit PO_4^{eq} is shown when the pause between HAp deposition and resetting is constrained to <45 days, and on the right, when it is unconstrained.

delay was estimated to be slightly shorter, at 22 days; data-model residuals are improved when PO_4 resetting is implemented and later optimized.

It is possible that the diverging results reflect the separate resetting processes that occur via different mechanisms in secretion and maturation, here treated as the same process. Another possibility is that the unconstrained delay of 71 days produces a plausible but incorrect drinking water history, resembling some inverse drinking water optimization trials. The implementation of phosphate resetting, and the optimization of resetting parameters, both improve model-data discrepancy (Fig. 4.8), and predict observed $\delta^{18}O$ patterns in animals from all treatment groups quite well (Fig. 4.9). Sensitivity testing of the phosphate-water offset parameter using tooth and blood measurements from all animals suggest that the phosphate water offset, $\Delta_{PO4\text{-}H2O}$, is likely

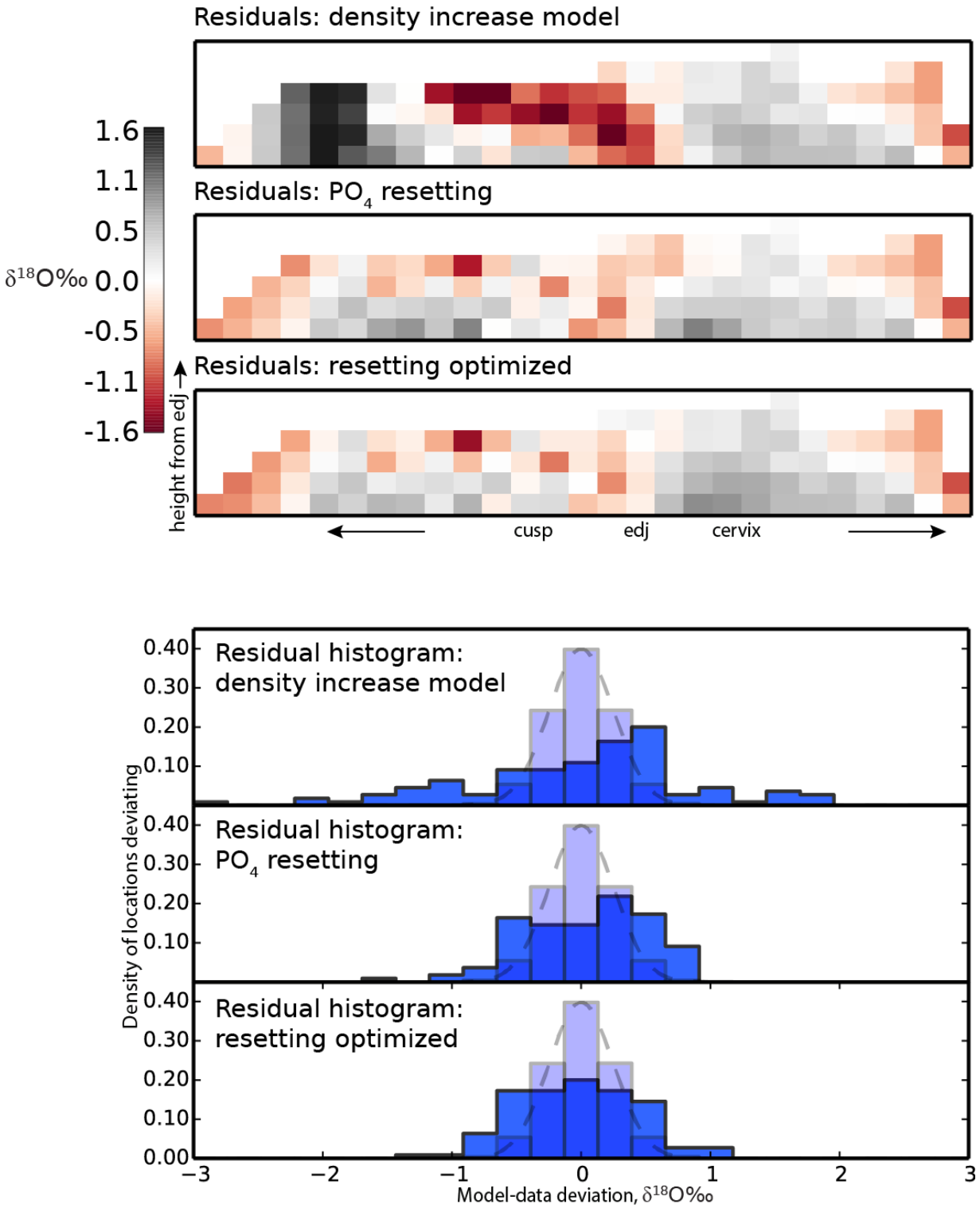

Figure 4.8 Above, residuals (discrepancies) between experimental M2 $\delta^{18}O$ data and model isomaps for the synchrotron-based density increase model, the first PO_4 resetting model, and the optimized PO_4 resetting model (constrained). Below, dark blue histograms show the normalized distribution of the residuals for the same comparisons. Light blue histograms and dashed black line show the expected pattern of residuals if model results perfectly predict data, and phosphate $\delta^{18}O$ measurement error is 0.25 ‰ (1 s.d.).

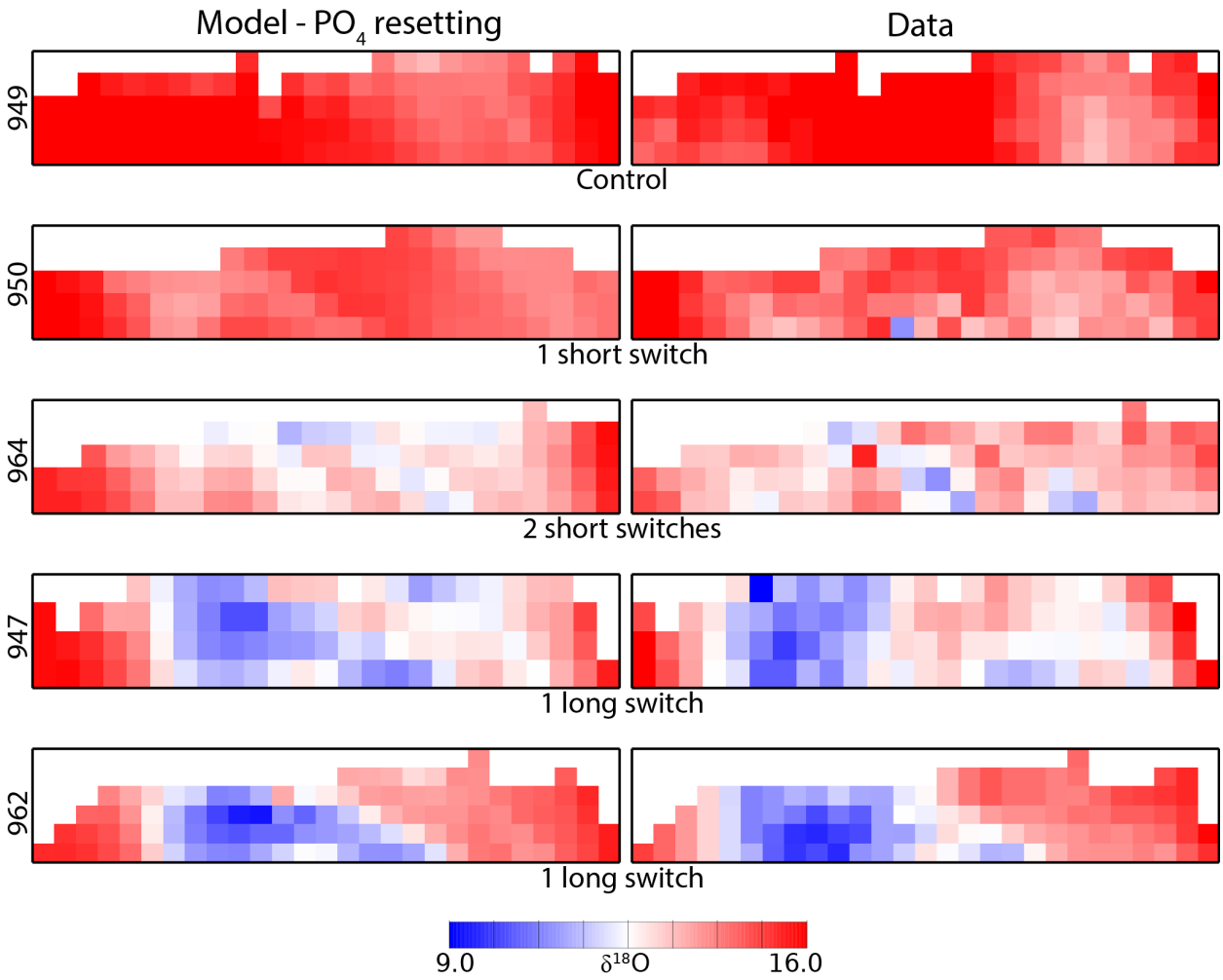

Figure 4.9 Modeled (right) and measured (left) M2 $\delta^{18}O$ data from five animals. Animal 949 drank only Quabbin water (control), while 950 drank LFC water once for 20 days, 964 drank LFC water again for 20 days after a 40 day pause, and both 947 and 962 drank LFC water for 60 days (Chapter 3). All animals consumed some amount of snow in the winter following the experiment.

between +18.8 – 19.4‰. Predicted offsets are highest for the control animal, and decrease for animals that drank more LFC water. One effect of increasing phosphate remodeling is to lower model-data discrepancies in all animals. Another effect is to cause $\Delta_{PO4\text{-}H2O}$ to converge on higher values for those animals that drank more LFC water: +19.0 - 19.4‰. This pattern of convergence is consistent with phosphate resetting during mineralization. Without model resetting, $\delta^{18}O$-

depleted LFC water is overrepresented in modeled enamel. When resetting is not modeled, this overrepresentation can be reduced by lowering the phosphate-water offset, which accounts for a $\Delta_{PO4\text{-}H2O}$ of +18.8‰ in 962. When resetting is included during modeling, best-fit $\Delta_{PO4\text{-}H2O}$ values increase, approaching those of the control animal. Constraining $\Delta_{PO4\text{-}H2O}$ to +19.0 - 19.4‰ in mammals would represent an important improvement for paleontological water $\delta^{18}O$ or temperature reconstructions: available models currently place this offset at anywhere from +16.8 – 19.7‰ (Longinelli and Nuti, 1973; Lecuyer 2013; Pucéat *et al.*, 2010; Chang and Blake 2015).

These observations support the finding that amorphous calcium phosphate forms the basis of initial mineral deposition, and that subsequent transition to more crystalline HAp is a fluctuating rather than linear process (Beniash *et al.*, 2009; Simmer *et al.*, 2012; Josephson *et al.*, 2010; Damkier *et al.*, 2014; Robinson 2014). Nevertheless, our model is imperfect in that it treats both secretion and maturation resetting equally. Differing mechanisms of exchange, namely amorphous to crystalline transitions during secretion and pH fluctuations leading to dissolution-reprecipitation reactions during maturation, would be expected to regulate resetting with differing magnitudes and timings. Furthermore, even when phosphate resetting is increased during sensitivity testing for the likely phosphate-water offset, most likely offsets for experimental animals fall slightly below the control animal. These results suggest that our model still underestimates the extent of resetting during either phase.

4.5 Conclusions

Paleoseasonality reconstructions from teeth can play a critical role in resolving debates about the onset of tropical monsoon patterns, shifting ecological pressures, or the magnitude of temperature changes at high latitudes. In human evolutionary history, climatic variability has been proposed as a driver of behavioral innovation (Potts 2013; Anton *et al.*, 2014), and seasonality may have influenced hominin foraging patterns, fallback food choice and extractive stone tool use (Isler and Van Schaik 2014; Melin *et al.*, 2014). Yet given the substantial geographic heterogeneity and ecological diversity in Africa, legitimate questions remain about the importance of seasonality. We integrate a new mineralization model, experimental results and recent advances in understanding the mechanisms of biomineralization to develop an inverse method for reconstructing $\delta^{18}O$ from abundant bovid molars. This method can distinguish between seasonal $\delta^{18}O$ rainfall patterns globally, including at different sites in East Africa, where these methods hold real promise for evaluating whether increased seasonal variability is observed at sites of early human stone tool manufacturing (Potts 2013). The method also highlights the importance of accounting for nonlinear mineralization patterns and the dampening of input signals during biomineralization when characterizing seasonality from tooth isotopes. Further study of mineralization among diverse taxa, continued improvements in seasonal reconstruction methods, and ongoing efforts to describe isotope hydrology will better resolve the complex relationship between climate, behavior and human evolution.

4.6 References

Antón SC, Potts R, Aiello LC (2014) Evolution of early Homo: An integrated biological perspective. *Science* 345:1236828.

Aubert M, Williams IS, Boljkovac K, Moffat I, Moncel MH, *et al.* (2012) In situ oxygen isotope micro-analysis of faunal material and human teeth using a SHRIMP II: a new tool for palaeo-ecology and archaeology. *J Arch Sci* 39:3184-3194.

Balasse M, Obein G, Ughetto-Monfrin J, Mainland I (2012) Investigating seasonality, birth in herds: a reference set of sheep enamel stable oxygen isotope ratios. *Archaeom* 54:349.

Beniash E, Metzler RA, Lam RSK, Gilbert P (2009) Transient amorphous calcium phosphate in forming enamel. *J Struc Bio* 166:133-143.

Blumenthal S, Cerling T, Chritz K, Bromage T, Kozdon R, Valley J (2014) Stable isotope time-series in mammalian teeth: In situ δ18O from the innermost enamel layer. *Geochim Cosmochim Acta* 124:223236.

Bowen GJ, Revenaugh J (2003) Interpolating the isotopic composition of modern meteoric precipitation. *Water Resources Res* 39.

Boyde A (1989) Enamel. In *Teeth* 309-473. *Springer Berlin Heidelberg*.

Brookman TH, Ambrose SH (2012) Seasonal variation in kangaroo tooth enamel oxygen and carbon isotopes in southern Australia. *Quat Res* 78:256-265.

Bryant, JD, Froelich PN, Showers WJ, Genna BJ (1996) A tale of two quarries: biologic and taphonomic signatures in the oxygen isotope composition of tooth enamel phosphate from modern and Miocene equids. *Palaios* 397-408.

Cerling TE, Sharp ZD (1996) Stable carbon and oxygen isotope analysis of fossil tooth enamel using laser ablation." *Palaeogeo, Palaeoclim, Palaeoecology* 126:173-186.

Chang SJ, Blake RE (2002) Precise calibration of equilibrium oxygen isotope fractionations between dissolved phosphate and water from 3 to 37° C. *Geochimica et Cosmochimica Acta* 150:314-329.

Colman AS (2002) The oxygen isotope composition of dissolved inorganic phosphate and the marine phosphorus cycle. *Yale University*.

Damkier HH, Josephsen K, Takano Y, Zahn D, Fejerskov O, Frische S (2014) Fluctuations in surface pH of maturing rat incisor enamel are a result of cycles of H(+)-secretion by ameloblasts and variations in enamel buffer characteristics. *Bone* 60:227-34.

Daux V, Lécuyer C, Héran MA, Amiot R, Simon L, *et al.* (2008) Oxygen isotope fractionation between human phosphate and water revisited. *J Hum Ev* 55:1138-1147.

De Yoreo JJ, Gilbert PUPA, Sommerdijk NAJM, Lee Penn R, *et al.* (2015) Crystallization by particle attachment in synthetic, biogenic, geologic environments. *Science* 349.

Diekwisch TG (1998) Subunit compartments of secretory stage enamel matrix. *Connect Tissue Res* 38:101-11.

Driessens F, Verbeeck RK (1990) Biominerals. *CRC Press*.

Fricke H, O'Neil J (1996) Inter-and intra-tooth variation in the oxygen isotope composition of mammalian tooth enamel phosphate: implications for palaeoclimatological and palaeobiological research. *Palaeogeogr, Palaeoclim, Palaeoecology* 126:91–100.

Garcia RA, Cabeza M, Rahbek C, Araújo MB (2014) Multiple dimensions of climate change and their implications for biodiversity. *Science* 344:1247579.

Gat J (1996) Oxygen and hydrogen isotopes in the hydrologic cycle. *Ann. Rev. Earth Plan. Sci.* 24:225262.

Gehler A, Tütken T, Pack A (2011) Triple oxygen isotope analysis of bioapatite as tracer for diagenetic alteration of bones and teeth. *Palaeogeogr, Palaeoclim, Palaeoecology* 310:84-91.

Good SP, Caylor KK (2011) Climatological determinants of woody cover in Africa. *Proc Natl Acad Sci USA* 108:4902-4907.

Goodwin SD (1998) Comparison of body temperatures of goats, horses, and sheep measured with a tympanic infrared thermometer, an implantable microchip transponder, and a rectal thermometer. *Journal of the American Association for Laboratory Animal Science* 37:51-55.

Gretebeck RJ, Schoeller DA, Socki RA, Davis-Street J, Gibson EK, Schultz LO, Lane HW (1997) Adaptation of the doubly labeled water method for subjects consuming isotopically enriched water. *J Appl Phys* 82:563-570.

Harvey FE, Welker JM (2000) Stable isotopic composition of precipitation in the semi-arid north-central portion of the US Great Plains. *Journal of Hydrology* 238:90-109.

Hoetzel S, Dupont L, Schefuß E, Rommerskirchen F, Wefer G (2013) The role of fire in Miocene to Pliocene C4 grassland and ecosystem evolution. *Nat Geosci* 6:1027-1030.

Hoppe KA, Stover SM, Pascoe JR, Amundson R (2004) Tooth biomineralization in horses: implications for isotopic microsampling. *Palaeogeogr, Palaeoclim, Palaeoecology* 206:355–365.

Hsiang SM, Burke M, Miguel E (2013) Quantifying the influence of climate on human conflict. *Science* 341:1235367.

Isler K, Van Schaik CP (2014) How Humans Evolved Large Brains: Comparative Evidence. *Ev Anthr* 23:65-75.

Josephsen K, Takano Y, Frische S, Praetorius J, Nielsen S, *et al.* (2010) Ion transporters in secretory and cyclically modulating ameloblasts: a new hypothesis for cellular control of preeruptive enamel maturation. *Am J Physiol Cell Physiol*. 299:C1299-307.

Kirsanow K, Makarewicz C, Tuross N (2008) Stable oxygen ($\delta^{18}O$) and hydrogen (δD) isotopes in ovicaprid dentinal collagen record seasonal variation. *J Arch Sci* 35:3159-3167.

Kirsanow K, Tuross N (2011) Oxygen and hydrogen isotopes in rodent tissues: Impact of diet, water and ontogeny. *Palaeogeogr, Palaeoclim, Palaeoecology* 310:9-16.

Kohn M (2004) Comment: Tooth Enamel Mineralization in Ungulates: Implications for Recovering a Primary Isotopic Time-Series, by B. H. Passey and T. E. Cerling (2002). *Geochim Cosmochim Acta* 68:403405.

Kohn MJ, Schoeninger MJ, Valley JW (1998) Variability in oxygen isotope compositions of herbivore teeth: reflections of seasonality or developmental physiology? *Chem Geo* 152:97.

Kohn M, Cerling T (2002) Stable Isotope Compositions of Biological Apatite. *Rev Min Geochem* 48:455-488.

Kucherenko S, Sytsko Y (2005) Application of deterministic low-discrepancy sequences in global optimization. *Computational Optimization and Applications*. 30:297-318.

Kumar P (2013) Hydrology: Seasonal rain changes. Nature Climate Change, 3(9):783-784.

Lécuyer C, Amoit R, Touzeau A, Trotter J (2013) Calibration of the phosphate δ 18 O thermometer with carbonate–water oxygen isotope fractionation equations. *Chemical Geology* 347:217-226.

Longinelli, A, Nuti S (1973) Revised phosphate-water isotopic temperature scale. *Earth and Planetary Science Letters* 19:373-376.

Longinelli A, Padalino AP (1980) Oxygen isotopic composition of water from mammal blood: first results. *Eur J Mass Spectrom Biochem Med Env Res* 1:135-139.

Longinelli A 1984. Oxygen isotopes in mammal bone phosphate: a new tool for paleohydrological and paleoclimatological research? *Geochim Cosmochim Acta* 48:385-390.

Marshall AJ, Wrangham RW (2007) Evolutionary consequences of fallback foods. *Int J Prim* 28:1219-1235.

Mayer AL, Khalyani AH (2011) Grass trumps trees with fire. Science, 334:188-189.

Melin AD, Young HC, Mosdossy KN, Fedigan LM (2014) Seasonality, extractive foraging and the evolution of primate sensorimotor intelligence. *J Hum Ev* 71:77-86.

Mine, A *et al.*, in press.

Moermanetal JW (2013) *Earth and Planetary Science Letters* 369–370:108–119.

Morin CW, Comrie AC (2010) Modeled response of West Nile virus vector *C. quinquefasciatus* to climate using dynamic mosquito simulation. *Int J Biometeor.* 54:517-529.

O'Grady PO, Wende AR, Remien CH, Valenzuela LO, Enright LE *et al.* (2010) Aberrant Water Homeostasis Detected by Stable Isotope Analysis. *PLoS ONE* 5(7):11699.

Passey BH, Cerling TE (2002) Tooth enamel mineralization in ungulates: implications for recovering a primary isotopic time-series. *Geochim Cosmochim Acta* 66:3225-3234.

Passey B, Cerling T, Schuster G, Robinson T, Roeder B, Krueger S (2005) Inverse methods for estimating primary input signals from time-averaged isotope profiles. *Geochim Cosmochim Acta* 69:4101-4116.

Passey BH, Cerling TE (2006) In situ stable isotope analysis (δ 13 C, δ 18 O) of very small teeth using laser ablation GC/IRMS. *Chem Geo*, 235:238-249.

Pellegrini M, Lee-Thorp JA, Donahue, RE (2011) Exploring the variation of the δ18Op and δ18Oc relationship in enamel increments. *Palaeogeogr, Palaeoclim, Palaeoecology* 310:71-83.

Podlesak DW, Torregrossa AM, Ehleringer JR, Dearing MD, Passey BH, Cerling TE (2008) Turnover of oxygen and hydrogen isotopes in the body water, CO 2, hair, and enamel of a small mammal. *Geochim Cosmochim Acta*, *72*:19-35.

Potts R (2013) Hominin evolution in settings of strong environmental variability. *Quat Science Rev* 73:1-13.

Powell MJD (1998) Direct search algorithms for optimization calculations. *Acta Numerica* 7:287-336.

Pucéat E, Joachimski MM, Bouilloux A, Monna F, Bonin A, Motreuil S, Moriniere P, Henard S, Mourin J, Dera G, Quesne D (2010) Revised phosphate–water fractionation equation reassessing paleotemperatures derived from biogenic apatite." *Earth and Planetary Science Letters* 298:135-142.

Refinetti R, Menaker M (1992) The circadian rhythm of body temperature. *Physiology & behavior* 51:613-637.

Robinson C (2014) Enamel maturation: background, implications for enamel dysplasias. *Front Physiol* 5.

Sellen DW (2000) Age, sex and anthropometric status of children in an African pastoral community. *Ann Hum Bio* 27:345-365.

Simmer J, Richardson A, Hu Y-Y, Smith C, Hu J (2012) A post-classical theory of enamel biomineralization… and why we need one. *Int J Oral Sci* 4:129–134.

Smith CE (1998) Cellular and Chemical Events During Enamel Maturation. *Crit Rev Oral Bio Med* 9:128-161.

Sponheimer M, Passey B H, de Ruiter D J, Guatelli-Steinberg D, *et al.* (2006) Isotopic Evidence for Dietary Variability in the Early Hominin P. robustus. *Science* 314:980-982.

Stevens R, Balasse M, O'Connell T (2011) Intra-tooth oxygen isotope variation in a known population of red deer: Implications for past climate and seasonality reconstructions. *Palaeogeogr, Palaeoclim, Palaeoecology* 301:64-74.

Suga S 1982. Progressive mineralization pattern of developing enamel during the maturation stage. *J Dent Res* 1532-1542.

Vennemann TW, Fricke HC, Blake RE, O'Neil JR, Colman A (2002) Oxygen isotope analysis of phosphates: a comparison of techniques for analysis of Ag3PO4. *Chem Geol* 185:321-336.

Vincens A, Garcin Y, Buchet G (2007) Influence of rainfall seasonality on African vegetation in the Late Quaternary: pollen evidence, Lake Masoko, Tanzania. *J Biogeogr* 34:1274-1288.

Watson JE, Iwamura T, Butt N (2013) Mapping vulnerability and conservation adaptation strategies under climate change. *Nat Clim Change* 3:989-994.

Weinert D, Waterhouse J (2007) The circadian rhythm of core temperature: effects of physical activity and aging. *Physiology & behavior* 90:246-256.

Wiedemann-Bidlack FB, Colman AS, Fogel ML (2008) Phosphate oxygen isotope analysis on microsamples of bioapatite: removal of organic contamination and minimization of sample size. *Rapid Comm Mass Spectrom* 22:1807-1816.

Zazzo A, Balasse M, Passey B, Moloney A, Monahan F, Schmidt O (2010) The isotope record of short- and long-term dietary changes in sheep tooth enamel: Implications for quantitative reconstruction of paleodiets. *Geochim Cosmochim Acta* 74:3571-3586.

Zazzo A, Bendrey R, Vella D, Moloney A, Monahan F, Schmidt O (2012) Refined sampling strategy for intra-tooth stable isotope analysis of enamel. *Geochim Cosmochim Acta* 84:113.

Zehner JW, Terndrup TE (1991) The impact of moderate ambient temperature variance on the relationship between oral, rectal, and tympanic membrane temperatures. *Clinical pediatrics* 30:61-64.

5

Conclusions: the future of seasonality reconstructions

5.1 A method for seasonality reconstruction. The seasonality of water resources on a landscape determines its resource predictability, community composition, and is therefore central to an understanding of the environmental context of human evolution (Chapter 1). This work has endeavored to create methods for reconstructing past seasonal hydrology from oxygen isotopes ($\delta^{18}O$) in herbivore teeth. To build these methods this research has adopted descriptive, experimental, and computational approaches, using sheep as a model organism for large herbivores. Together, these approaches can recreate the paths taken by water through the body, the formation of teeth, and accurately predict tooth $\delta^{18}O$ values from known seasonal isotopic variation in drinking water. More importantly, these approaches can also work backwards, and reconstruct seasonal water $\delta^{18}O$ values from tooth measurements. Ultimately these methods should be applied using taxa and paleontological materials abundant in fossil assemblages throughout the world, including at sites relevant to human origins.

5.2 Importance of modeling mineralization. The mineralization process revealed here through synchrotron imaging and MCMC modeling supports the prediction by Suga (1982) that maturation is a complex process, but resembles Passey and Cerling (2002)'s model where maturation occurs in a single wave (Chapter 2). While findings here build a new, more comprehensive and dynamic model compared to earlier work, they are consistent with much of what we know about tooth mineralization at the cellular level. Once ameloblasts have completed apposition, they change conformation and pump Ca^{2+}, PO_4^{3-}, CO_3^{2-} and OH^- species into the

mineralization matrix, supersaturating the matrix medium and promoting crystallite growth (Robinson 2014). Our observation that mineralization pauses until maximum crown width has been achieved is consistent with this knowledge. So is the diffusive spatial character of maturation. Lastly, our observation that extension rates progressively slow is consistent with observations in other sheep breeds and taxa made through traditional light microscope histology and tooth length at death measurements (Zazzo *et al.*, 2012; Kierdorf *et al.*, 2013; Bendry *et al.*, 2015).

Because the ultimate goal of this research is reconstructing landscape seasonal climatic patterns, mapping tooth mineralization features in great detail appears to be a tedious task. However, anatomically and geochemically, fossil teeth record phenomena far larger than themselves. The complex processes of landscape hydrology that drive plant community composition, animal behavior, and adaptation and evolution are embedded within microscopic anatomical structures. For this reason, even small details of mineralization assume a far greater significance because they produce microcosms of the larger environment: spatial patterns of $\delta^{18}O$ values in teeth are records of seasonal variation in hydrology. Chapter 4 demonstrates that if mineralization processes that dampen and distort environmental inputs into the body are simply ignored, serial sample values may not resemble these inputs at all (Fig. 5.1). Unfortunately the vast majority of publications reporting serial isotope samples do not address mineralization offsets. Even details of secretion, including declining extension rates, have a major impact upon the temporal scale of reconstructions (Chapter 4). Fossil assemblages with hominin remains from the Pliocene until the late Pleistocene derive from tropical sites. The importance of appropriately modeling

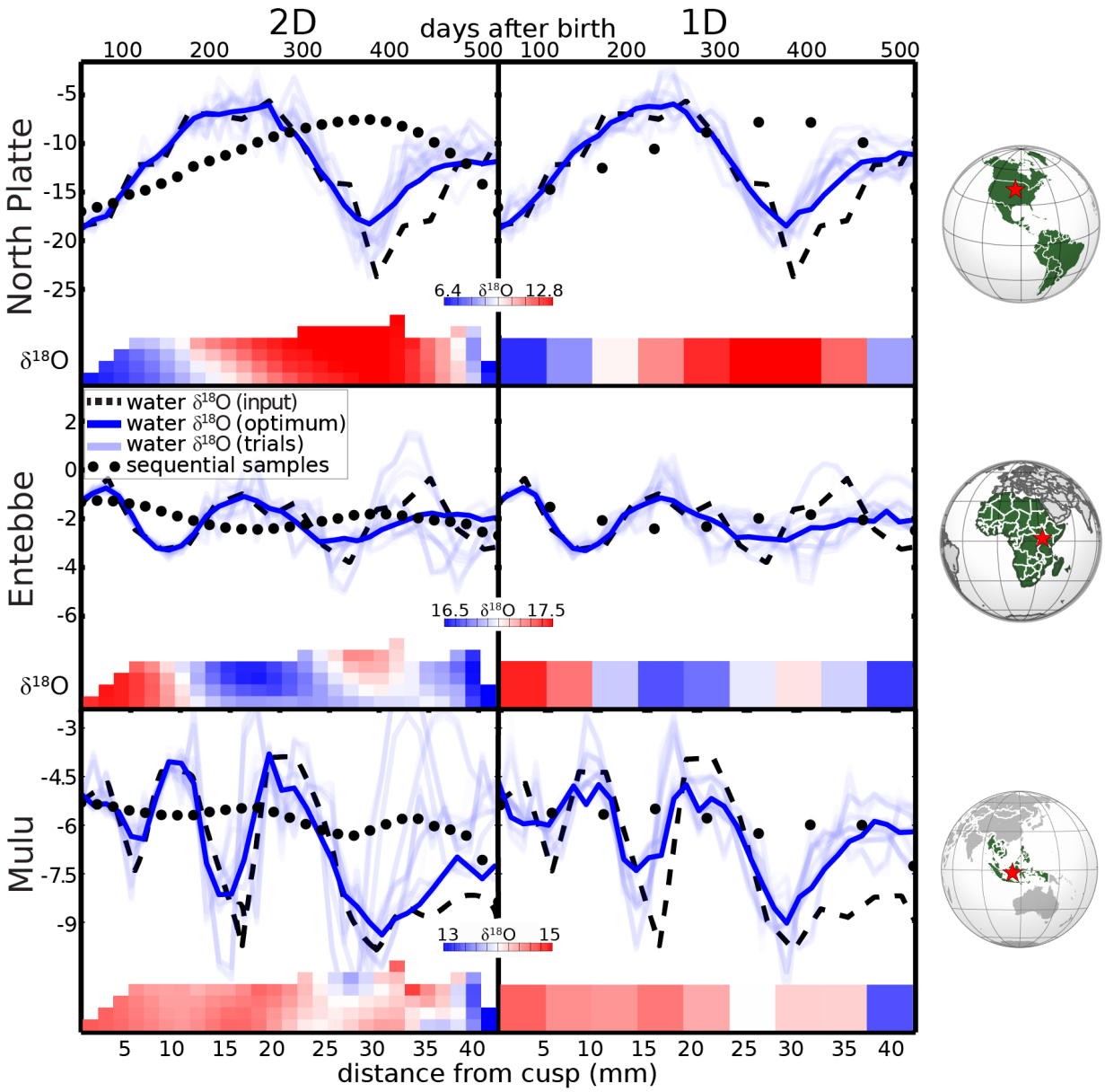

Figure 5.1 Reconstructing water inputs from tooth $\delta^{18}O$ values. Seasonal rainfall isotopic compositions (black dashed lines) for North Platte, Nebraska (top row), Entebbe, Central Uganda (middle row), and Mulu, Borneo (bottom row) produce simulated tooth $\delta^{18}O$ values (bottom of each plot), sampled at either high (left) or low (right) resolution. The color coded (blue to red) scale bar denotes tooth $\delta^{18}O$ composition. These tooth values are calculated using a forward model that integrates drinking water $\delta^{18}O$ with animal physiology (Ch. 2), and an isotopic model for enamel mineralization (all three combined in Ch. 4). Note that scaling of the y-axis and tooth $\delta^{18}O$ scale bar are site specific and differ for the three rows of figures: variation in Nebraska is higher than in the tropical sites.

Conventional, serial isotope sampling at high (1.5mm samples, left) or low (5mm samples, right) resolution produce original drinking/rain water estimates (black dots) that do not resemble inputs (black dashed line), especially at tropical sites. For instance, black dots are out of phase with input seasons at every site (x-axis, days), and grossly underestimate drink/rain $\delta^{18}O$ variation (y-axis) in the tropics.

By contrast, inverse methods presented in this work can estimate most likely reconstructed drinking water inputs (blue) and a sample of the most likely 30% of discovered solutions (light blue) that are far more faithful to inputs. Reconstructions are derived from tooth $\delta^{18}O$ values sampled at either high (1.5 x 0.18 mm spacing, left) or low (5mm, full enamel thickness spacing, right) resolution.

mineralization is only amplified in the tropics, where seasonal patterns tend to be more complex, and their effects on landscape $\delta^{18}O$ values more subtle (Fig. 5.1).

5.3 Human mineralization patterns. An obvious application of the methods developed in chapter two is the modeling of primate tooth mineralization. One reason for mapping primate teeth in detail using synchrotron density imaging is that primate teeth are very different morphologically from those of large ungulates. In this sense, primate teeth could provide an ideal comparison with sheep teeth, to test the pattern of maturation when tooth formation is slowed, and relative crown width is greater. It is possible that in this context, Suga's estimate of four maturation stages will be supported (Suga, 1989), and modeling maturation will be more important for quantitative isotopic or other trace element reconstruction. On the other hand, barium/calcium ratios in modern macaques, and in a Neanderthal tooth, show that elemental ratios in primate teeth may primarily reflect secretory geometry (Austin *et al.*, 2013). These results leave the relative importance of secretion and maturation for past dietary reconstruction unresolved.

From a paleontological perspective, mapping mineralization in primate teeth is important because it will aid in the interpretation of isotopic data from fossil hominins. Hundreds of samples have already been taken from hominin enamel throughout south and east Africa, and some of these samples have been collected serially (Sponheimer *et al.*, 2006; Cerling *et al.*, 2013; Sponheimer *et al.*, 2013; Wynn *et al.*, 2013). While seasonality reconstruction from large herbivore teeth may provide important environmental context to human evolution, sampling from hominins directly can indicate how they interacted with seasonal landscapes.

Mapping human mineralization patterns also contributes towards the goal of understanding and improving human oral health. The discoveries of evolving mineral phases during secretion and pH fluctuations during maturation in mice indicate that the processes leading to healthy, mature enamel remain poorly understood, even in the best studied mammals (Beniash *et al.*, 2009; Damkier *et al.*, 2014) Because these critical steps in the building of mature enamel are intimately linked to the timing and geometry of mineralization phases, their characterization promotes spatial and temporal understanding of all associated maturation processes. These include the expression, regulation and phosphorylation patterns in amelogenins and enamelins found within the developing enamel matrix (Kwak *et al.*, 2009; Josephsen *et al.*, 2010; Kwak *et al.*, 2011). Research presented here on the timing of phosphate resetting may contribute to a more nuanced picture of all those steps required to produce a healthy and resilient tooth. It is possible that prolonged ion species exchange during maturation, which complicates seasonality reconstruction by further dampening environmental signals, is actually crucial to healthy enamel formation (Robinson 2014).

5.4 Inverse modeling in other taxa. One reason Passey and Cerling (2002)'s mineralization model and inverse method (Passey *et al.*, 2005) have been infrequently used is that the model was explicitly designed for ever-growing teeth. To make models presented here both testable and applicable to a wider range of taxa, we have produced methods that adapt our models to other mineralization patterns (Chapter 2; Chapter 4). It should be possible to adapt mineralization models to many herbivore teeth. Despite the great variety of tooth morphology in mammals, at the genetic and cellular level tooth mineralization is a highly conserved process. Furthermore, the

high, hypsodont enamel crowns of many ungulates appear similar in cross section, even among distantly related taxa. Assuming that the general weights of secretion and maturation are preserved, secretion and maturation can be modeled for any taxon once extension rate and angle of apposition has been characterized histologically. Because our model produces concrete predictions of enamel spatial hydroxyapatite (HAp) density at a given point in time, it can be tested by density mapping from a single, developing tooth. Though we do not observe multiple waves of maturation, it is possible that in some taxa with especially thick enamel crowns, multiple waves are required to complete the maturation process. Ideal taxa for mineralization characterization beyond sheep would include horses, suids, and a number of representative bovids including alcelaphines, reduncines, and antilopines. These taxa are abundant in fossil assemblages, and many have large teeth that form over substantial periods of time and may therefore capture more information about past seasonality.

Another difficulty in applying mineralization and blood models for seasonal input reconstruction is that the models presented here, as well as earlier models (Kohn 1996; Passey *et al.*, 2005, Podlesak *et al.*, 2008), are unfamiliar and therefore inaccessible to most researchers who might wish to employ them. This difficulty can be resolved in part by converting the empirical model presented here into a simplified parametric (wholly parameter-defined) model. The model can then be provided as a package with a user interface, or hosted online, to allow use by researchers who do not have the time to become familiar with model code.

5.5 Probability frameworks for seasonality reconstruction. While mineralization patterns appear complex, interpreting reconstructed blood $\delta^{18}O$ histories to describe past seasonal

hydrology is a far more demanding task. In theory, blood and tooth $\delta^{18}O$ values are closely linked to meteoric water values (Longinelli 1984), and these vary in characteristic temporal and geographic patterns with landscape hydrology (Gat 1996; Bowen 2010). Several steps must be made however to infer seasonal meteoric water precipitation from initial tooth $\delta^{18}O$ values. First, blood $\delta^{18}O$ histories must be derived from tooth $\delta^{18}O$ values through an inverse method that accurately characterizes tooth mineralization and blood turnover. Next, $\delta^{18}O$ values must be simultaneously estimated for all animal feeding and drinking sources, along with the magnitude of these sources. This task requires a model of the diversity of water and plant $\delta^{18}O$ available on the landscape, a model of how the animal interacts with that landscape, and a model of how landscape and animal behavior fluctuate seasonally. Physiological constraints including evaporative water loss must be estimated as a part of this modeling. Lastly, any modeled seasonal meteoric water reconstruction must be placed within a statistical framework that evaluates the extent to which the reconstruction is representative of landscape patterns over larger timescales.

As daunting as this task appears, advances in the modeling of landscape hydrology and animal behavior provide avenues forward. Mapping of contemporary patterns of landscape $\delta^{18}O$ availability, and of present or past water sourcing, is an important first step for reconstructing the range of contexts in which herbivores may have foraged, and is a central focus of characterizing sedimentary sequences (Feibel *et al.*, 1994; Levin *et al.*, 2013; Quinn 2015). Characteristic animal behaviors, apparently unchanged through the Plio-Pleistocene for some taxa, can further help characterize $\delta^{18}O$ distributions on past landscapes (Cerling *et al.*, 2015). For instance, the reliance of hippos upon standing water sources, of Equids, Alcelaphines and *Ceratotherium* rhinos upon graze, and of giraffes and *Diceros* rhinos upon browse make these taxa recorders of landscape

standing water ($\delta^{18}O$ depleted) or evaporated leaf water ($\delta^{18}O$ enriched) values (Levin *et al.*, 2006; Wynn *et al.*, 2013; Cerling *et al.*, 2015; Quinn 2015). In general and following Bayes' theorem, inverse methods presented here (Chapter 2; Chapter 4) can be developed to approach the problem of understanding seasonal meteoric water δ_M from reconstructed blood $\delta^{18}O$ histories δ_{bw}:

$$p(\delta_M, \delta_L, \boldsymbol{B}_f, \boldsymbol{B}_{ev} | \delta_{bw}) = p(\delta_{bw} | \delta_M, \delta_L, \boldsymbol{B}_f, \boldsymbol{B}_{ev}) * p(\delta_M, \delta_L, \boldsymbol{B}_f, \boldsymbol{B}_{ev}) \quad \text{(eq. 5.1)}$$

where δ_L are available landscape water $\delta^{18}O$ values, B_f is an animal's foraging behavior for available waters, and B_{ev} is an animal's evaporative state over time. The parameter space required to solve for likely seasonal meteoric water can be reduced by binning δ_L, B_f and B_{ev} into dry and wet season values.

As in all models, uncertainty of output predictions is contingent upon uncertainty of input parameters. A crucial step for implementing any model predicting seasonal rainfall regimes from tooth and blood $\delta^{18}O$ values will be validation of the model in the wild. This work has shown that even under controlled conditions, blood $\delta^{18}O$ variation in a population of herbivores may be as high as the magnitude of rainfall $\delta^{18}O$ variation in the Turkana Basin (Chapter 3). Variation in the wild is almost certainly larger in most cases than for domesticated animals in captivity. More work measuring blood, tooth and landscape $\delta^{18}O$ in wild herbivorous and tropical populations can evaluate to what extent animal physiology and foraging behavior predict this variation. One outcome of testing blood and meteoric water $\delta^{18}O$ variation over time might be the discovery

that, even without understanding specific foraging and evaporative water loss behaviors, seasonal blood $\delta^{18}O$ in some taxa can be strong predictors of meteoric $\delta^{18}O$ values.

5.6 Multiproxy approach to paleoseasonality. Recent ecometric analyses have revealed similar relationships between herbivore tooth morphology and rainfall amount during dry and wet seasons (Eronen *et al.*, 2010; Fortelius *et al.*, 2014; Zlobaite *et al.*, 2016). While serial isotope values can be a powerful tool for reconstructing past seasonality, they are one tool among many that may document patterns over longer timeframes or larger geographic scales. Collecting multiple lines of evidence for past seasonal climatic and environmental conditions helps avoid conclusions that are based upon the limitations of any particular source of evidence. For instance, increasingly positive $\delta^{13}C$ values from herbivore tooth samples, leaf waxes and soil carbonates have led many researchers to conclude that grassland has become more abundant throughout the Miocene and Plio-Pleistocene of east Africa, even though pollen record show a decline in grasses over this interval (Feakins *et al.*, 2013; Chapter 1). Ideally, climatic reconstructions should employ both local and regional data that include insolation, dust, pollen, plant biomarkers, soil carbonates, faunal assemblages, ecomorphic traits, and tooth isotope values when available.

5.7 Conclusions. Tooth isotope values have been used as recorders of past seasonality for two decades due to the ordered, incremental character of tooth formation, and its preservation of environmental isotopic chemistry within enamel apatite. Despite widespread use of serial isotope sampling to infer aspects of seasonality, interpreting measurements has been difficult because the bulk of mineralization – maturation – has been poorly characterized. To address this problem,

this work has reconstructed mineralization in sheep as a proxy for large herbivores, using a new method that employs synchrotron x-ray density mapping. Density measurements from a population of animals were assembled into a single, dynamic model of mineralization that captures the timing and geometry of maturation, with the aid of Bayesian inference and Markov Chain Monte Carlo (MCMC sampling). This work has also evaluated a number of models predicting blood $\delta^{18}O$ from environmental sources by raising a population of sheep under controlled conditions. Experiments have demonstrated that blood $\delta^{18}O$ values may reflect rapid changes in environmental water sources. Even under controlled conditions, blood $\delta^{18}O$ variation within and between individuals approaches the magnitude of meteoric water $\delta^{18}O$ variation in present-day Turkana. Experimental work on sheep has shown that modeling evaporative water loss as a function of temperature greatly improves model performance in the context of seasonal variation.

Lastly, this research has integrated mineralization and blood oxygen isotope modeling, tested both experimentally, and built a method for estimating seasonal water $\delta^{18}O$ from teeth. Model-data comparisons argue that mineral phase transitions, common in other organisms, also help form sheep teeth and influence mature $\delta^{18}O$ values. Armed with this refined mineralization model, this work has yielded a computational routine that can estimate seasonal water $\delta^{18}O$ inputs from tooth $\delta^{18}O$ data. The routine iteratively proposes seasonal $\delta^{18}O$ input histories and associated tooth $\delta^{18}O$ maps, and compares these to data until proposed and measured $\delta^{18}O$ values converge. Convergence upon environmentally realistic seasonal $\delta^{18}O$ histories is aided by Bayesian inference and the use of priors, which are manipulated in a heuristic to dramatically reduce search times. With accurate mineralization models, it is shown that even conventional

isotope sampling procedures can be used to quantitatively reconstruct seasonal blood $\delta^{18}O$ variation.

The processes that record large climatic and environmental change through the microcosm of teeth are highly complex. Nevertheless I anticipate that paleoseasonality reconstruction from tooth isotope values will become common practice at fossil assemblages throughout the world. Increasingly sophisticated reconstructions of landscape hydrology, animal behavior, and community composition at locations of past hominin occupation, combined with the inverse methods presented here, make these methods even more feasible. Reconstructing the seasonality of resource availability and use by hominins as they developed stone tool industries will help us understand the ecological forces that shaped hominin behavior, adaptation and the origin of our own species.

5.8 References

Austin C, Smith TM, Bradman A, Hinde K, Joannes-Boyau R, Bishop D, Hare DJ, Doble P, Eskenazi B, Arora M (2013) Barium distributions in teeth reveal early-life dietary transitions in primates. Nature 498(7453):216-9.

Bendrey R, Vella D, Zazzo A, Balasse M, Lepetz S (2015) Exponentially decreasing tooth growth rate in horse teeth: implications for isotopic analyses. Archaeometry.

Beniash E, Metzler RA, Lam RSK, Gilbert P (2009) Transient amorphous calcium phosphate in forming enamel. *J Struc Bio* 166:133-143.

Bowen GJ (2010) Isoscapes: Spatial Pattern in Isotopic Biogeochemistry. *Annual Reviews in Earth and Planetary Sciences* **38**:161-87.

Chang SJ, Blake RE (2015) Precise calibration of equilibrium oxygen isotope fractionations between dissolved phosphate and water from 3 to 37 C. Geochimica et Cosmochimica Acta. 150:314-29.

Damkier HH, Josephsen K, Takano Y, Zahn D, Fejerskov O, Frische S (2014) Fluctuations in surface pH of maturing rat incisor enamel are a result of cycles of H(+)-secretion by ameloblasts and variations in enamel buffer characteristics. *Bone* 60:227-34.

Dawson TE, Mambelli S, Plamboeck AH, Templer PH, Tu KP (2002) Stable isotopes in plant ecology. Annual review of ecology and systematics. 507-59.

De Yoreo JJ, Gilbert PUPA, Sommerdijk NAJM, Lee Penn R, *et al.* (2015) Crystallization by particle attachment in synthetic, biogenic, geologic environments. *Science* 349.

Gat J. (1996) Oxygen and hydrogen isotopes in the hydrologic cycle. *Annual Review of Earth and Planetary Sciences* **24**:225262.

Gretebeck RJ, Schoeller DA, Socki RA, Davis-Street J, Gibson EK, Schulz LO, Lane HW (1997) Adaptation of the doubly labeled water method for subjects consuming isotopically enriched water. Journal of Applied Physiology. 82(2):563-70.

Josephsen K, Takano Y, Frische S, Praetorius J, Nielsen S, *et al.* (2010) Ion transporters in secretory and cyclically modulating ameloblasts: a new hypothesis for cellular control of preeruptive enamel maturation. *Am J Physiol Cell Physiol.* 299:C1299-307.

Kierdorf H, Kierdorf U, Frölich K, Witzel C (2013) Lines of Evidence–Incremental Markings in Molar Enamel of Soay Sheep Revealed by Fluorochrome Labeling, Backscattered Electron Imaging Study. *PLoS ONE* 8.9:e74597.

Lécuyer C, Amiot R, Touzeau A, Trotter J. Calibration of the phosphate δ18O thermometer with carbonate–water oxygen isotope fractionation equations (2013) Chemical Geology. 347:217-26.

Levin NE, Cerling TE, Passey BH, Harris JM, Ehleringer JR (2006) A stable isotope aridity index for terrestrial environments. Proceedings of the National Academy of Sciences. 103(30):11201-5.

Levin NE, Zipser EJ, and Cerling TE (2009) Isotopic composition of waters from Ethiopia and Kenya: Insights into moisture sources for eastern Africa. *Journal of Geophysical Research* **114**:D23306.

Longinelli A, Nuti S. Revised phosphate-water isotopic temperature scale (1973) Earth and Planetary Science Letters. 19(3):373-6.

Longinelli A, Padalino AP (1980) Oxygen isotopic composition of water from mammal blood: first results. *Eur J Mass Spectrom Biochem Med Env Res* 1:135-139.

Longinelli A (1984) Oxygen isotopes in mammal bone phosphate: a new tool for paleohydrological and paleoclimatological research? *Geochim Cosmochim Acta* 48:385-390.

Luz B, Kolodny Y, and Horowitz M (1984) Fractionation of oxygen isotopes between mammalian bone-phosphate and environmental drinking water. *Geochimica et Cosmochimica Acta*. 48:1689-93.

Passey BH, Cerling TE (2002) Tooth enamel mineralization in ungulates: implications for recovering a primary isotopic time-series. *Geochim Cosmochim Acta* 66:3225-3234.

Passey B, Cerling T, Schuster G, Robinson T, Roeder B, Krueger S (2005) Inverse methods for estimating primary input signals from time-averaged isotope profiles. *Geochim Cosmochim Acta* 69:4101-4116.

Podlesak DW, Torregrossa AM, Ehleringer JR, Dearing MD, Passey BH, Cerling TE (2008) Turnover of oxygen and hydrogen isotopes in the body water, CO 2, hair, and enamel of a small mammal. *Geochim Cosmochim Acta*, *72*:19-35.

Pucéat E, Joachimski MM, Bouilloux A, Monna F, Bonin A, Motreuil S, Morinière P, Hénard S, Mourin J, Dera G, Quesne D (2010) Revised phosphate–water fractionation equation reassessing paleotemperatures derived from biogenic apatite. Earth and Planetary Science Letters. 298(1):135-42.

Quinn RL (2015) Influence of Plio-Pleistocene basin hydrology on the Turkana hominin enamel carbonate δ18O values. Journal of human evolution. 86:13-31.

Robinson C (2014) Enamel maturation: background, implications for enamel dysplasias. *Front Physiol* 5.

Suga S 1982. Progressive mineralization pattern of developing enamel during the maturation stage. *J Dent Res* 1532-1542.

Suga S (1989) Enamel hypomineralization viewed from the pattern of progressive mineralization of human and monkey developing enamel. Advances in dental research. 3(2):188-98.

Taylor CR (1970) Dehydration and heat effects on temperature East African ungulates. American Journal of Physiology. 219(4)1136-9.

Wynn JG, Sponheimer M, Kimbel WH, Alemseged Z, Reed K, Bedaso ZK, Wilson JN (2013) Diet of Australopithecus afarensis from the Pliocene Hadar formation, Ethiopia. Proceedings of the National Academy of Sciences. 110(26):10495-500.

Zazzo A, Bendrey R, Vella D, Moloney A, Monahan F, Schmidt O (2012) Refined sampling strategy for intra-tooth stable isotope analysis of enamel. *Geochim Cosmochim Acta* 84:113.